

**IMPACT OF LAND USE AND CLIMATE CHANGE ON
MONSOON FLOW OF GANGES RIVER BASIN USING
SWAT MODEL**

M. Sc. Engineering Thesis

by

Md. Motiur Rahman Khan



**DEPARTMENT OF WATER RESOURCES ENGINEERING
BANGLADESH UNIVERSITY OF ENGINEERING AND TECHNOLOGY
DHAKA-1000**

FEBRUARY, 2021

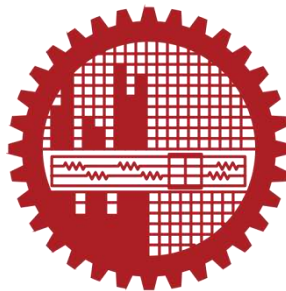
IMPACT OF LAND USE AND CLIMATE CHANGE ON MONSOON
FLOW OF GANGES RIVER BASIN USING SWAT MODEL

A Thesis Submitted

by

Md. Motiur Rahman Khan
(Roll No. 1015162037P)

In partial Fulfillment of the requirements for the Degree of
MASTER OF SCIENCE IN WATER RESOURCES ENGINEERING



DEPARTMENT OF WATER RESOURCES ENGINEERING
BANGLADESH UNIVERSITY OF ENGINEERING AND TECHNOLOGY
DHAKA-1000

FEBRUARY, 2021

Bangladesh University of Engineering and Technology, Dhaka
Department of Water Resources Engineering

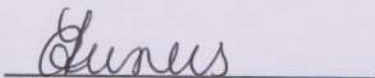
CERTIFICATION OF APPROVAL

The thesis titled “**Impact of Land Use and Climate Change on Monsoon Flow of Ganges River Basin Using Swat Model**”, submitted by Md. Motiur Rahman Khan, Roll no. 1015162037 P, Session October 2015, to the Department of Water Resources Engineering, Bangladesh University of Engineering and Technology, has been accepted as satisfactory in partial fulfillment of the requirements for the degree of Master of Science in Water Resources Engineering on 9th February, 2021.



Dr. Umme Kulsum Navera
Professor
Department of Water Resources Engineering,
Bangladesh University of Engineering and Technology, Dhaka.

Chairman
(Supervisor)



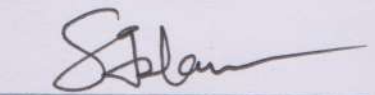
Dr. Anika Yunus
Professor and Head
Department of Water Resources Engineering,
Bangladesh University of Engineering and Technology, Dhaka.

Member
(Ex- Officio)



Dr. Md. Sabbir Mostafa Khan
Professor
Department of Water Resources Engineering,
Bangladesh University of Engineering and Technology, Dhaka.

Member



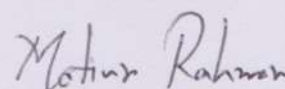
Dr. A.K.M. Saiful Islam
Professor
Institute of Water and Flood Management
Bangladesh University of Engineering and Technology, Dhaka.

Member
(External)

CANDIDATE'S DECLARATION

This is to certify that this M.Sc. thesis entitled "**Impact of Land Use and Climate Change on Monsoon Flow of Ganges River Basin Using Swat Model**" has been done by me under the supervision of Dr. Umme Kulsum Navera, Professor, Department of Water Resources Engineering, Bangladesh University of Engineering and Technology, Dhaka. I do hereby declare that this thesis or any part of it has not been submitted elsewhere for the award of any degree or diploma from any other institution.

9th February, 2021



Md. Motiur Rahman Khan

Roll No. 1015162037 P

Session: October 2015

Table of Content

| | Page No. |
|---|-----------------|
| TABLE OF CONTENTS | iv |
| LIST OF FIGURES | viii |
| LIST OF TABLES | xi |
| LIST OF SYMBOLS | xiii |
| LIST OF ABBREVIATION | xiv |
| ACKNOWLEDGEMENT | xv |
| ABSTRACT | xvi |
| CHAPTER 1 INTRODUCTION | |
| 1.1 Background and Present State of the Problem | 1 |
| 1.2 Scope of the Research Work | 3 |
| 1.3 Objective of the Study | 4 |
| 1.4 Organization of the Thesis | 4 |
| CHAPTER 2 LITERATURE REVIEW | |
| 2.1 General | 6 |
| 2.2 Previous Studies and Research on River Basin Water flow | 6 |
| 2.2.1 Basin wise River Flow Related Studies around the World | 6 |
| 2.2.2 Basin wise River Flow Related Studies in Bangladesh | 8 |
| 2.3 Water Flow change related study in Ganges River Basin | 11 |
| 2.4 Studies related to Impact of Climate Change on Water Resources using Hydrological Model | 12 |
| 2.5 Studies related to Impact of Land Use change on Water Resources using Hydrological Model | 14 |
| 2.6 Recent Literature on SWAT | 17 |
| 2.7 Summary | 19 |

| | Page No. |
|---|-----------------|
| CHAPTER 3 THEORETICAL BACKGROUND | |
| 3.1 General | 21 |
| 3.2 Assessment of Hydrological Processes | 21 |
| 3.3 Review of Physically Based Hydrological Modeling | 24 |
| 3.3.1 Modeling Concepts of Hydrologic Processes | 26 |
| 3.3.2 Advantages and Limitations of Physically Based Hydrologic Modelling | 28 |
| 3.4 Soil and Water Assessment Tool (SWAT) Model | 30 |
| 3.4.1 Conceptual Basis | 30 |
| 3.4.2 Theory on Water Balance | 31 |
| 3.4.3 Hydrology | 40 |
| 3.4.4 Advantages of Using SWAT Model | 44 |
| 3.5 Model Calibration and Validation | 44 |
| 3.6 Model Performance Evaluation | 46 |
| 3.7 Climate Change Modeling based on General Circulation Models (GCM) | 48 |
| 3.7.1 Climate Change Scenarios | 50 |
| 3.8 Summary | 51 |
| CHAPTER 4 STUDY AREA AND METHODOLOGY | |
| 4.1 General | 52 |
| 4.2 Methodology of the Study | 52 |
| 4.3 Study Area | 54 |
| 4.3.1 Topography | 55 |
| 4.3.2 Flow Regime | 57 |
| 4.3.3 Land Use Classes | 58 |
| 4.3.4 Climate of Ganges Basin | 60 |

| | Page No. |
|--|-----------------|
| 4.4 Data Collection | 63 |
| 4.4.1 Digital Elevation Model (DEM) | 63 |
| 4.4.2 River Network Data | 64 |
| 4.4.3 Land use Data | 64 |
| 4.4.4 Soil Type Data | 65 |
| 4.4.5 Weather and Discharge Data | 67 |
| 4.5 Steps of SWAT Model Setup | 68 |
| 4.6 Climate Model and Scenario Generation | 69 |
| 4.7 Climate and Land Use Change Impact Assessment | 69 |
| 4.8 Summary | 70 |
| CHAPTER 5 RESULT AND DISCUSSION | |
| 5.1 General | 71 |
| 5.2 Steps of Model Setup | 72 |
| 5.2.1 Watershed delineation | 72 |
| 5.2.2 Hydrologic Response Units Analysis | 75 |
| 5.2.3 Weather Data Definition | 77 |
| 5.2.4 Creating the SWAT Input datasets | 78 |
| 5.2.5 Simulation Method Selection | 79 |
| 5.2.6 Sensitivity Analysis | 80 |
| 5.3 Model Calibration and Validation | 82 |
| 5.4 Model Performance Evaluation | 86 |
| 5.5 Water Balance of the Ganges River Basin | 88 |
| 5.6 Selection of Climate Change Scenarios | 91 |
| 5.6.1 Analyzing the GCM Climate data | 92 |
| 5.6.2 Selection of Scenarios for Climate Change Analysis | 95 |

| | Page No. |
|---|-----------------|
| 5.7 Climate Change Impact Analysis on Flow of Ganges River Basin | 98 |
| 5.7.1 Change of Monthly Flow for 2020s projection | 98 |
| 5.7.2 Change of Monthly Flow for 2050s projection | 100 |
| 5.7.3 Change of Monthly Flow for 2080s projection | 101 |
| 5.7.4 Change of Monthly Flow for different Period for different scenarios | 103 |
| 5.7.5 Change of Future Seasonal Flow of Ganges River Basin | 105 |
| 5.7.6 Change of Mean Annual Flow of Ganges River Basin at Hardinge Bridge | 108 |
| 5.8 Impact of Land Use changes on Flow of Ganges River Basin | 110 |
| 5.8.1 Changes on Flow due to Urbanization | 110 |
| 5.8.2 Changes on Flow due to Deforestation | 111 |
| 5.9 Comparison between previous study and this study | 112 |
| 5.10 Summary | 115 |
| CHAPTER 6 CONCLUSIONS AND RECOMMENDATIONS | |
| 6.1 General | 116 |
| 6.2 Conclusions of the Study | 116 |
| 6.3 Recommendations for Future Studies | 117 |
| REFERENCES | 118 |
| APPENDIX-A | A1-A3 |
| APPENDIX-B | B1-B4 |
| APPENDIX-C | C1-C9 |

LIST OF FIGURES

| Figure No. | Title | Page No. |
|-------------------|--|-----------------|
| Figure 1.1: | Location of the Ganges and the Brahmaputra River basins overlaid by the administrative boundaries (Source: Pervez et. al, 2014) | 1 |
| Figure 3.1: | Hydrologic process: Water is transferred between the land surface, the water body and the atmosphere (Source: Encyclopedia Britannica, Inc) | 22 |
| Figure 3.2: | Hydrologic process in SWAT | 31 |
| Figure 3.3: | HRU/Sub-basin in command loop (Neitsch et al., 2005) | 33 |
| Figure 3.4: | Schematic representation of conceptual water balance of the SWAT model | 37 |
| Figure 3.5: | In-stream processes modeled by SWAT | 38 |
| Figure 3.6: | Total RF (anthropogenic plus natural) for RCPs and extended concentration pathways (ECP)—for RCP2.6, RCP4.5, and RCP6, RCP8.5 (Source: IPCC, 2013) | 50 |
| Figure 4.1: | Methodology of the Study | 53 |
| Figure 4.2: | Ganges River Basin in GBM basins (JRCB, 2018) | 54 |
| Figure 4.3: | Topography of Ganges River Basin (Source: Riccardo, 2015) | 55 |
| Figure 4.4: | The longitudinal section of its course of flow upto Farakka (Source: Hydrological inventory of River basin by NIH 1998-1999) | 56 |
| Figure 4.5: | Mean annual discharge hydrograph of the Ganges River at Hardinge Bridge transit from 1990 to 2003 (Stephanie, 2007) | 57 |
| Figure 4.6: | Landuse pattern for different years on Ganges River Basin (Source: Anand et al., 2018) | 59 |
| Figure 4.7: | Monthly average precipitation of Ganges River Basin for normal period (Source: Riccardo, 2015) | 60 |
| Figure 4.8: | Monthly average temperature of Ganges River Basin for normal period (Source: Riccardo, 2015) | 61 |
| Figure 4.9: | Digital Elevation Model (DEM) of Ganges River Basin | 63 |
| Figure 4.10: | Land use map of Ganges River Basin | 65 |
| Figure 4.11: | Soil type map of Ganges River Basin | 66 |

LIST OF FIGURES (Contd.)

| Figure No. | Title | Page No. |
|-------------------|--|-----------------|
| Figure 4.12: | Flow chart of model setup in SWAT | 68 |
| Figure 5.1: | Sub basins and delineated stream network of Ganges River Basin | 73 |
| Figure 5.2: | Automatic Watershed Delineation Dialogue box in SWAT | 74 |
| Figure 5.3: | ArcSWAT window after Watershed Delineation | 75 |
| Figure 5.4: | ArcSWAT window of HRU definition | 76 |
| Figure 5.5: | Meteorological Station grid of NASA-POWER on Watershed | 78 |
| Figure 5.6: | SWAT dialogue box to Run the Model | 79 |
| Figure 5.7: | SWAT output dialogue box and output.std file | 80 |
| Figure 5.8: | Global sensitivity analysis of calibration parameters | 82 |
| Figure 5.9: | Output window of SWAT-CUP for Calibration | 83 |
| Figure 5.10: | Monthly observed and simulated flows for the Calibration period of 2000 to 2007 | 84 |
| Figure 5.11: | Monthly observed and simulated flows for the Validation period 2000 to 2016 | 85 |
| Figure 5.12: | Scatter plot of observed vs simulated flow at Hardinge Bridge station for 2000-2016. | 88 |
| Figure 5.13 | Schematic figure of water balance of Ganges River Basin (SWAT- : Check) | 89 |
| Figure 5.14: | Average (2000-2016) monthly water availability of Ganges River Basin (all in mm) | 90 |
| Figure 5.15: | Climate Change Grid Locations in the Ganges River Basin | 92 |
| Figure 5.16: | ΔT vs ΔP Plot for 2020s | 95 |
| Figure 5.17: | ΔT vs ΔP Plot for 2050s | 96 |
| Figure 5.18 | ΔT vs ΔP Plot for the 2080s : | 96 |
| Figure 5.19: | Mean monthly discharge (m ³ /s) for 2020s at Hardinge Bridge station for Ganges River Basin | 99 |
| Figure 5.20: | Change in monthly flow of the Ganges Basin at Hardinge Bridge for 2020s | 99 |
| Figure 5.21: | Mean monthly discharge (m ³ /s) for 2050s at Hardinge Bridge station for Ganges River Basin | 100 |

LIST OF FIGURES (Contd.)

| Figure No. | Title | Page No. |
|-------------------|---|-----------------|
| Figure 5.22: | Change in monthly flow of the Ganges Basin at Hardinge Bridge for 2050s | 101 |
| Figure 5.23: | Mean monthly discharge (m ³ /s) for 2080s at Hardinge Bridge station for Ganges River Basin | 102 |
| Figure 5.24: | Change in monthly flow of the Ganges Basin at Hardinge Bridge for 2080s | 102 |
| Figure 5.25: | Average monthly discharge (m ³ /s) of Wettest Scenario for 2020s, 2050s and 2080s | 103 |
| Figure 5.26: | Average monthly discharge (m ³ /s) of Driest Scenario for 2020s, 2050s and 2080s | 103 |
| Figure 5.27: | Average monthly discharge (m ³ /s) of Coolest Scenario for 2020s, 2050s and 2080s | 104 |
| Figure 5.28: | Average monthly discharge (m ³ /s) of Warmest Scenario for 2020s, 2050s and 2080s | 105 |
| Figure 5.29: | Box-plot of Average annual discharge (m ³ /s) of all the scenarios for 2020s, 2050s and 2080s | 108 |
| Figure 5.30: | Box-plot of % Change of Average annual discharge of all the scenarios for 2020s, 2050s and 2080s | 109 |
| Figure 5.31: | Percentage change of Q ₉₀ (High Flow) compared with the baseline period | 109 |
| Figure 5.32: | Average annual discharge for different urbanization scenarios | 111 |
| Figure 5.33: | Average annual discharge for different deforestation scenarios | 112 |
| Figure 5.34: | Comparison of climate change scenarios with base for the Ganges basin (Source: Islam, M. A. et al., 2017) | 113 |
| Figure 5.35: | Change in seasonal and annual flow against different climate change scenario for the Ganges basin (Source: Islam, M. A. et al., 2017) | 114 |

LIST OF TABLES

| Figure No. | Title | Page No. |
|-------------------|--|-----------------|
| Table 3.1: | Selected physically based hydrologic model, spatial description and discretization type. | 27 |
| Table 3.2: | Advantages and limitations of physically based distributed hydrologic models over lumped conceptual models | 29 |
| Table 3.3: | Model performance rating. | 48 |
| Table 3.4: | Spatial Resolution of different GCMs in IPCC TAR and AR5 | 49 |
| Table 3.5: | Overview of Representative Concentration Pathways (RCPs) adopted by IPCC AR5. | 51 |
| Table 4.1: | Land use distribution in Ganges River Basin | 64 |
| Table 4.2: | Properties of soil used in SWAT setup for Ganges River basin. | 66 |
| Table 4.3: | Basic input data used in this study. | 67 |
| Table 5.1: | The Sequential Uncertainty Fitting (SUFI2) optimized value with optimization range of the SWAT model parameters included in the final calibration. | 81 |
| Table 5.2: | Mean observed and simulated flow for calibration (2000-2007) and validation period (2008-2016) of the Ganges River basin. | 86 |
| Table 5.3: | General Reported ratings for Nash-Sutcliffe efficiency (NSE), Mean relative bias (PBIAS), Root mean square error-standard deviation ratio (RSR) and Coefficient of determination (R ²) for calibration and validation process. | 87 |
| Table 5.4: | Model performance statistics for calibration (2000-2007) and validation period (2008-2016) of the Ganges River basin. | 87 |
| Table 5.5: | Annual average Water balance of Ganges River Basin (2000-2016). | 89 |
| Table 5.6: | Average monthly water availability of Ganges River Basin. | 90 |
| Table 5.7: | Precipitation change (%) for RCP 2.6. | 93 |
| Table 5.8: | Temperature increase (°C) for RCP 2.6. | 93 |
| Table 5.9: | Precipitation change (%) for RCP 4.5. | 93 |
| Table 5.10: | Temperature increase (°C) for RCP 4.5. | 94 |
| Table 5.11: | Precipitation change (%) for RCP 8.5. | 94 |

LIST OF TABLES (Contd.)

| Figure No. | Title | Page No. |
|-------------------|--|-----------------|
| Table 5.12: | Temperature increase (°C) for RCP 8.5. | 94 |
| Table 5.13: | Selected Scenarios for 2020s. | 97 |
| Table 5.14: | Selected Scenarios for 2050s. | 97 |
| Table 5.15: | Selected Scenarios for 2080s. | 97 |
| Table 5.16: | Change in Discharge (%) for all the four scenarios for 2020s. | 106 |
| Table 5.17: | Change in Discharge (%) for all the four scenarios for 2050s. | 106 |
| Table 5.18: | Change in Discharge (%) for all the four scenarios for 2080s. | 107 |
| Table 5.19: | Percentage of Area cover for different land use scenarios. | 110 |
| Table 5.20: | Monthly flow volume change of climate scenarios with respect to base scenario for the Ganges basin at Hardinge Bridge. | 114 |

LIST OF SYMBOLS

| | |
|-----------------------|---|
| α_{bnk} | Bank flow recession constant |
| f_{trans} | Fraction of transmission losses |
| R_{tc} | Rainfall during the time of concentration |
| R_{Sfi} | Water equivalent of the snow precipitation |
| Ψ | Suction head (negative depth) |
| $\Delta\theta$ | Moisture content difference at two levels |
| f | Infiltration rate |
| λ | Latent heat of vaporization |
| ρ | Density of the air |
| e_a | Saturation vapor pressure at mean air temperature |
| e_d | Saturation vapor pressure at dew point |
| r_s | Total surface resistance |
| γ | Psychrometric constant |
| Δ | Rate of change of e_s with temperature |
| φ_d | Drainable porosity of |
| L_{hill} | Hill slope length (m) |
| S | Retention parameter |
| aniso | Anisotropic factor |
| K_{sat} | Saturated hydraulic conductivity |

LIST OF ABBREVIATION

| | |
|-------------------|---|
| 2020s | 2010-2039 |
| 2050s | 2040-2069 |
| 2080s | 2070-2099 |
| BWDB | Bangladesh Water Development Board |
| DEM | Digital Elevation Model |
| FAO | Food and Agriculture Organization |
| GBM | Ganges-Brahmaputra-Meghna |
| GCM | General Circulation Model |
| m ³ /s | Cubic meter per second |
| HRU | Hydrological Response Unit |
| IPCC | Intergovernmental Panel on Climate Change |
| LH-OAT | Latin Hypercube One-factor-at-A-Time |
| NASA POWER | NASA Prediction of Power Worldwide Energy Resources |
| NSE | Nash-Sutcliffe efficiency |
| RMSE | Root Mean Square Error |
| RCP | Representative Concentration Pathways |
| SUFI | Sequential Uncertainty Fitting |
| SWAT | Soil and Water Assessment Tool |
| SWAT-CUP | SWAT Calibration and Uncertainty Program |
| USGS | United State Geological Survey |

ACKNOWLEDGEMENT

At first and foremost, the author would like to express his gratitude and gratefulness to the almighty Allah the creator of the world. Without the kindness of Allah, the author could not have finished the research work.

The author acknowledges his deepest sense of gratitude and respect to his supervisor Dr. Umme Kulsum Navera, Professor, Department of Water Resources Engineering, BUET for her guidance, encouragement, efficient supervision, proficiency and all kind of help she provided which results in successful completion of the thesis.

The author also expresses profound gratitude to his thesis committee member Dr. Anika Yunus, Professor and Head, DWRE, BUET and Dr. Md. Sabbir Mostafa Khan, Professor, DWRE, BUET for their support and encouragement for the research. Their constructive suggestions immensely contributed to the improvement of this thesis.

The author wishes his sincere gratitude to external member of thesis committee Dr. A.K.M. Saiful Islam, Professor, IWFM, BUET for his support and consultations while completing this thesis.

The author is grateful to Md. Asif Ahmed Abir, Graduate Research Assistant, Department of Civil Geological and Environmental Eng., University of Saskatchewan, Canada for his frequent support and guidance during the completion of this research.

The author would like to express his heartfelt thanks to Mrs. Farjana Akter Dipa, Senior Lecturer, Department of Civil Engineering, Stamford University Bangladesh for her suggestions and inspiration.

The author is thankful to all the officials of Department of WRE and the authority for allowing him to use the WRE library.

The author finally expresses his profound thanks his parents (Md. Rustom Ali Khan and Monowara Begum) and rest of family members for their blessing, love and inspiration.

ABSTRACT

Ganges River Basin is a part of Ganges-Brahmaputra-Meghna (GBM) basin which is second largest river basin system in the world based on drainage. This basin system with an area of 10,87,500 km² carries enormous volume of 525 km³/yr water through Bangladesh. Water related issues of the basin are due to both high and low flows which will be more effected due to climate change and also due to land use changes. Now a days, global warming causes the change in frequency of rainfall and temperatures. It is alarming that many studies identified significant changes in the climate of this larger South Asian region due to global warming. These changes are very likely to affect the hydrological regimes of the whole Ganges River Basins including the sub-basins and subsequently the flows that enter into Bangladesh from the system. The present study focuses on developing a hydrological model of Ganges River Basin using Soil Water Assessment Tools (SWAT) model to estimate present and future discharge considering the climate change and land use changes.

A semi-distributed hydrological model of the Ganges River Basin has been developed using SWAT. A 90-m resolution DEM derived from the Shuttle Rader Topography Mission (SRTM) has been used to delineate catchment boundary. A 300- m resolution of land use data of 2009 has been used. The soil map of the catchment has been extracted from the FAO digital soil map of the world. The gridded rainfall and temperature data have been obtained from Nasa-POWER. The evaluation process of model comprises of sensitivity analysis, calibration and validation. This hydrological model has been calibrated from 2000 to 2007 and validated for 2008 to 2016 at Hardinge Bridge transit (SW 90). The NSE, PBIAS, RSR, R² values showed satisfactory result for calibration and validation period respectively.

The calibrated hydrological model of Ganges River Basin has been used to assess the impact of climate change on discharge of Ganges River Basin by applying different climate change scenarios of selected GCMs. Four climate change scenarios, such as warmest, coolest, driest and wettest were selected based on the projected precipitation and temperature of the 21st century obtained from four RCPs (RCP 2.6, RCP 4.5 and RCP 8.5) of three GCMs (BCC-CSM 1.1, IPSL-CM5A-LR and HadGEM-2 ES). Ganges River Basin projected an increase in the mean annual streamflow for 21st century under the climate projections for almost all the four scenarios considered in this study. It is found that the average annual flow generated from the Ganges River Basin is 330,175.21 Mm³. The results also indicate that the discharge will be changed during dry period and also during monsoon. The average annual flow volume has an increasing rate for 2020s, 2050s and 2080s. An increase in urbanization and deforestation area for all over Ganges River Basin, have been done to analyze the changes of discharge. It has been found that the increasing trend of discharge for land use change scenarios towards the 21st century.

CHAPTER 1

INTRODUCTION

1.1 Background and Present State of the Problem

Ganges-Brahmaputra-Meghna (GBM) basin is the second largest river basin system in the world based on drainage (Coleman, 1969). Ganges River basin is a part of this basin system (Khandu, 2016). Approximately 1,086,000 km² catchment area have been drained by the river. This is a trans-boundary river basin and 79% of the catchment is in India, 14% is in Nepal, 4% is in Bangladesh and 3% is in China (JRCB, 2018). The river originates at an elevation about 3892m above mean sea level at Gangotri Glacier at Uttarakhand, India (Bhutiani et. al., 2014).

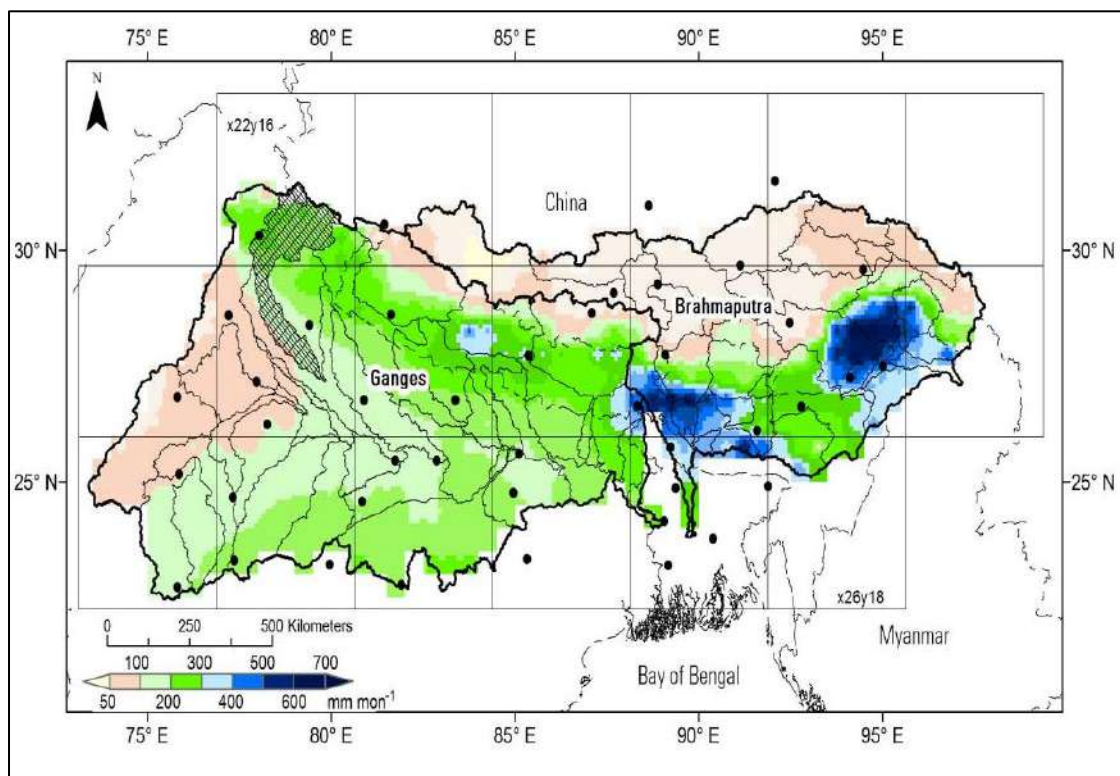


Figure 1.1: Location of the Ganges and the Brahmaputra River basins overlaid by the administrative boundaries (Source: Pervez et. al, 2014)

Many small streams comprise the headwaters of Ganges River. At Devprayag, where Alaknanda river joins Bhagirathi, the river acquires the name Ganges. It traverses a course of 2,525 km before flowing into the Bay of Bengal. The important tributaries of Ganges River are Yamuna, Ramganga, Gomti, Ghagra, Sone, Gandak, Burhi-Gandak, Kosi, Mahananda river and the important distributaries are Hugli, Gorai-Modhumati, Mathabhanga and Arial khan river. In Bangladesh, the Ganges River is joined by the

mighty Brahmaputra near Goalondo ghat and combined flow is known as the Padma. Bangladesh is the lower most riparian country of Ganges River basin. A large amount of discharge from upstream countries passes through Bangladesh towards the Bay of Bengal. The average annual discharge at the mouth with a flow of Ganges River is about 11,400 m³/s (Jian et al., 2009). The most important sources of water in the river are rainfall, snowmelt water from the Himalayas and base flow. The average annual rainfall in the GRB varies from 350 mm at the western end to 2000 mm near the delta at the eastern part. The amount of rainfall received by the basin not only changes throughout the region, it is also limited to only few months of the year mainly during monsoon months of June through October thus causing low flow conditions in the Ganges River as well as its tributaries during the dry periods of November through May. The temperature during winter season ranges from 2°C to 15°C, while that during summer season varies from 25°C to 45°C (Singh, 1994).

Bangladesh being a part of this greatest deltaic GBM plain. This basin is highly vulnerable to climate changes. The quantity of water flows is affected due to natural variability in hydrological conditions, as well as changes in land use, water use, and climate (Chalov et. al., 2015). Now a days, global warming causes the change in frequency of rainfall and temperatures. The average temperature of the world will be increased about 1.5°C between 2030-2052 (IPCC-5, 2014). Due to the warming of the earth's climate system, the global hydrologic cycle is apprehended to be perturbed to alarming scales and the existing level of water resources scarcity in the South Asian region is likely to face more stress and uncertainty in the coming years. Water-related issues of the basin are due to both high and low flows. Flood is the common phenomena in this area and severe flood occurs almost every year (Kumar, 2017). Low flows are caused by scarcity of rainfall outside the summer Monsoon, and sometimes by failure of this monsoon to develop to its normal extent.

The Ganges River Basin has a population of more than 500 million, making it as the most populated river basin in the world. Land use types are changing continuously and also will change in the future because of huge population which has and will have a major impact on the flow of the river. Changes of climate and land use change have some major impact on the peak flow and the hydrology of the Ganges River basin which leads to increase in the frequency of water-induced occurrences in Bangladesh. In recent years, a number of studies have assessed the impact of climate change on

water resources in Bangladesh. However, very few studies have been considered to assess the national and sub-national water flow incorporating climate change and land use change scenarios.

In this context, an approach has been developed in this study to establish a hydrological model for the Ganges River basin which has been selected as the study area. Soil Water Assessment Tools, SWAT 2012.10_2.19 (Arnold et. al., 1998a) is a useful tool for developing a hydrological model at Hardinge Bridge Transit (SW 90) for the Ganges River Basin.

1.2 Scope of the Research Work

The Ganges Basin today is one of the most climate vulnerable areas in the world. Melting glaciers, intensified monsoons and water-induced disasters, and sea level rise – all the ills of climate change – are expected to manifest in the basin. The countries of the basin have little capacity to deal with today’s weather and hydrological variability, much less the intensification expected with climate change. Maplecroft’s 2011 rankings of vulnerability to climate change placed the Ganges’ three main riparian as the first, second, and fourth most climate-vulnerable countries in the world. These changes are very likely to affect the hydrological regimes of the Ganges basins (Shrestha et. al, 2015), and subsequently the flows that enter into Bangladesh from these basins. This basin contains a wide variety of land use classes because more than 500 million population lives in this basin area which makes this basin the most densely populated river basin in the world. Land use types are changing continuously and also will change in future because of huge population which has and will have a major impact on the flow of the river. So, Land-use and climate change might affect the flow of the Ganges river basin, which experiences monsoon flooding almost every year.

The scope of the research study has been assessing the Ganges basin and its sub-basin for the assessment of flow of Ganges River Basin considering climate change impacts, and future Land use change scenarios. For this purpose, a hydrological model had developed by SWAT and calibrated and validated the model for Ganges River Basin. This study has focused only on the simulation of hydrological processes related to streamflow. The model has been calibrated and validated for present climatic condition and then developed possible future scenarios considering climate change impacts, and future Land use change scenarios for assessing the flow of Ganges River Basin.

1.3 Objective of the Study

The objective of this study is to assess the streamflow of Ganges River Basin through Bangladesh from 2000 to 2016 period and also assess the impact of land use and climate change on flow of Ganges River Basin Using SWAT Model. However, the specific aims of the study are as follows:

1. To develop a hydrological model for Ganges River basin by using Soil Water Assessment Tools (SWAT) and to calibrate and validate the model for monsoon flow.
2. To analyze the impact of land use changes in the major portion of the upstream basin area on the monsoon flow of Ganges River in Bangladesh.
3. To assess the impact of changes of Rainfall and Temperature (climatic parameters) on monsoon flow of Ganges River.

The expected output of this research is a hydrologically calibrated and validated model of the Ganges River basin. Furthermore, the impact of climate change for different scenarios from selected GCM models have been assessed along with the baseline mode. This helps to better understand the changes in water flow of the Ganges Basin due to the impacts of climate change. As well as analyzing the probable impact of Land use changes on the Ganges River basin can be visualized from this study. So, the possible outcomes of the research work can be summarized as follows:

- A baseline calibrated and validated hydrologic model of Ganges River Basin by using SWAT model will be available from the study.
- Probable impact of climate changes scenarios on water flow of Ganges River basin.
- Impact of Land use changes which will affect the flow of Ganges River.

1.4 Organization of the Thesis

The thesis contains six chapters. The organization of the chapters is as follows:

Chapter 1 is an introduction to the thesis. Here, the background and present state of the study and objective of the thesis have been discussed.

Chapter 2 is literature review. This chapter contains review of literature on several topics which include- review of previous studies for climate change impact assessment on different basins, impact of Land use change on water availability of different river basin have been described. Mainly focuses on the reviews of literature related to the objectives and outcomes of this study. Findings of the previous research works related to this study have also been summarized in this chapter.

Chapter 3 is theoretical background. This chapter contains the basic concepts and theories of different hydrological processes in SWAT. This chapter also deals with the basic theory and equations behind the model study.

Chapter 4 is methodology and study area. This chapter contain the hydro-morphological status of the study area, Ganges River basin. And also deals with the steps followed in the present thesis to setup, from data collection to calibration/validation of models and assess the impact of climate and land use changes on flow of Ganges River Basin.

Chapter 5 is results and discussions which describes the detail procedure followed to setup model of Ganges River Basin. This chapter also describes the parameters used to calibrate the model and evaluate the performance of calibration/validation. This chapter also gives the selection of GCM models for RCP 4.5, 8.5 for assessing impact of climate change on water flow and discussion on impact of land use changes on river flow at Hardinge Bridge transit (SW 90).

Chapter 6 is conclusions and recommendations. This chapter gives a summary of the results obtained in this study and also includes recommendations for further study relevant to this topic.

CHAPTER 2

LITERATURE REVIEW

2.1 General

This chapter provides a brief literature review of Ganges River Basin, climate change, land use change scenarios and impact of these scenarios on hydrology model. Doing a careful and thorough literature review is essential for research at any level. It is basic homework that is assumed to have been done vigilantly, and a given fact in all research papers. It not only surveys what research has been done in the past on your topic, but it also appraises, encapsulates, compares and contrasts, and correlates various scholarly books, research articles, and other relevant sources that are directly related to this research. The available study reports, project documents, published scientific articles have collected and reviewed to get information on the study area and corresponding water resources related to this study. Some of the important and selected previous studies are briefly described in this chapter around the world and in Bangladesh.

2.2 Previous Studies and Research on River Basin Water flow

Several studies on water flow in Ganges River Basin have been conducted by different researcher. However, only a few studies have been conducted to assess the water flow of Ganges river basin. In most of the cases empirical or regression model were developed relating the climate parameters to the streamflow. Due to the non-linearity of the hydrologic processes, it is not sufficient to use conceptual, empirical or regression models to predict streamflow. Also, some calibrated model parameters of these models may not be valid when the hydrologic regime of the river basin changes because of anthropogenic impacts.

2.2.1 Basin wise River Flow Related Studies around the World

Watson (2009) represented a forested watersheds model on the Boreal Plain in Canada. The model, called SWAT_{BF}, was applied to the Willow Creek watershed (15.1 km²) in north central Alberta. The performance of the model for the calibration period (2001–2003) was good with coefficients of efficiency of 0.89 and 0.81 being achieved for the prediction of monthly and daily runoff, respectively. However, it was found that SWAT_{BF} did not perform as well for the validation period (2004–2006) with the monthly and daily coefficients of efficiency being 0.44 and 0.27, respectively. Potential

sources of error to explain the decline in model performance for the validation period are discussed. SWAT_{BF} has the potential to be used as a tool by forest managers for predicting the effects of land use change on the Boreal Plain provided that it can be satisfactorily validated.

Nina (2007) presented that the hydrologic modeling for the development of management scenario and the simulation of the effect of management practices on water and sediment yielding in Gharasu watershed (5793 km²) using the Soil and Water Assessment Tool (SWAT2000) model. This basin is located in the north west of Karkheh River Basin in the far western corner of Iran. The SWAT2000 interfaced with Arc View GIS data layers including digital elevation model (DEM), land cover and soil map by AVSWAT2000 software. The model was calibrated from 1991 to 1996 and validated from 1997 to 2000. The calibrated model for hydrological conditions was used to assess suspended sediment load. Eventually, the model was used to predict the effect of changing land use and conservation practices on sediment yield within the basin.

Anaba (2017) simulated stream flow for the Murchison Bay catchment as a result of land use changes by SWAT. The SWAT model was calibrated and validated for stream flow for extended periods. The Sequential Uncertainty Fitting (SUFI-2) global sensitivity method within SWAT Calibration and Uncertainty Procedures (SWAT-CUP) was used to identify the most sensitive stream flow parameters. The model satisfactorily simulated stream discharge from the catchment. The model performance was determined with different statistical methods. The results showed a satisfactory model stream flow simulation performance. The results of runoff and average upland sediment yield estimated from the catchment showed that, both have increased over the period of study. The increasing rate of runoff can lead to severe and frequent flooding, lower water quality and reduce crop yield in the catchment. The results showed that, if all uncertainties are minimized, a well calibrated SWAT model can generate reasonable hydrologic simulation results in relation to land use, which is useful to water and environmental resources managers and policy and decision makers.

Gashawa (2018) analyze the hydrological impacts of LULC changes in the Andassa watershed for a period of 1985–2015 and to predict the LULC change impact on the hydrological status in year 2045. The hybrid land use classification technique for

classifying Landsat images (1985, 2000 and 2015); Cellular-Automata Markov (CA-Markov) for prediction of the 2030 and 2045 LULC states; the Soil and Water Assessment Tool (SWAT) for hydrological modeling were employed in the analyses. In order to isolate the impacts of LULC changes, the LULC maps were used independently while keeping the other SWAT inputs constant. The results showed that there was a continuous expansion of cultivated land and built-up area, and withdrawing of forest, shrubland and grassland during the 1985–2015 periods, which are expected to continue in the 2030 and 2045 periods. The LULC changes, which had occurred during the period of 1985 to 2015, had increased the annual flow (2.2%), wet seasonal flow (4.6%), surface runoff (9.3%) and water yield (2.4%).

Kumar (2018) analyzed the effects of LULC changes on hydrological processes governing the Tons River Basin (TRB). The LULC (1985–2035) result showed an increase in URBN from 0.29 to 2.81% while the rate of change (RoC) for URBN was calculated to be 8.71%. A continuous reduction was seen in FRSD from 15.57 to 9.77% giving the RoC as -0.37% . The FRST increased at the RoC of 1.95% from 0.6 to 1.77% while the mixed crop (RWSW) increased from 72.68 to 78.27% at the RoC of 0.77% . The other LULC classes showed similar results. Evaluation of the impact of LULC changes revealed that there was decrease in surface runoff, from 62.29 to 62.14% and lateral flow from 2.39 to 0.261% for the period of 2015 to 2035. The groundwater flow showed a slight increment from 37.42 to 37.62% while the total water yield increased from 774.74 to 776.74 mm. The simulated results for TRB showed that the hydrological processes in the watershed were minimally influenced by LULC changes. It was concluded that the basin's LULC change was not pronounced and was minimally affected by natural and artificial changes.

2.2.2 Basin wise River Flow Related Studies in Bangladesh

Mohammed (2018) assessed the possible changes in floods in the Bangladesh part of the densely populated Ganges– Brahmaputra–Meghna (GBM) delta at 1.5°C , 2°C , and 4°C global warming levels. This study was undertaken with the aim of joining the efforts of the global scientific community to assist in the preparation of the upcoming Special Report on 1.5 Degrees by the Intergovernmental Panel on Climate Change. The future changes in the possibilities of peak synchronization of nearby large rivers were assessed for the first time. Peak synchronization is critical for flood assessment in low-

lying delta regions like Bangladesh. Results indicate that the flood peaks of the GBM Rivers are more likely to synchronize in the future. Results also indicate that the flood magnitudes may become more severe in the future. At global warming levels of 1.5°C, 2°C, and 4°C, flood flows with a 100-year return period are projected to increase by about 27%, 29%, and 54% for the Ganges; 8%, 24%, and 63% for the Brahmaputra; and 15%, 38%, and 81% for the Meghna, respectively, compared with a baseline of 1986–2005.

Farzana (2019) used the Soil and Water Assessment Tool (SWAT) to predict stream runoff in Halda Basin in Bangladesh. While the calibrated model's performance was satisfactory ($R^2 = 0.80$, $NSE = 0.71$), the model was unable to track the extreme low flow peaks due to the temporal and spatial variability of rainfall which may not be fully captured by using data from one rainfall gauging station. Groundwater delay time, baseflow alpha factor and curve number were the most sensitive parameters influencing model performance. This study improves understanding of the key processes of a catchment in a data-poor, monsoon driven, small river basin and could serve as a baseline for scenario modelling for future water management and policy framework.

Tanvir (2009) attempted has been made to establish a basin scale hydrological model for the Ganges basin to predict the impact of climate change on water resources availability. A water balance model has been setup using physical based, semi-distributed hydrological model SWAT. Temperature and precipitation data from 9 GCMs and two SRES scenarios (A1B and A2) are used along with various input data (e.g., DEM, land use/cover, soil type, weather). Besides, assessment of statistical confidence of the results from different GCM is done utilizing the non-parametric Mann-Whitney U test. It is found that the average annual flow generated from the Ganges basin is 361,593 Mm³. The results also indicate that the water availability will decrease during dry period and increase during monsoon. The average annual flow volume increases 22% by 2030, 26% by 2050 and 19% by 2080 for A1B scenario. A similar situation is observed for A2 also.

Imran (2018) assessed the potential changes to the water balance of the Teesta River basin due to climate change using SWAT (Soil Water Assessment Tool). After assessing the results of GCM solutions for 2080s, four scenarios have been selected for detail analysis. They are: Wettest, Driest, Warmest and Coolest. Among the selected

scenarios, for the wettest scenario the precipitation had increased by 11.71% while it decreased by 1.76% for the driest scenario. The increase in temperature for the coolest and the warmest scenario is found to be 2.24°C and 5.34°C. The developed hydrological model of 1998-2013 timeframe served as the base model output to be compared against climate change model results. Comparing the water balance of the climate change model with the base model, it has been found that the monsoon season will become more wetter (as much as 48% increase of precipitation) and the dry season become more drier (as much as 43% reduction of precipitation) due to climate change for all the climate change scenarios. The general trend emerging from the flow analysis is that the Dalia point will experience a more severe shortage of water during the lean season where, as much as 25% decrease of flow has been found even without any upstream controls.

Nishat (2009) provide useful insights on future water availability scenarios for downstream nations in anticipation of proposed upstream water resources projects in large international river basins (IRBs). However, model set up can be challenging due to the large amounts of data requirement on both static states (soils, vegetation, topography, drainage network, etc.) and dynamic variables (rainfall, streamflow, soil moisture, evapotranspiration, etc.) over the basin from multiple nations and data collection agencies. Under such circumstances, satellite remote sensing provides a more pragmatic and convenient alternative because of the vantage of space and easy availability from a single data platform. In this paper, water resources management model set up in MIKE BASIN, over the Ganges, Brahmaputra, and Meghna (GBM) river basins. Using an array of satellite remote sensing data on topography, vegetation, and rainfall from the transboundary regions, we demonstrate that it is possible to calibrate MIKE BASIN to a satisfactory level and predict streamflow in the Ganges and Brahmaputra rivers at the entry points of Bangladesh at relevant scales of water resources management. Simulated runoff for the Ganges and Brahmaputra rivers follows the trends in the rated discharge for the calibration period. However, monthly flow volume differs from the actual rated flow by (–) 8% to (+) 20% in the Ganges basin, by (–) 15 to (+) 12% in the Brahmaputra basin, and by (–) 15 to (+) 19% in the Meghna basin. Our large-scale modeling initiative is generic enough for other downstream nations in IRBs to adopt for their own modeling needs.

2.3 Water Flow change related study in Ganges River Basin

Mirza (1997) used an empirical model to test the sensitivity of runoff of Ganges-Brahmaputra-Meghna basin to the change in temperature and precipitation from -1°C to $+5^{\circ}\text{C}$ and -10% to $+20\%$ respectively. It was observed that Ganges basin is relatively sensitive to the changes in temperature and precipitation. For temperature and precipitation change of $+2^{\circ}\text{C}$, $+10\%$ and $+4^{\circ}\text{C}$, 20% runoff at Delhi station precipitation change was found $+19\%$ and 29% respectively. For temperature beyond 4°C runoff tend to decrease. Whereas at Gauhati station on Brahmaputra river runoff change for $+2^{\circ}\text{C}$ temperature and $+10\%$ precipitation changes were found $+13\%$ which is lower than Ganges. On the other hand, runoff increase in Meghna basin at Sylhet station for $+2^{\circ}\text{C(P)}$, $+10\%(P)$ was $+11\%$. For $+5^{\circ}\text{C(T)}$, $+20\%(P)$ scenario runoff change at Gauhati, Delhi and Sylhet were found $+22\%$, $+35\%$ and 21% .

Masood (2014) assessed the impact of climate change on GBM basin in three time slices- present-day (1979–2003), near-future (2015–2039) and far-future (2075–2099) periods. He used MRI AGCM3.2S data as input in a macro scale hydrologic model H08. It was found that by the end of 21st century $+14$, $+15$, and $+18\%$ changes in runoff will occur in the Brahmaputra, Ganges and Meghna basin due to the mean change in precipitation of $+14.0$, $+10.4$, and $+15.2\%$ (entire GBM is projected to be warmed 3°C).

Kamal (2012) assessed climatic variability over Ganges-Brahmaputra-Meghna (GBM) basin which have a significant impact on the natural flow regime of its rivers. An artificial neural network (ANN) model, based on future climate projections of HadCM3 GCM, was constructed to examine the potential changes in the river flow regime assuming that climate tend to change as per the SRES scenarios A1B, A2 and B1. The results showed a trend of increasing monsoon flows for these scenarios during the periods of 2020s, 2050s and 2080s with a projected shift in the seasonal distribution of flows. Examining the monthly projected flows for different scenarios and comparing with the observed condition, it was found that the peak flow may increase $4.5 - 39.1\%$ in monsoon and the dry period low flows may drop by $4.1 - 26.9\%$ indicating high seasonality as a result of climate change. The results indicate the exacerbation of flooding potential in the central part of Bangladesh due to the largest increase of peak flows during monsoon.

Anand (2015) developed a hydrological model by Soil and Water Assessment Tool (SWAT) to the Ganga basin having a total drainage area of around 1.08 M sq. km extending over Tibet, Nepal, India and Bangladesh has been made. The model is calibrated to determine the spatial deviations in runoff at sub-basin level. Manual calibration approach was used for calibrating the SWAT model by following multi-step procedure to get to the realistic present situation as close as possible. Simulations were then further made with and without proposed future projects to obtain various scenarios. The various statistical parameters used for the evaluation of the monthly runoff simulation showed that SWAT performed well in mimicking the monthly stream flow for Ganga River basin. The model under predicted the flows in the non-perennial region during non-monsoon season, due to low rainfall and regulated flows and seepage taking place from the reservoirs. The impacts of the interventions, both existing as well as proposed, on the water balance of the basin were evaluated and quantified. The derived results suggest that there is a substantial reduction in overall water resources availability in the study basin on account of the current level of development and further, future developments, as are being proposed, may require a careful study of their potential impact on currently sanctioned water use. The study showcases that efficacy of the model for simulating the stream flow is admirable.

2.4 Studies related to Impact of Climate Change on Water Resources using Hydrological Model

Mirza et al. (2003) investigated impacts of climate change on the magnitude, extent and depth of flooding in Bangladesh. A sequence of empirical models and the MIKE11-GIS hydrodynamic model were used. Climate scenarios were constructed from the results of four climate models: CSIRO09, UKTR, GFDL and LLNL. Surprisingly, the model results indicate that most changes in the mean flooded areas occur between 0 and 2°C in relation to the increases in the peak discharges of the Ganges, Brahmaputra and Meghna Rivers rather than at higher temperature increases. In the range of 0–2, 2–4 and 4–6°C increases in temperature, increases in flooded area for per degree warming is $0.44\text{--}0.55 \times 10^6$, $0.015\text{--}0.09 \times 10^6$ and $0.015\text{--}0.075 \times 10^6$ ha, respectively.

Narsimlu (2013) used the SWAT model to simulate future climate scenarios in the upper Sind River Basin (3,806.34 km²) in India. The dominant soil types are Alfisols and Vertisols (FAO1976) and the main soil groups are alluvial soils and medium to

deep black soils. The model was simulated for a period of 16 years (1990–2005) by considering the first 2 years as warm up and next 9 years (1992–2000) for calibration and the last 5 years (2001– 2005) used for validation. The model performance was assessed by comparing observed versus simulated monthly flows during calibration and validation periods. These performance indicators of the model were found to be 0.82, 0.80, 0.73 and 0.42, respectively, and indicated a good performance of the model. For climate scenarios the author used the output of PRECIS RCM which is A1B scenarios based on availability of data, past experiences and use in other studies for India. The resolution of the RCM was 50*50 km and the authors chose baseline (1961-1990), midcentury (2021-2050) and end century (2071-2098) for simulating SWAT model. They reported that average annual stream flow could increase by 16.4 % for the midcentury and a significant increase of 93.5 % by the end century and stream flow may rise drastically in monsoon season, but will decrease in non-monsoon season due to the projected future climate change.

Zahabiyoun (2011) tested SWAT model for investigation of the effect of climate change on the runoff of Gharesou basin (5793 km²) in Iran. The authors 17 selected HadCM3-AR4 global climate model data under the A2 scenario – from the SRES scenario which was downscaled. During calibration period from 1992 to 1996, the R² and Nash coefficient were found to 0.82 and 0.8 respectively and validation period from 1998 to 2000 were found to be 0.77 and 0.73 respectively. They compared between observable and simulated climate variables with the help of the climate model during the period 2040–2069 shows that during different months, the temperature region will grow warmer by 1–48°C than the base period. Precipitation will witness a change between -30 and +30 in all months expect those without rainfall, which can affect the total available water, peak time, and external events. Since temperature and precipitation exhibit the most effects on the hydrology of the basin, simulations indicate a change from -11 to 25 m³/s in the basin runoff.

Panjwani et al. (2019) evaluated 12 CMIP5-GCMs for India for precipitation, minimum temperature and maximum temperature. They employed fuzzy analytic hierarchy process (FAHP) and reliability index to assess their ability. Indicators employed were agreement index (AI), RMSE and CC. FAHP was found suitable to rank GCMs. IPSL-CM5A-LR, MIROC5, GFDLCM3 and FIO-ESM for minimum

temperature; IPSL-CM5A-LR, GFDL-ESM2M, HadGEM2, MIROC5 and CSIRO for precipitation were found suitable.

Sreelatha & Raj (2020) evaluated average temperature for Telangana region, South India. Indicators chosen were SS, CC, normalized root mean square deviation (NRMSD), Nash–Sutcliffe efficiency (NSE), and absolute normalized mean bias deviation (ANMBD). CP and group decision-making were considered for ranking pattern. BCC-CSM1.1(m), MIROC5, CNRM-CM5 and ACCESS1.0 were found to be suitable GCMs.

Salehin (2011) used grid-based model over the Ganges-Brahmaputra-Meghna for both conditions as coarser and fine model. The coarse grid model has a snowmelt runoff module, which calculates snowmelt and glacial melt runoff in the Ganges and Brahmaputra basins following the temperature index method. The coarse grid model is verified against observed daily discharge at important locations, Bahadurabad on the Brahmaputra and Hardinge Bridge on the Ganges and against available monthly discharge data in the Nepalese part of the Ganges basin. The author used CRU (climate Research units) data as precipitation source for their model. And also recommended the use of meteorological satellite data (Tropical Rainfall Measuring Mission or TRMM data) for this kind of hydrological model.

2.5 Studies related to Impact of Land Use change on Water Resources using Hydrological Model

Kebede (2017) analyze the LULC changes in Finchaa watershed on geographic information system (GIS) version-based SWAT has been used to evaluate sensitivities and patterns of LULCC. To predict stream flow because of LULCC calibration and validation of the soil and water assessment tool were applied using the compatible version of SWAT-CUP against stream flow for Finchaa hydropower reservoir were taken to estimate model performance on monthly basis. To predict stream flow changes the analysis were performed on surface runoff, sediment yield and flow of ground water. It was found that the SWAT model predict stream flow due to LULCC reasonably well having R2 values of 0.71 & 0.74 and Nash-Sutcliffe efficiency was found to be 0.68 & 0.72 for calibration and validation of the model resulting the best model to predict hydrological process of the basin or catchment.

Samie (2019) determined the effect of land use change on runoff in Chenar Rahdar watershed. Land use map of the studied basin was determined using Landsat satellite imagery for 2004 and 2015 using ENVI software. According to results, 6 classes of land use were investigated. 21 model parameters were calibrated with monthly runoff using 2004-2012 data and validated using 2012-2015 data. The efficiency coefficient for calibration and validation were between 0.88 and 0.94, respectively. The land use changes trend within the time interval showed that the highest percentage of incremental changes is related to urban lands with 108.45%, whereas, the highest decline was observed for agricultural land with 12.46%. In order to investigate the effect of land use change on surface runoff, different land use maps were applied to SWAT model, supposing constant condition for other parameters of the model. The results show that surface runoff increased by 11%, in 2015 compared to 2004. Comprehensive water management can reduce surface runoff in the watershed. The results showed that if all uncertainties were minimized, the calibrated SWAT model can give acceptable runoff simulation results regarding the land use change.

Yingkui (2013) evaluated that hydrological impact of urban planning and water/land resource management of St. Charles County, a suburb of St. Louis, Missouri, has undergone significant urban expansion in recent decades. Rapid urban sprawl in the Dardenne Creek watershed within the county has had a profound influence on surface runoff. We examined the patterns of land use/land cover (LULC) change in this watershed using Landsat TM/ETM+ imagery in 1982, 1987, 1991, 1999, and 2003. Calibrated with the observed hydrological data in 2003, a Long-Term Hydrologic Impact Assessment (L-THIA) model was used to evaluate the effect of LULC change on surface runoff. Results indicated a rapid increase of urban areas in the watershed, from 3.4% in 1982 to 27.3% in 2003, dominated by changes in the lower portion of the watershed close to the metropolitan area. Model simulations suggest >70% increase in average direct runoff in the watershed from 1982 to 2003, and the runoff increase is highly correlated with urban expansion. This work helps raise awareness of the scale of hydrologic impacts of urbanization in this watershed, and provides a simple calibrated tool for local planners to assess potential hydrological impacts of future planning and development activities.

Kumar (2018) evaluated the impacts of LULC changes on hydrological processes governing the Tons River Basin (TRB). Landsat satellite images based on seven landuse classes which were defined for this basin are forest deciduous (FRSD), forest mixed (FRST), mixed crop (RWSW), barren land (BARN), hay (HAY), residential (URBN) and water body (WATR). The LULC (1985–2035) result showed an increase in URBN from 0.29 to 2.81% while the rate of change (RoC) for URBN was calculated to be 8.71%. A continuous reduction was seen in FRSD from 15.57 to 9.77% giving the RoC as -0.37% . SWAT was run for five decades from 1985 to 1995, 1995–2005, 2005–2015 (before baseline scenario) and 2015–2025, 2025–2035 (after baseline scenario) assuming 2015 as a baseline scenario. Evaluation of the impact of LULC changes revealed that there was decrease in surface runoff, from 62.29 to 62.14% and lateral flow from 2.39 to 0.261% for the period of 2015 to 2035. The groundwater flow showed a slight increment from 37.42 to 37.62% while the total water yield increased from 774.74 to 776.74 mm. The simulated results for TRB showed that the hydrological processes in the watershed were minimally influenced by LULC changes. It was concluded that the basin's LULC change was not pronounced and was minimally affected by natural and artificial changes.

Fengping (2019) assessed land use changes and their hydrological impacts in the Nenjiang River Basin (NRB) by using Soil and Water Assessment Tool (SWAT) model. The Cellular Automata-Markov model was used to predict a land use map in 2038. The results showed that there was a significant expansion of agriculture area at the expense of large areas of grassland, wetland, and forest during 1975–2000. The land use changes during the period of 1975 to 2000 had decreased the water yield (3.5%), surface runoff (1.7%), and base-flow (19%) while they increased the annual evapotranspiration (2.1%). For impacts of individual land use type, the forest proved to have reduced streamflow in the flood season (10%–28%) and increased surface runoff in the drought season (20%–38%). Conversely, grassland, dry land, and paddy land scenarios resulted in increase of streamflow during summer months by 7%–37% and a decrease of stream flow in the cold seasons by 11.7%–59.7%. When the entire basin was changed to wetland, stream flow reduced over the whole year, with the largest reduction during January to March. The 2038 land use condition is expected to increase the annual water yield, surface runoff and wet season flow, and reduce evapotranspiration and base-flow.

Michael (2017) analyzed the separate and the combined impacts of climate and land use changes on hydrology on the Bonsa catchment in Ghana, West Africa, using the ACRU hydrological model. The study used five RCP 8.5 climate change scenarios from the CMIP5 AR5 models for near (2020 – 2039) and far (2060 – 2079) future time slices. Change factors were used to downscale the GCM scenarios to the local scale, using observed climate data for the control period of 1990 to 2009. The land use of 1991 and 2011 were used as the baseline and current land use as well as three future land use scenarios (BAU, EG, EGR) for two time slices (2030 and 2070) were used. The study showed that under all separate climate change scenarios, overall flows reduced, but under combined climate and land use changes, stream flows increased. Under the combined scenarios, streamflow responses due to the different future land use scenarios were not substantially different. Also, land use is the dominant controlling factor in streamflow changes in the Bonsa catchment under a dry climate change, but under a wet climate change, climate controls streamflow changes. The spatial variability of catchment streamflow changes under combined land use and climate changes were greater than the spatial variability of streamflow changes under climate change. The range of plausible future stream flows changes derived in this study provides natural resources and environmental managers of the Bonsa catchment, the first ever and the most current information to develop suitable adaptation and mitigation strategies, to prepare adequately for climate and land use changes.

2.6 Recent Literature on SWAT

Roy (2021) has been assessed the flood inundation of the Arial Khan River and its floodplain for the predicted climate change scenario of RCP 8.5 (Representative Concentration Pathway 8.5) using open-source mathematical models. A calibrated and validated hydrologic model of GBM basins in SWAT (Soil and Water Assessment Tool) model has been used to estimate the future flow magnitudes at Bahadurabad Transit (Brahmaputra River) and Hardinge Bridge (Ganges River) using extreme emission scenario RCP 8.5. Using the flow magnitude of these two stations as the upstream boundaries, an HEC-RAS 1D model has been set up for the Brahmaputra, Ganges, and Padma rivers for generating future flow magnitude at the offtake of the Arial Khan River. Later, an HEC-RAS 1D-2D coupled model is set up for the Arial Khan River floodplain and flood maps are prepared considering flood depth, duration, and inundation extent. The flood assessment for different projections of RCP 8.5 shows

that there is an increasing trend of flood in terms of depth, duration, and inundation from the 2020s to the 2080s. Hence, the floodplain becomes more hazardous by the end of this century. The climate change impact on the projected population for the RCP 8.5 scenario is assessed under SSP5 (Shared Socioeconomic Pathways 5) which indicates that the total flood-affected population will be nearly twice in the 2080s compared to the 2020s. So, future climate change is going to have a dreadful effect on the flood situation of the Arial Khan River floodplain.

Afonso (2021) focused on a basin in the Brazilian Amazon and had the following three objectives: (1) to perform an effective diagnosis of flow and sediment yield, (2) to evaluate the impacts of LULC changes over the last 40 years on the hydro-sedimentological variables, and (3) to investigate the impacts of the possible trends or breaking points in the flow, surface runoff, and sediment yield series. The Soil and Water Assessment Tool (SWAT) model validation showed that the simulated results were consistent with the data measured in the dynamic reproduction of flow seasonality. Furthermore, changes in LULC altered surface runoff, sediment yield, and flow according to the Mann-Kendall and Pettitt non-parametric tests. It was also observed that the sub-basins in which pastureland is predominant are more susceptible to increased surface runoff and sediment yield. On the other hand, in the sub-basins whose land cover is predominantly forest, the time series is homogeneous and trendless.

Khan (2021) attempts to address these issues by utilizing the semi-distributed hydrological model “Soil and water assessment tool” (SWAT) with new climate datasets and better spatial and altitudinal representation as well as a wider range of future climate forcing models (general circulation model/regional climate model combinations (GCMs_RCMs) from the “Coordinated Regional Climate Downscaling Experiment-South Asia (CORDEX-SA) project to assess different aspects of future hydrology (mean flows, extremes and seasonal changes). The overall results of these future SWAT hydrological projections indicate similar trends of changes in magnitudes, seasonal patterns and extremes of the UIB—stream flows for almost all climate scenarios/models/periods—combinations analyzed. In particular, all but one GCM_RCM model—the one predicting a very high future temperature rise—indicated mean annual flow increases throughout the 21st century, wherefore, interestingly, these are stronger for the middle years (2041–2070) than at its end (2071–2100). The

seasonal shifts as well as the extremes follow also similar trends for all climate scenario/model/period combinations, e.g., an earlier future arrival (in May–June instead of July–August) of high flows and increased spring and winter flows, with upper flow extremes (peaks) projected to drastically increase by 50 to >100%, and with significantly decreased annual recurrence intervals, i.e., a tremendously increased future flood hazard for the UIB. The future low flows projections also show more extreme values, with lower-than-nowadays-experienced minimal flows occurring more frequently and with much longer annual total duration.

Akoko (2021) analyzed impacts and mitigation measures on the environment and provided insights into better environmental management. Erosion and sedimentation studies using the SWAT model were done to quantify sediment yield and evaluate soil conservation measures. Climate-change context studies mainly demonstrated streamflow sensitivity to weather changes. The model parameterization studies highlighted parameter selection in streamflow analysis, model improvements, and basin scale calibrations. The challenges and advantages of the SWAT model's applications, which range from data availability and prediction uncertainties to the model's capability in various applications, are highlighted. Discussions on considerations for future simulations such as data sharing, and potential for better future analysis are also highlighted. Increased efforts in local data availability and a multidimensional approach in future simulations are recommended.

2.7 Summary

The review of findings of previous study is very much needed before undertaking any research work. Therefore, the literature review of the previous studies around the world as well as in Bangladesh has been carried out in this chapter. It is necessary to acquire a clear concept about the previous research works which is the base of the present research and also to identify the scope of the work. Based on these literature review works; findings of the results are as follows: the hydrological modulation of the different river basin by SWAT well documented in the literature. There are three major river enters through Bangladesh. Ganges river is one of them. In previous studies hydrological modeling of Brahmaputra and Meghna is well studied. The main focus of those studies has been climate change effect on particular river basin water flow. But the understanding about the land use change impact on water flow of Ganges River

basin is still limited. The flow of Ganges River is very important for Bangladesh on basis of flood and irrigation (Mirza et al., 2004). So, this research intends to close this knowledge gap by evaluate the water flow according to future land use scenarios and also climate change scenarios.

Various surface hydrology models have been developed to quantify water flow in hydrological components. SWAT is among the very few models that have the capacity to incorporate predicted changes in temperature, precipitation, and land cover simultaneously while simulating the hydrological components. Numerous studies have been conducted implementing the SWAT model to assess climate, land use, and agricultural impacts in the Ganges basins. This research seeks to extend the knowledge base about the responses of the streamflow to climate and land use and land cover change in the Ganges basin. The SWAT model has been implemented for the Ganges basin and has been run with gridded precipitation to quantify water flow in the basin. A sensitivity assessment of the basin has also been incorporated to understand the basin's sensitivity to climate change.

Based on the above literatures on this chapter, there exist scopes to focus in the Ganges river basin water flow, this research has been chosen. Under this research, a hydrological model has been developed for this area for better understanding of the existing situation of discharge. Future scenarios have been developed considering climate change issues and land use changes. These scenarios will eventually help to find suitable measures to make the concept about streamflow change of Ganges river basin in future.

CHAPTER 3

THEORETICAL BACKGROUND

3.1 General

Hydrology is the study of the amount and quality of water being stored or conveyed on the land surface, and in soils and rocks near the surface. The hydrological response of a catchment is controlled by a combination of climate, vegetation, drainage, soils and land use. A hydrologic model is a simplification of a real-world system (e.g., surface water, soil water, wetland, groundwater, estuary) that aids in understanding, predicting, and managing water resources. Both the flow and quality of water are commonly studied using hydrologic models. Hydrological modeling can be defined as the characterization of real hydrologic features and system by the use of small-scale physical models, mathematical analogues, and computer simulations (Allaby, 1999).

SWAT model is physically based and computationally efficient, uses readily available inputs and users to study long term. SWAT modeling is gaining importance in recent times owing to its ease of usage and accuracy. SWAT is a hydrologic model which is effective tool for assessment future flow using climate data and also future land use change data. To know the basic concept and equation about SWAT model help to understand how to improve this model. For this purpose, this chapter has been discussed about basic concept and basic equations of different component about SWAT model.

3.2 Assessment of Hydrological Processes

Hydrologic process that involves the continuous circulation of water in the Earth-atmosphere system. Of the many processes involved in the water cycle, the most important are evaporation, transpiration, condensation, precipitation, and runoff. Although the total amount of water within the cycle remains essentially constant, its distribution among the various processes is continually changing. This cycle consists of a group of reservoirs containing water, the processes by which water is transferred from one reservoir to another (or transformed from one state to another), and the rates of transfer associated with such processes.

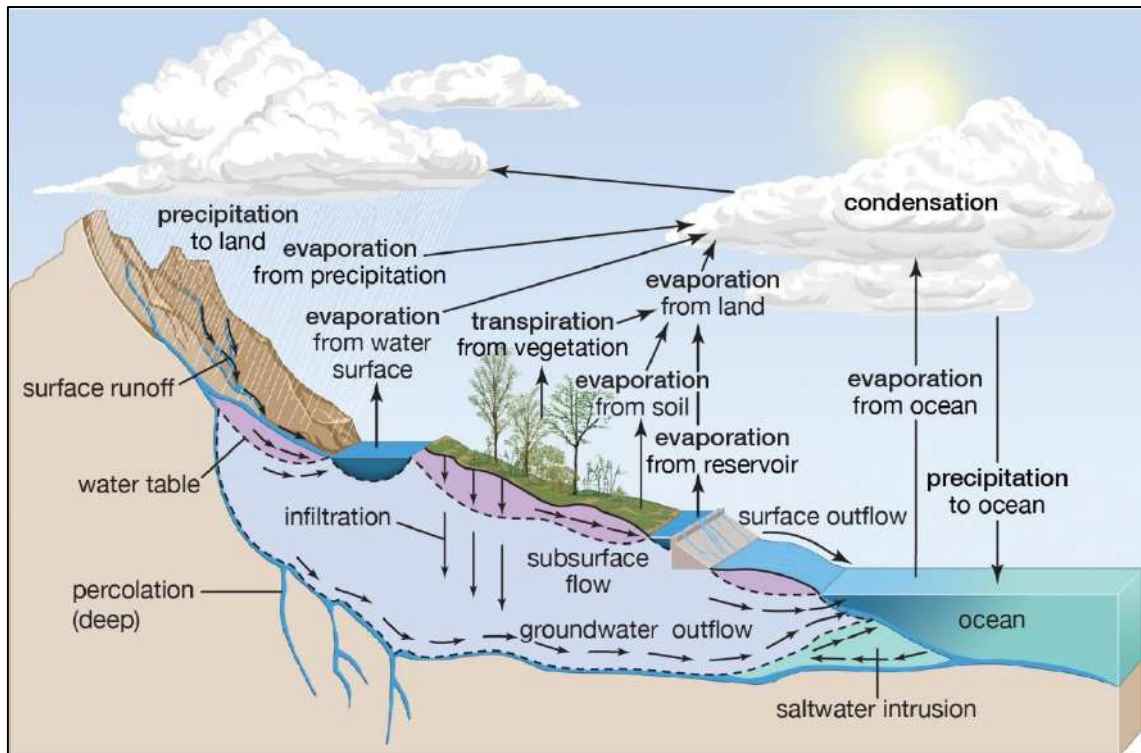


Figure 3.1: Hydrologic process: Water is transferred between the land surface, the water body and the atmosphere (Source: Encyclopedia Britannica, Inc)

The main component of Hydrological processes as follows:

- Rainfall or precipitation
- Evapotranspiration
- Infiltration
- Percolation
- Surface storage
- Interflow
- Groundwater flow

A brief description of the water cycle follows:

Rainfall or precipitation

Precipitation, either in the form of rainfall or snow, is the main input component of watershed modelling. The reliable output of the model highly depends upon accurate input. Therefore, precipitation is the key input component of watershed modelling. In humid regions, rainfall is the main source of precipitation whereas in cold regions, snow often becomes the main contributor of precipitation, which explicitly defines the surface and subsurface hydrological cycle (Faria et al., 2000).

Evapotranspiration

Evapotranspiration is a collective term for all processes by which water in the liquid or solid phase at or near the earth's surface becomes atmospheric water vapor. Evapotranspiration includes evaporation from rivers and lakes, bare soil, and vegetative surfaces; evaporation from within the leaves of plants (transpiration); and sublimation from ice and snow surfaces.

Potential evapotranspiration is the rate at which evapotranspiration would occur from a large area completely and uniformly covered with growing vegetation which has access to an unlimited supply of soil water. This rate is assumed to be unaffected by micro-climatic processes such as advection or heat-storage effects.

Infiltration

Infiltration refers to the entry of surface water into the underlying soil layers. The infiltration process plays an important role to supply water for plant growth and to recharge the ground water aquifers. The rate of infiltration depends upon the physical properties of the soil, vegetation cover on the ground, initial water content of the soil, soil temperature, and the intensity of rainfall or rate of snowmelt.

Percolation

Percolation is the movement of water through the soil, and its layers, by gravity and capillary forces. The prime moving force of groundwater is gravity. Water that is in the zone of aeration where air exists is called vadose water. Water that is in the zone of saturation is called groundwater. For all practical purposes, all groundwater originates as surface water. Once underground, the water is moved by gravity. The boundary that separates the vadose and the saturation zones is called the water table. Usually the direction of water movement is changed from downward and a horizontal component to the movement is added that is based on the geologic boundary conditions.

Surface runoff

Overland flow is categorized into two portions: infiltration excess overland flow and saturation excess overland flow (Beven, 2000). Generally, when rainfall intensity exceeds the infiltration capacity of the soil, then infiltration excess runoff is generated. Saturation excess runoff mechanism may occur in either of the following situations: (1) on areas of high antecedent soil moisture conditions; (2) where there is a thin soil layer

and the storage capacity of soil is limited; and (3) in areas of low permeability and low slope (Beven, 2000). Hence, surface runoff depends upon the infiltration capacity and degree of saturation of underlying soil layers. It also depends upon the vegetation cover of the ground as well as in the degree of ground slope.

Lateral subsurface flow

Lateral subsurface flow, or interflow, originates below the ground surface but above the zone where the soil and bedrock profile is saturated with water. The lateral subsurface flow contributes to the streamflow within the watershed. Lateral subsurface flow, or interflow in the soil profile is calculated using a kinematic storage model developed by Sloan and Moore (1984). The kinematic wave approximation of saturated subsurface or lateral flow assumes that the lines of flow in the saturated zone are parallel to the impermeable boundary and the hydraulic gradient equals the slope of the bed.

Groundwater flow

Ground water moves very slowly, and a particle of water may take anywhere from days or months to years or even hundreds of years to move to the ocean, where it starts the process all over again. This is a main reason why ground water supplies are impossible to artificially replenish after being depleted. Wells go dry because the pump used to bring up ground water no longer reaches the water table. Ground water may take hundreds of years to replenish (through percolation) in particularly dry areas.

3.3 Review of Physically Based Hydrological Modeling

Hydrologic modelling involves formulating the mathematical models to represent the hydrologic processes such as, precipitation, snowmelt, interception, evapotranspiration, infiltration, sub-surface flow and surface flow, as well as the interaction between them. Hydrologic modeling can be challenging because it involves highly non-linear processes, complex interactions and high spatial variabilities at basin scale. Starting from the mid of the 19th century, the evolution of hydrologic modelling is continuing from lumped conceptual models to physically based distributed models with the development of understanding the physical processes, computational efforts and data retrieving facilities. Lumped conceptual hydrologic models consider three basic processes within a river basin: the loss of water from storage to atmosphere; storage of water in soil, vegetation, aquifer, and in rivers; routing of flow over the surface (Gosain

et al., 2009). Physically based hydrologic models are based on known scientific principles of energy and water fluxes whereas, conceptual models are based on conceptual storages and model parameters that require calibration, or they are moisture accounting models without explicitly considering energy fluxes, and so they mimic physical processes in a simplified manner. Focus on the physically based distributed hydrologic modelling started in order to minimize or overcome the deficiencies of the conceptual models. In physically based hydrologic modelling the hydrologic process of water movement are modeled either by the finite difference approximation of the partial differential equation representing the mass, momentum and energy balance or by empirical equations (Abbott et al., 1986b).

Typically, the primary components of hydrologic cycle related to the land phase are taken into consideration. These are: interception, snowmelt, evapotranspiration, sub-surface runoff, groundwater flow, surface runoff and channel routing. Physically based hydrologic models can be fully distributed where a river basin is discretized as a rectangular grid mesh, or be semi-distributed when the basin is divided into limited number of sub-basins based on the terrain features and the drainage network. Resolution of horizontal discretization could be an important factor in physically based hydrologic modelling.

Hydrologic models can be classified according to the physical processes involved in modelling as conceptual and physically based (Refsgaard, 1996). In conceptual models each of the hydrologic processes, that showed into observations of the catchment, are represented by simplified mathematical relationships, where as in physically based model the detail physical processes can be represented in a deterministic way by representations of mass, momentum and energy conservation (Refsgaard, 1996). According to the spatial description of the watershed process, hydrologic models can be classified as lump and distributed models. In a lumped model the spatial variability of watershed characteristics is ignored, while in a distributed model the spatial variability of vegetation, soil, topography, etc. are taken into account. The conceptual models are usually lumped while the physically based model in practice has to be distributed in manner (Refsgaard, 1996). The development of physically based hydrologic modelling started around the late 1960s. Freeze and Harlan (1969) set out a blueprint for a physically based digitally simulated hydrologic response model. Their

purpose of study was to assess the feasibility of the development of physically based mathematical model of complete hydrologic system. They concluded that, though the present level of sophistication allows the treatment of one- or two-dimensional unsteady soil moisture flow in heterogeneous soil, three-dimensional steady state groundwater flows in nonhomogeneous anisotropic formation, and one-dimensional open channel flow with lateral inflow, the level of development is not adequate to develop complete physically based hydrologic model (Freeze and Harlan, 1969).

Later studies by Freeze (1971, 1972a, 1972b) on saturated and unsaturated flow in groundwater and their role on surface runoff are still considered as the pioneering work of physically based hydrologic modelling (Abbott et al.,1986a). In 1976, three European organizations, namely, the British Institute of Hydrology, the Danish Hydraulic Institute and French Consulting Company SOGREAH, joined to develop a fully distributed physically based hydrologic model SHE (European Hydrologic System) and it became operational in 1983 (Abbott et al., 1986a, 1986b). Since then, the development of physically based hydrologic models is one of the major interests of hydrologic research community.

3.3.1 Modeling Concepts of Hydrologic Processes

In physically based hydrologic modeling the hydrologic process of water movement are modeled either by the finite difference approximation of the partial differential equation representing the mass, momentum and energy balance or by empirical equations (Abbott et.al., 1986b).

Typically, the primary components of hydrologic cycle related to the land phase are taken into consideration. These are: interception, snowmelt, evapotranspiration, sub-surface runoff, groundwater flow, surface runoff and channel routing.

A number of physically based hydrologic models have been reviewed and modeling concepts of these physical processes used by various hydrologic models will be discussed in the following sections. Table 3.1. Shows the selected model acronyms and principal references.

Table 3.1: Selected physically based hydrologic model, spatial description and discretization type.

| Model Acronym | Model Definition | Principle Reference(s) | Semi/Fully Distributed | Distributed type* |
|-------------------|---|---|------------------------|-------------------|
| TOPMODEL | Topography based hydrological MODEL | Beven and Kirby (1976,1979) | Semi | HRU |
| WATBAL | | Knusden et.al. (1986) | Semi | OG |
| SHE | European Hydrologic System | Abbot et.al. (1986a, 1986b) | Fully | OG |
| ISBA | Interaction Soil Biosphere Atmosphere | Nolihan and Planton (1989) Nolihan and Mahfouf (1995) | Fully | OG |
| IHDM | Institute of Hydrology Distributed Model | Beven et.al. (1987) Calver and Wood (1995) | Fully | HRU |
| THALES | | Grayson et.al. (1992a; 1995) | Fully | IE |
| SLURP | Semi-distributed Land Use-based Runoff Processes | Kite (1995) | Semi | GRU |
| MIKE SHE | MIKE System Hydrologique European | Refsgaard and Storm (1995) | Fully | OG |
| SWAT | Soil and Water Assessment Tool | Arnold et.al. (1998a) | Semi | HRU |
| WATFLOOD/ SPL9 | Waterloo Flood Forecasting Model | Kouwen (1988) Kouwen (2000) Kouwen and Mousavi (2002) | Fully | OG |
| HRCDHM | Hydrologic Research Centre Distributed Hydrologic Model | Carpenter et.al. (2001) | Semi | HRU |
| DPHM-RS | Semi-distributed Physically based Hydrologic Model using Remote Sensing and GIS | Biftu and Gan (2001, 2004) | Semi | HRU |
| R.WATER.FEA | | Vieux and Gaver (1994) | Fully | IE |
| iRIBS | TIN-based Real-time Integrated Basin Stimulator | Ivanov et.al., 2004 | Fully | TIN |
| TOPNET | | Bandaragoda et.al. (2004) | Semi | HRU |
| MISBA | Modified Interaction Soil Biosphere Atmosphere | Kerkhoven and Gan (2006) | Fully | OG |
| LISTFLOOD | | Van der Knijff et.al. (2010) De Roo et.al. (2000) | Fully | OG |
| HydroGeoSphere | | Therrien et.al. (2005; 2010) | Fully | OG |
| PAWS | Process-based Adaptive Watershed Simulator | Shen and Phanikumar (2010) | Fully | OG |
| CREST | The Coupled Routing and Excess Storage | Wang et.al. (2011) | Fully | OG |

Source: Islam, 2011b

* Abbreviation used for Discretization type: OG= Orthogonal Grid, HRU= Hydrologic Response Unit, GRU=Grouped Response Unit, IE=Irregular Elements, TIN=Triangulated Irregular Network.

3.3.2 Advantages and Limitations of Physically Based Hydrologic Modelling

Lumped conceptual hydrologic models consider three basic processes within a river basin: the loss of water from storage to atmosphere; storage of water in soil, vegetation, aquifer, and in rivers; routing of flow over the surface (Gosain et. al., 2009). Focus on the physically based distributed hydrologic modeling started in order to minimize or overcome the deficiencies of the conceptual models. Conceptual models are controlled by various parameters to represent the hydrologic processes. Parameters of these models are estimated either by manual curve fitting or by optimizing the objective functions, thus making less or no physical interpretation of the fitted parameters.

Therefore, unrealistic parameter values may be obtained through errors in measurements. In lumped conceptual models the mathematical representation of hydrologic processes is only an approximate representation of the real world. So, the errors in parameter estimation also can be raised from model structure. The calibration of conceptual models requires long meteorological and hydrological records which are not always available, especially for the un-gauged catchments (Gosain et. al., 2009). Spatial heterogeneities of landuse, soil, and input variables are not considered in lumped conceptual models (Abbott et al., 1986a). The effects of landuse changes resulting from the human's activities on the hydrologic cycle cannot be undertaken by altering the parameter values to reflect changes as the parameters values to reflect changes as the parameters are not based on physical processes (Abbott et.al. 1986a).

The calibration and validation of lumped conceptual models depends on the accuracy of both inputs and outputs. So, uncertainty is involved in estimating the input variables, especially the evapotranspiration may cause significant changes in calibration and validation processes. Different set of parameter values may result equal quality of good results in a lumped conceptual model (Beven, 1989).

As discussed in the previous paragraph, the development of physically based hydrologic model was initiated to overcome the deficiencies associated with the lumped conceptual models, by using parameter values with physical interpretation and considering their spatial variability (Abbott et al., 1986a). However, the physics on which the equations of physically based hydrologic models are based is the small-scale physics of homogeneous system and in application these models lump up the small-

scale physics to the model grid scale without considering any theoretical framework (Beven, 1989).

Table 3.2: Advantages and limitations of physically based distributed hydrologic models over lumped conceptual models

| Advantages Over Lumped Conceptual Model |
|--|
| <ul style="list-style-type: none"> • Parameters in physically based models are based on physics. • Physically based are developed from well-established scientific laws at micro-scale to water behavior at the meso-scale or regional scale. • Can consider the effects of the land use changes on the hydrologic cycle. • Consider the spatial heterogeneities of land use, soil, and input variables. • Less (or no) calibration is needed. |
| Limitations |
| <ul style="list-style-type: none"> • Lump up the small-scale physics to the model grid scale without considering any theoretical framework. • Calibration by the comparison of the predicted and observed hydrograph cannot be considered a sufficient test of model that implies the internal response of catchment. • Context of original purpose of development is often lost when models applied beyond the scope of their capabilities. • Development of some physically based model is not dynamic nor it is in conjunction of a field program • Many models are developed from limited data sources. • Calibration testing on one or two catchments is also insufficient test of model's universal applicability. |

Source: Islam, 2011b.

Calibration of most physically based hydrologic models is usually performed by the comparison of predicted and observed hydrograph which is a necessary test but cannot be considered a sufficient test of model that implies the internal response of catchment (Beven, 1989). In application of physically based hydrologic models, the context of their original purpose of development is often lost when they are applied beyond the scope of their capabilities (Grayson et al., 1992a). Development of some physically based model is not dynamic nor is it in conjunction of a field program (Dunne, 1983). Many models are developed from limited data sources. Calibration testing on one or two catchments is also insufficient test of model's universal applicability (Grayson et al., 1992a). A summary of advantages and limitations of physically based distributed hydrologic models over lumped conceptual models discussed in the aforementioned paragraphs is listed in below.

3.4 Soil and Water Assessment Tool (SWAT) Model

SWAT is a spatially distributed, continuous time scale watershed scale model developed by Dr. Jeff Arnold for the USDA-ARS. It was developed to predict the impact of land management practices on water, sediment and agricultural chemical yields in large complex watersheds with varying soils, landuse and management conditions over long periods of time. SWAT divides a watershed into sub-watersheds. Each sub-watershed is connected through a stream channel and further divided into Hydrologic Response Unit (HRU). HRU is a unique combination of a soil and a vegetation type in a sub-watershed, and SWAT simulates hydrology, vegetation growth, and management practices at the HRU level. Weather, soil properties, topography, vegetation and land management practices are the most important inputs for SWAT to model hydrologic and water quality in a watershed (Neitsch, 2002) SWAT allows a basin to be subdivided into sub-basins to evaluate hydrology, weather, sediment yield, nutrients and pesticides, soil temperature, crop growth, tillage and agricultural management practices.

3.4.1 Conceptual Basis

The Soil and Water Assessment Tool (SWAT) is a watershed scale conceptual model that operates on a daily time step (Arnold et al. 1998) which is also a physically based model (Gassman et al., 2007) that can simulate long term water yield and water quality from watersheds with varying soils and land management practices. The SWAT model is applicable for hydrological prediction in both large- and small-scale watersheds. The comprehensive SWAT model is capable of simulating different hydrological components such as climate, hydrology, soil temperature, plant growth, erosion, nutrient transport, pesticide transport, and land management practices (Arnold et al., 1998; Neitsch et al., 2005). The model accounts for spatial details and is a better predictor of long term yields rather than a single flood event (Arnold et al., 1998).

In the SWAT model, a watershed can be partitioned into smaller units on the basis of two-levels of discretization. First, a watershed can be divided into any number of smaller spatial units called sub-watersheds. Thereafter, the sub-watersheds are further subdivided into non- spatial groupings called hydrologic response units (HRUs) on the basis of the identical soil and land use characteristics. Hence, the SWAT model can preserve the spatially distributed parameters of the entire basin (Srinivasan et al. 1998).

3.4.2 Theory on Water Balance

Water balance is the driving force behind everything that happens in the watershed. To accurately predict the movement of pesticides, sediments or nutrients, the hydrologic cycle as simulated by the model must conform to what is happening in the watershed.

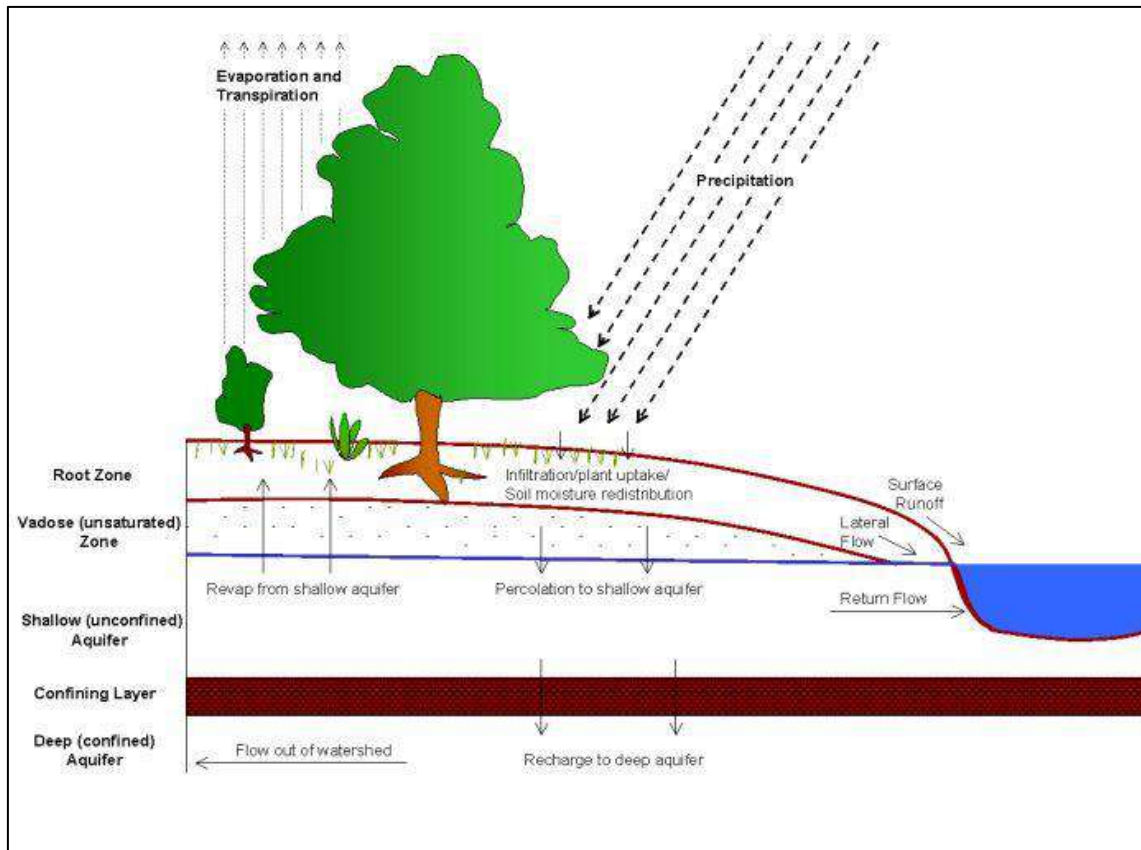


Figure 3.2: Hydrologic process in SWAT

The simulation of hydrologic cycle can be separated into land phase and water or routing phase. Land phase controls the amount of water, sediment, nutrient and pesticide loading to the main channel in each sub-basin whereas routing phase defines the movement of water, sediments, etc. through the channel network of the watershed to the outlet. Schematic of pathways available for water movement in SWAT is shown in the Figure 3.2. It involves various elements such as snow, canopy storage, infiltration, evapotranspiration, lateral subsurface flow, surface runoff, transmission losses, return flow etc.

Land phase of the hydrologic cycle

Hydrologic cycle simulated by swat is based on the water balance equation

$$SW_t = SW_0 + \sum_{i=1}^t (R_{day} - Q_{surf} - E_a - W_{seep} - Q_{gw}) \quad \dots\dots\dots(3.1)$$

Where SW_t is the final soil water content (mm H₂O), SW_0 is the initial soil water content on day i (mm H₂O), R_{day} is the amount of precipitation on day i (mm H₂O), Q_{surf} is the amount of surface runoff on day i (mm H₂O), E_a is the amount of evapotranspiration on day i (mm H₂O), W_{seep} is the amount of water entering the vadose zone from the soil profile on day i (mm H₂O), and Q_{gw} is the amount of return flow on day i (mm H₂O).

Snow

Swat classifies precipitation as rain or freezing rain/snow using the average daily temperature. The snow melt is calculated in the SWAT model by considering the air and snow pack temperature, a melting factor, and the snow cover. In the SWAT model, the melted snow (snow water equivalent) is added to the precipitation input in the calculation of surface runoff and percolation.

The snowpack increases with additional snowfall, but decreases with snowmelt or sublimation. The mass balance for the snowpack is computed as:

$$SNO_i = SNO_{i-1} + R_{sfi} - E_{subi} + SNO_{mli} \quad \dots\dots\dots(3.2)$$

where SNO_i and SNO_{i-1} are the water equivalents of the snowpack on the current day (i) and previous day ($i-1$), respectively, R_{sfi} is the water equivalent of the snow precipitation on day i , E_{subi} is the water equivalent of the snow sublimation on day i , and SNO_{mli} is the water equivalent of the snowmelt on day i .

Canopy Storage

Canopy storage is the water intercepted by vegetative surfaces where it is held and made available for evaporation. When using the curve number method to compute surface runoff, canopy storage is taken into account in the term initial abstractions. However, if methods such as Green & Ampt are used to model infiltration and runoff, canopy storage must be modeled separately.

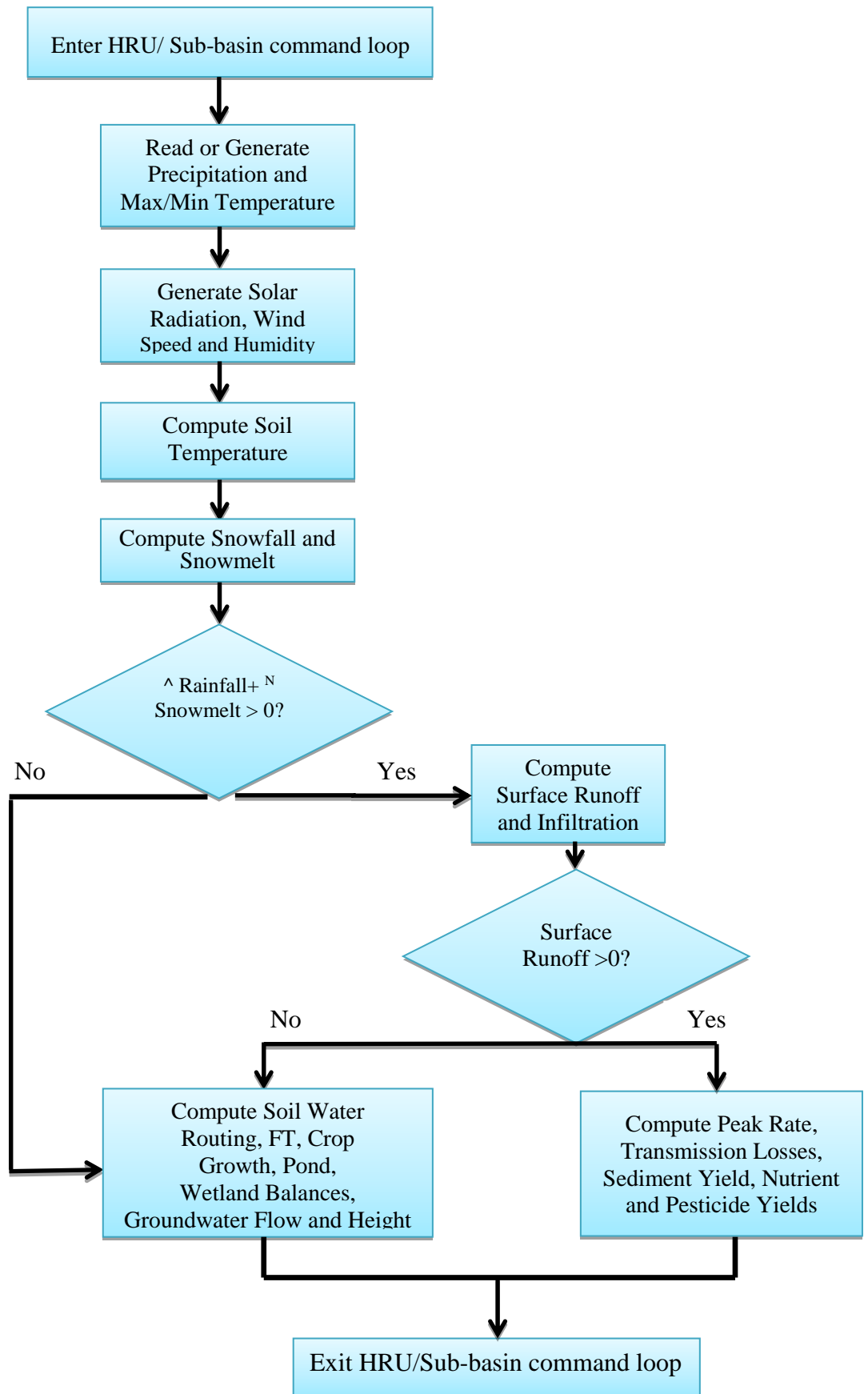


Figure 3.3: HRU/Sub-basin in command loop (Neitsch et al., 2005)

SWAT allows the user to input the maximum amount of water that can be stored in the canopy at the maximum leaf area index for the land cover. This value and the leaf area index are used by the model to compute the maximum storage at any time in the growth cycle of the land cover/crop. When evaporation is computed, water is first removed from canopy storage.

Infiltration

In the SWAT model, the amount of water infiltrating into the soil profile is calculated indirectly because the surface runoff is computed directly using either of the previously mentioned methods (Neitsch et al., 2005). Hence, the infiltrated water is calculated as a difference between the amount of rainfall and the amount of surface runoff. The Green and Ampt infiltration equation (Green and Ampt, 1911) does directly model infiltration, but it requires precipitation data in smaller time increments.

$$f_t = K \left(\frac{\psi \Delta \theta}{F_t} + 1 \right) \dots\dots\dots(3.3)$$

$$F_{t+\Delta t} = F_t + K\Delta t + \psi \Delta \theta \ln \left[\frac{F_{t+\Delta t} + \psi \Delta \theta}{F_t + \psi \Delta \theta} \right] \dots\dots\dots(3.4)$$

Where f: infiltration rate (depth/time); F: Cumulative infiltration depth (depth); K: Vertical hydraulic conductivity (depth/time); ψ : Suction head (negative depth); $\Delta\theta$: Moisture content difference at two levels

Evapotranspiration

The model computes evaporation from soils and plants separately as described by Ritchie (1972). Potential soil water evaporation is estimated as a function of potential evapotranspiration and leaf area index (area of plant leaves relative to the area of the HRU). Actual soil water evaporation is estimated by using exponential functions of soil depth and water content. Plant transpiration is simulated as a linear function of potential evapotranspiration and leaf area index. Numerous methods have been developed to estimate ET. Three of these methods have been incorporated into SWAT2000: The Penman-Monteith method (Monteith, 1965; Allen, 1986; Allen et al., 1989), the Priestley-Taylor method (Priestley and Taylor, 1972) and the Hargreaves method (Hargreaves et al., 1985).

The Penman-Monteith equation is:

$$E = \frac{\Delta H + \frac{\rho c p (e_a - e_d)}{r_a}}{\lambda \left[\Delta + \gamma \left[1 + \left(\frac{r_s}{r_a} \right) \right] \right]} \dots\dots\dots(3.5)$$

Where

ρ : Density of the air, c : Specific heat of the air, e_a : Saturation vapor pressure at mean air temperature, e_d : Saturation vapor pressure at dew point, r_s : Total surface resistance, r_a : Aerodynamic resistance, λ : Latent heat of vaporization, γ : Psychrometric constant, Δ : Rate of change of e_s with temperature.

The model offers three options for estimating potential evapotranspiration: Hargreaves (Hargreaves et. al., 1985), Priestley-Taylor (Priestley and Taylor, 1972), and Penman-Monteith (Monteith, 1965). The three PET methods included in swat vary in the amount of required inputs. The Penman-Monteith method requires solar radiation, air temperature, relative humidity and wind speed. The Priestley-Taylor method requires solar radiation, air temperature and relative humidity. The Hargreaves method requires air temperature only.

Lateral Subsurface Flow

Lateral subsurface flow, or interflow in the soil profile is calculated using a kinematic storage model developed by Sloan and Moore (1984). The kinematic wave approximation of saturated subsurface or lateral flow assumes that the lines of flow in the saturated zone are parallel to the impermeable boundary and the hydraulic gradient equals the slope of the bed. The drainable volume of water stored in the saturated zone of the hill slope segment per unit area, $SW_{ly,excess}$, is

$$SW_{ly,excess} = \frac{(1000 * H_0 * \phi_d * L_{hill})}{2} \dots\dots\dots(3.6)$$

where, $SW_{ly,excess}$ is the drainable volume of water stored in the saturated zone of the hill slope per unit area (mm), H_0 is the saturated thickness normal to the hill slope at the outlet expressed as a fraction of the total thickness (mm/mm), ϕ_d is the drainable porosity of the soil (mm/mm), L_{hill} is the hill slope length (m), and 1000 is a factor needed to convert meters to millimeters.

Surface Runoff

Surface runoff, or overland flow, is flow that occurs along a sloping surface. Using daily or sub-daily rainfall amounts, SWAT simulates surface runoff volumes and peak runoff rates for each HRU.

Surface runoff component simulates the surface runoff volume and the peak runoff rates provided daily rainfall data are fed. Surface runoff is computed using a modification of the SCS curve number (USDA Soil Conservation Service, 1972) or the Green & Ampt infiltration method (green and Ampt, 1911). In the curve number method, the curve number varies none linearly with the moisture content of the soil. The curve number drops as the soil approaches the wilting point and increases to near 100 as the soil approaches saturation. The Green & Ampt method requires sub-daily precipitation data and calculates infiltration as a function of the wetting front matric potential and effective hydraulic conductivity. Surface runoff volume predicted in SWAT using SCS curve number method is given below:

$$Q_{surf} = \frac{(R_{day} - 0.2S)^2}{(R_{day} + 0.8S)} \dots\dots\dots(3.7)$$

Where $R > 0.2S$ where, Q_{surf} is the accumulated runoff or rainfall excess (mm), R_{day} is the rainfall depth for the day (mm), and S is retention parameter (mm). Runoff will occur when $R_{day} > 0.2S$. The retention parameter varies spatially due to changes in soils, land use, management and slope and temporally due to changes in soil water content. The retention parameter is defined as

$$S = 25.4 \left(\frac{1000}{CN} - 10 \right) \dots\dots\dots(3.8)$$

Where CN is the curve number for the day.

Peak Runoff Rate

The model calculates the peak runoff rate with a modified rational method. The rational method is based on the assumption that if a rainfall of intensity i begins at time $t = 0$ and continues indefinitely, the rate of runoff will increase until the time of concentration, $t = t_{conc}$, when the entire sub-basin area is contributing to flow at the outlet.

The rational formula is:

$$q_{peak} = \frac{C * i * Area}{3.6} \dots\dots\dots(3.9)$$

Where, q_{peak} is the peak runoff rate (m^3/s), C is the runoff coefficient, i is the rainfall intensity (mm/hr), $Area$ is the sub-basin area (km^2) and 3.6 is a unit conversion factor.

Return Flow

Return flow, or base flow, is the volume of stream flow originating from groundwater. SWAT partitions groundwater into two aquifer systems: a shallow, unconfined aquifer which contributes return flow to streams within the watershed and a deep, confined aquifer which contributes return flow to streams outside the watershed (Arnold et.al., 1993). Water percolating past the bottom of the root zone is partitioned into two fractions—each fraction becomes recharge for one of the aquifers.

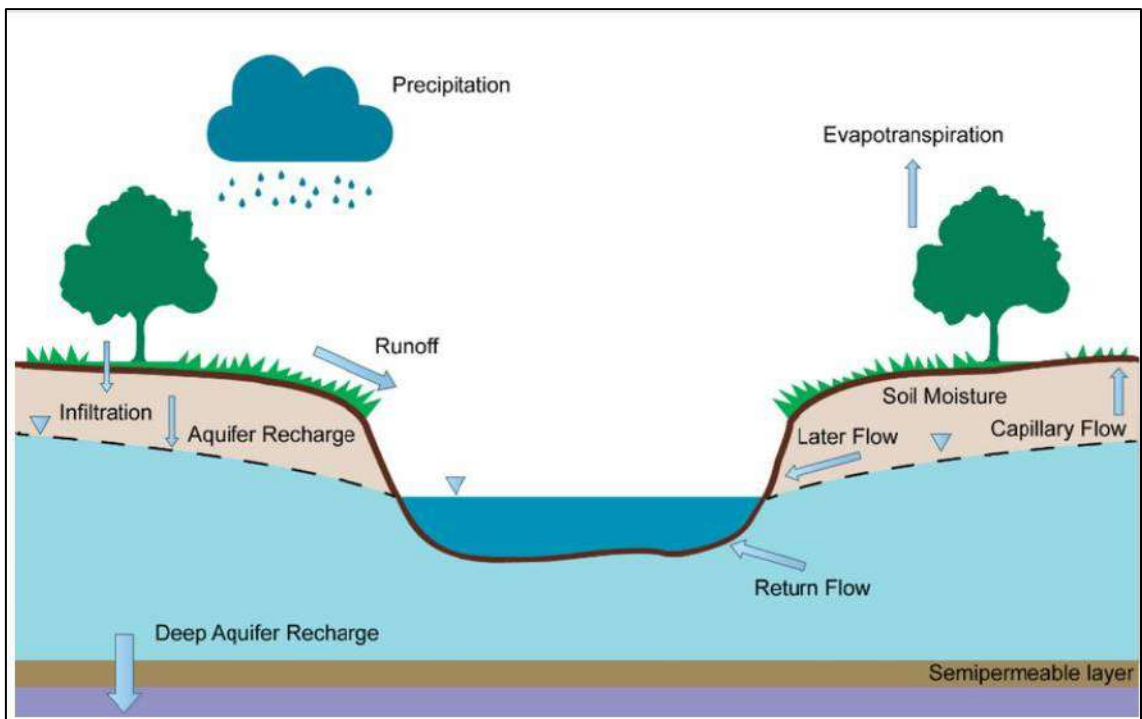


Figure 3.4: Schematic representation of conceptual water balance of the SWAT model
 In addition to return flow, water stored in the shallow aquifer may replenish moisture in the soil profile in very dry conditions or be directly removed by plant. Water in the shallow or deep aquifer may be removed by pumping.

Routing Phase of Hydrologic Cycle

Once swat determines the loading of water, sediment, nutrients and pesticides to the main channel, the loading is routed through the stream network of the watershed using a command structure similar to that of HYMO (Williams and Hann, 1972). Additionally, swat also models the transformation of chemicals in the stream and streambed.

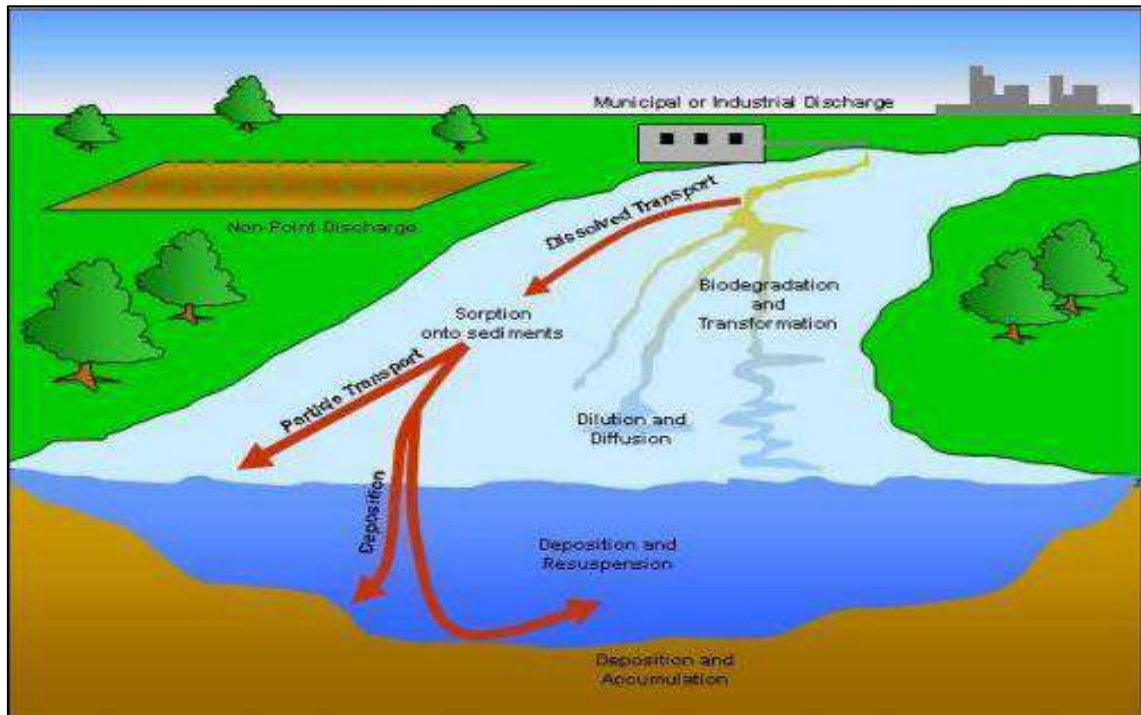


Figure 3.5: In-stream processes modeled by SWAT

Routing in the Main Channel or Reach

As water flows downstream, a portion may be lost due to evaporation and transmission through the bed of the channel. Another potential loss is removal of water for agricultural or human use. Flow may be supplemented by the fall of rainfall or addition of water from point source. In swat flow is routed using variable storage coefficient method developed by Williams (1969) or the Muskingum routing method.

Variable Storage Routing

The variable storage routing method was developed by Williams (1969) and used in the HYMO (William and Hann, 1973) and ROTO (Arnold et.al., 1995) models.

For a given reach segment, storage routing is based on the continuity equation:

$$V_{in} - V_{out} = \Delta V_{stored} \dots\dots\dots(3.10)$$

Where V_{in} is the volume of inflow during the time step ($m^3 H_2O$), V_{out} is the volume of outflow during the time step ($m^3 H_2O$), ΔV_{stored} is the change in volume of storage during time step ($m^3 H_2O$).

After rearranging the equation, it can be written as

$$Q_{out,2} = SC (q_{in,ave} + V_{stored,1}/\Delta t) \dots\dots\dots(3.11)$$

SC is the storage coefficient, $q_{in,ave}$ is the average of $q_{in,1}$ and $q_{in,2}$ where $q_{in,1}$ is the inflow rate at the beginning of the time (m^3/s), $q_{in,2}$ is the inflow rate at the end of the time step (m^3/s), $q_{out,2}$.

Muskingum Routing

The Muskingum method is a commonly used hydrologic routing method in situations requiring a variable storage-discharge relationship (Chow et. al., 1988). The Muskingum method models the storage volume of flooding in a river channel using a combination of wedge and prism storage (see schematic below). The key parameters in Muskingum routing are K (travel time) and X (weighting coefficient). The value of X depends on the shape of the wedge storage to be modeled, and the value of X ranges from 0 for reservoir type storage to 0.5 for a full wedge. In natural streams, X is between 0 and 0.3 with a mean value near 0.2 (Chow et. al., 1988). K is the time required for an incremental flood wave to traverse its reach, and it may be estimated as the observed time of travel of peak flow through the reach (Chow et.al., 1988). If observed inflow and outflow hydrographs are available for a river reach the values of K and X can be determined to provide the best fit (or narrowest loop) relative to the observed flows.

It is necessary to enter a bankfull discharge, Manning's N parameter, slope, length, width, number of segments to represent the reach, an averaging weighting coefficient (X), and weighting coefficient for celerity. The weighting coefficient for celerity is the weight that should be given to the celerity calculated for the bankfull discharge. The weighting coefficient should be between 0 and 1. A weight of 1 uses the bankfull

discharge celerity; a weight of zero uses only the celerity calculated for discharge at 10 percent of bankfull. In any case, the weighted estimate of celerity is used for all routing, regardless of changes in inflow. This differs from variable parameter Muskingum Cunge routing, where the celerity is calculated with each change in flow.

3.4.3 Hydrology

Rainfall Intensity

The rainfall intensity is the average rainfall rate during the time of concentration. Based on this definition, it can be calculated with the equation

$$I = R_{tc} / t_{conc} \dots\dots\dots(3.12)$$

Where I is the rainfall intensity (mm/hr), R_{tc} is the amount of rain falling during the time of concentration (mm H₂O), and t_{conc} is the time of concentration for the sub-basin (hr).

Percolation

Percolation is calculated for each soil layer in the profile. Water is allowed to percolate if the water content exceeds the field capacity water content for that layer and the layer below is not saturated.

The volume of water available for percolation in the soil layer is calculated

$$SW_{ly,access} = SW_{ly} - FC_{ly}; \text{ if } SW_{ly} > FC_{ly} \dots\dots\dots(3.13)$$

$$SW_{ly,access} = 0 \quad ; \text{ if } SW_{ly} < FC_{ly} \dots\dots\dots(3.14)$$

Where $SW_{ly,access}$ is the drainable volume of water on a given day (mm H₂O), SW_{ly} is the water content of the soil layer on a given day (mm H₂O). The amount of water that moves from one layer to the underlying layer is calculated using storage routing methodology.

Lateral Flow

Lateral flow will be significant in areas with soils having high hydraulic conductivities in surface layers and an impermeable semi permeable layer at a shallow depth. In such a system, rainfall will percolate vertically until it encounters the impermeable layer. The water then ponds above the impermeable layer forming a saturated zone of water,

i.e. a perched water table. This saturated zone is the source of water for lateral subsurface flow.

SWAT incorporates a kinematic storage model for subsurface flow developed by Sloan et al., (1983) and summarized by Sloan and Moore (1984). This model simulates subsurface flow in a two-dimensional cross-section along a flow path down a steep hillslope.

This kinematic storage model is represented by the following equation:

$$Q_l = 0.024 \left(\frac{2SW_d \times K_{sat} \times aniso \times S}{\phi_d \times L_h} \right) \dots\dots\dots(3.15)$$

where Q_l is the lateral flow (mm), SW_d is the drainable volume of water in the soil layer (mm), K_{sat} is the saturated hydraulic conductivity (mm/h), $aniso$ is the anisotropic factor, S is the slope (mm/mm), ϕ_d is the drainable porosity of the soil layer (mm/mm), L_h is length of the hill slope (m), and 0.024 is a conversion factor.

Groundwater System

An aquifer whose upper boundary is the water table whereas a confined aquifer is bounded above and below by geologic formations whose hydraulic conductivity are significantly lower than that of the aquifer.

Shallow Aquifer

The water balance for the shallow aquifer is:

$$aq_{sh,i} = aq_{sh,i-1} + W_{rchrg,sh} - Q_{gw} - W_{revap} - W_{pump,sh} \dots\dots\dots(3.16)$$

where $aq_{sh,i}$ is the amount of water stored in the shallow aquifer on day i (mm H₂O), $aq_{sh,i-1}$ is the amount of water stored in the shallow aquifer on day $i-1$ (mm H₂O), $W_{rchrg,sh}$ is the amount of recharge entering the shallow aquifer on day i (mm H₂O), Q_{gw} is the groundwater flow, or base flow, into the main channel on day i (mm H₂O), W_{revap} is the amount of water moving into the soil zone in response to water deficiencies on day i (mm H₂O) and $W_{pump,sh}$ is the amount of water removed from the shallow aquifer by pumping on day i (mm H₂O).

Deep Aquifer

The water balance for the deep aquifer is:

$$a_{q_{dp,i}} = a_{q_{dp,i-1}} + W_{deep} - W_{pump,dp} \quad \dots\dots\dots(3.17)$$

where $a_{q_{dp,i}}$ is the amount of water stored in the deep aquifer on day i (mm H₂O), $a_{q_{dp,i-1}}$ is the amount of water stored in the deep aquifer on day $i-1$ (mm H₂O), W_{deep} is the amount of water percolating from the shallow aquifer into the deep aquifer on day I (mm H₂O), and $W_{pump,dp}$ is the amount of water removed from the deep aquifer by pumping on day i (mm H₂O). If the deep aquifer is specified as the source of irrigation water or water removed for use outside the watershed, the model will allow an amount of water up to the total volume of the deep aquifer to be removed on any given day.

Transmission Loss

Transmission losses are losses of surface flow via leaching through the streambed. This type of loss occurs in ephemeral or intermittent streams where groundwater contribution occurs only at certain time of the year, or not at all. SWAT uses Lane ‘s method described to estimate transmission losses. Transmission losses are estimated with the equation:

$$t_{loss} = K_{ch} * TT * P_{ch} * L_{ch} \quad \dots\dots\dots(3.18)$$

Where, t_{loss} are the channel transmission losses (m³), K_{ch} is the effective hydraulic conductivity of the channel alluvium (mm/hr), P_{ch} is the wetted perimeter (m), and L_{ch} is the channel length (km). Transmission losses from the main channel are assumed to enter bank storage or the deep aquifer.

Evaporation Loss

Evaporation losses from the reach are calculated:

$$E_{ch} = CO_{efev} * E_o * L_{ch} * W * f_r \Delta t \quad \dots\dots\dots(3.19)$$

Where E_{ch} is the evaporation from the reach for the day (m H₂O), CO_{efev} is an evaporation coefficient, E_o is the potential evaporation (mm H₂O), L_{ch} is the channel length (km), W is the channel width at water level (m), and $f_r \Delta t$ is the fraction of the time step in which water is flowing in the channel.

The evaporation coefficient is a calibration parameter for the user and is allowed to vary between 0 and 1. The fraction of the time step in which water is flowing in the channel is calculated by dividing the travel time by the length of the time step.

Bank Storage

The amount of water entering bank storage on a given day is calculated

$$bnk_{in} = t_{loss} \times (1 - fr_{trans}) \dots\dots\dots(3.20)$$

Where bnk_{in} is the amount of water entering bank storage ($m^3 H_2O$), t_{loss} are the channel transmission losses ($m^3 H_2O$), and fr_{trans} is the fraction of transmission losses portioned to the deep aquifer.

Bank storage contributes flow to the main channel or reaches within the sub-basin. Bank flow is simulated with a recession curve similar to that used for groundwater. The volume entering the reach from bank storage is calculated

$$V_{bnk} = bnk \times (1 - \exp[-\alpha_{bnk}]) \dots\dots\dots(3.21)$$

Where V_{bnk} is the volume of water added to the reach via return flow from bank storage ($m^3 H_2O$), bnk is the total amount of water in bank storage ($m^3 H_2O$), and α_{bnk} is the bank flow recession constant or constant of proportionality.

Channel Water Balance

Water storage in the reach at the end of the time step is calculated

$$V_{stored,2} = V_{stored,1} + V_{in} - V_{out} - t_{loss} - E_{ch} + div + V_{bnk} \dots\dots\dots(3.22)$$

Where $V_{stored,2}$ is the volume of water in the reach at the end of the time step ($m^3 H_2O$), $V_{stored,1}$ is the volume of water in the reach at the beginning of the time step ($m^3 H_2O$), V_{in} is the volume of water flowing into the reach during the time step ($m^3 H_2O$), V_{out} is the volume of water flowing out of the reach during the time step ($m^3 H_2O$), t_{loss} is the volume of water lost from the reach via transmission through the bed ($m^3 H_2O$), E_{ch} is the evaporation from the reach for the day ($m^3 H_2O$), div is the volume of water added or removed from the reach for the day through diversions ($m^3 H_2O$), and V_{bnk} is the volume of water added to the reach via return flow from bank storage ($m^3 H_2O$).

3.4.4 Advantages of Using SWAT Model

The main advantage of SWAT is the capability to run simulations for large watersheds without extensive monitoring data and the capacity to predict changes in hydrological parameters under different management practices and physical environmental factors (Gassman et al., 2007; Daloglu et al., 2014). Some advantages of SWAT model had given below:

- Physically based.
- Requires generally available information as input.
- Computationally efficient.
- Capable of being used on un-gauged watersheds.
- Enables users to study long-term impact.

3.5 Model Calibration and Validation

Calibration

Calibration means adjustment of the model parameters so that simulated and observed data will match within the desired accuracy. Model parameters may require adjustment due to a number of reasons. There are numerous parameters in hydrological models which can be classified as physical parameters (i.e. parameters that can be physically measurable from the properties of watershed) and process parameters (i.e, parameters represent properties which are not directly measurable) (Sorooshian and Gupta, 1995). In reality, all models require some degree of calibration to fine tune the predictive ability of the model. After some test simulations it was clear that four parameters had greater influence on the shape and magnitude of the output hydrographs. They are:

SCS Curve Number Calculation

SCS (Soil Conservation Service) Curve Number (CN) is an empirical parameter used or predicting direct runoff or infiltration from rainfall excess. There are actually two ways that the program can calculate the surface runoff, one is the SCS Curve number method (1972) the other is the Green & Ampt infiltration method (1911). However, the Green & Ampt infiltration method requires sub daily in precipitation data which is very hard to get. That is why SCS curve number method of surface runoff calculation was used. The main parameter for the curve number calculation is CN2 which is the initial

SCS runoff curve number for moisture condition II. The SCS CN is function of the soil's permeability, land use and antecedent soil water condition. The CN has a range from 30 to 100. Lower numbers indicate low runoff potential while larger numbers are for increasing runoff potential. So, the lower the curve number, the more permeable the soil is. It is worth mentioning that the CN2 parameter is highly sensitive. With the slightest change of this parameter the SWAT model completely changes the simulated runoff magnitude. Initially the SWAT model assigns a CN2 value based on the soil data and land use pattern but more often than not a user needs to change this value for better calibration. The default value of CN2 is 60-95, so only minor changes from the initial value of CN2 was required for model calibration.

Ground Water Delay Time

The ground water delay time parameter of the SWAT model actually represents the lag time between the times that the water exits the soil profile and enters the shallow aquifer. This parameter cannot be directly measured but will mainly depend on the depth of the water table and the hydraulic properties of the geologic formation in the vadose (region of aeration above the water table) and ground water zones. In terms of model behavior, increasing the ground water delay time actually increases the base flow of the model and generates more flow in the dry periods, damping out the hydrograph a lot. While the default value is 31 days, during the calibration process, the value of Ground Water Delay time was chosen as 32 Days.

Baseflow recession constant

The baseflow recession constant is a direct index of ground water flow response to change in charge (Smedema and Rycroft, 1983). The value may vary from 0.1 to 0.3 with slow response to recharge and from 0.9-1 for land with rapid response. Although the baseflow recession constant may be calculated, it requires a lot of data on baseflow contribution into the main channel as well as data of recharge rate of shallow aquifer and storage of the shallow aquifer. Thus, it will be a very hard job to calculate the baseflow recession constant. In the swat model environment, the baseflow recession constant has a significant effect on the shape of the hydrograph. The default value of the parameter was set to 0.048 which represent a very slow responding soil. Increasing the base flow recession constant will make the slope of the hydrograph a lot steeper,

meaning that peaks will be reached faster and the recession limb of the hydrograph will also be a lot steeper hence meaning quicker drainage. The default value of baseflow recession constant.

Ground water Revap

Water may move from the shallow aquifer into the overlying unsaturated zone. In periods when the material overlying the aquifer is dry, water in the capillary fringe that separate the saturated and unsaturated zone will evaporate and diffuse upward. As this water gets removed, more water from the underlying aquifer will replace the evaporated one. This process is modeled by SWAT using the “GW_REVAP” parameter. The default value of GW_REVAP 0.02 was taken during calibration.

Validation

Validation is the process of determining the degree to which a model or simulation is an accurate representation of the real world from the perspective of the intended uses of the model or simulation. Once the model parameters have been finalized during calibration process, the model is simulated with that set of parameters for a different time frame to see the model’s performance. If the model performs well in predicting the output for the different timeframe it can be said to be validated. Calibration is generally done with the latest available data series. But it is not necessary to calibrate the model with latest data. After finalizing the parameters, the model was simulated for the entire time frame and simulation period was chosen as the validation period for the model. In calibration and validation stage of the model, the performance of the model is evaluated both statistically as well as graphically. The model generated mean monthly discharge and observed mean monthly discharge at the desire outlet.

3.6 Model Performance Evaluation

Statistically the performance of the model has been evaluated using the Nash-Sutcliffe Efficiency value (NSE), the coefficient of determination (proportion of the variance in the observations explained by the model, R^2), percent bias (PBIAS) and the ration of the root mean square error between the simulated and the observed values to the standard deviation of the observations (RSR) Moriasi et al., (2007) and Krauseet et al., (2005).

R² (Coefficient of determination)

R² estimates the combined dispersion against the single dispersion of the observed and predicted series and provides the relationship strength between observed and simulated values. Its value ranges from 0 to 1; a value close to 0 means very low correlation whereas a value close to 1 represents high correlation between observed and simulated discharge.

$$R^2 = \frac{\left[\sum_{i=1}^n (Q_i - \bar{Q}_i) \cdot (Q'_i - \bar{Q}'_i) \right]^2}{\sum_{i=1}^n (Q_i - \bar{Q}_i)^2 \cdot \sum_{i=1}^n (Q'_i - \bar{Q}'_i)^2} \dots\dots\dots(3.23)$$

NSE (Nash–Sutcliffe efficiency)

NSE determines the relative magnitude of the residual variance compared to that of the measured data (Moriassi et al., 2007) and is one of the most widely used statistical indicators for hydrological model performance (Shrestha et al., 2013). Its value ranges from ∞ to 1, where 1 indicates a perfect model and a value of less than 0 indicates that the mean value of the observed time series would have been a better predictor than the model.

$$NSE = 1 - \frac{\sum_{i=1}^n (Q_i - Q'_i)^2}{\sum_{i=1}^n (Q_i - \bar{Q}_i)^2} \dots\dots\dots(3.24)$$

PBIAS (Percentage bias)

PBIAS indicates the average tendency of the simulated results to be greater or larger than their observed data. It measures the difference between the simulated and observed quantity and its optimum value is 0. The positive value of the model represents underestimation whereas negative value represents overestimation.

$$PBIAS = \frac{\sum_{i=1}^n (Q_i - Q'_i)^2}{\sum_{i=1}^n Q_i} * 100 \dots\dots\dots(3.25)$$

RSR (RMSE-observation standard deviation ratio)

The lower value of RMSE (root mean square error) is commonly acceptable and one of the widely used error parameters. However, the satisfactory threshold of RMSE

is case specific. Therefore, RSR is chosen as a complementary indicator to RMSE. The optimum value of RSR is 0 and higher value indicates lower model performance.

$$RSR = \frac{RMSE}{STDEV_{obs}} = \frac{\sqrt{\sum_{i=1}^n (Q_i - Q'_i)^2 / n}}{\sqrt{\sum_{i=1}^n (Q_i - \bar{Q}_i)^2 / n}} \dots\dots\dots(3.26)$$

The threshold value of goodness-of-fit for all models was based on Moriasi et al., (2007), as shown in Table 3.3.

Table 3.3: Model performance rating.

| Performance rating | NSE | PBIAS | RSR |
|---------------------------|-------------|--------------|------------|
| Very good | 0.75 | <±10 | 0 to 0.5 |
| Good | 0.65-0.75 | ± 10 to ± 15 | 0.5 to 0.6 |
| Acceptable | 0.5 to 0.65 | 15 to ±25 | 0.6 to 0.7 |
| Unsatisfactory | <0.5 | >±25 | > 0.7 |

Source: Moriasi et al., (2007).

3.7 Climate Change Modeling based on General Circulation Models (GCM)

Development of General Circulation Models (GCMs) is one of the most prominent climate change research advancements starting from the early 1990s onwards, and they are the most advanced tools currently available for simulating the response of the global climate system to changing atmospheric composition (e.g. increase in atmospheric CO₂ on the mean global climate) (IPCC, 2001; Shackley et. al., 1998). GCMs are numerical atmospheric model coupled with three-dimensional dynamic ocean models, together with complex land surface schemes and sea ice models, and can provide considerable potential for the study of climate change and variability (Fowler et.al., 2007; Shackley et. al., 1998). GCMs used to solve equations describing the movement of energy and momentum, along with the conservation of mass at discrete points on the entire surface of the Earth, at a fixed time interval, and for separate layers in the atmosphere defined by a regular grid (Wilby, 2009).

Initially atmospheric General Circulation Models (GCMs) were run to equilibrium under current (1xCO₂) and doubled (2xCO₂) emissions forcing to estimate their potential effect on global climate. After being coupled with Oceanic Circulation Models, these GCMs are forced with transient greenhouse emissions to allow for the

estimation of the rate at which climate changes might occur. Table 3.4 shows different GCMs available, their institution and resolutions.

Table 3.4: Spatial Resolution of different GCMs in IPCC TAR and AR5

| | Model | Institution | Resolution Lat x Long | Reference |
|----|-------------------|---|----------------------------------|---|
| 1 | BCC-CSM 1.1 | Beijing Climate Center, China Meteorological | 2.8125 x 2.8125 | Wu, T., 2012 |
| 2 | BCC-CSM 1.1(m) | Beijing Climate Center, China Meteorological Administration | 2.8125 x 2.8125 | Wu, T., 2012 |
| 3 | CSIRO- Mk3.6.0 | Commonwealth Scientific and Industrial Research Organization and the Queensland Climate Change Centre of Excellence | 1.875 x 1.875 | Collier, M.A.et. al., 2011 |
| 4 | FIO-ESM | The First Institute of Oceanography | 2.812 x 2.812 | Song, Z., Qiao, F., Song, Y. |
| 5 | GFDL-CM3 | Geophysical Fluid Dynamics Laboratory | 2.0 x 2.5 | Donner, L.J.et. al., 2011 |
| 6 | GFDL- ESM2G | Geophysical Fluid Dynamics Laboratory | 2.0 x 2.5 | Dunne, J.P.et. al., 2012 |
| 7 | GFDL- ESM2M | Geophysical Fluid Dynamics Laboratory | 2.0 x 2.5 | Dunne, J.P.et. al., 2012 |
| 8 | GISS-E2-H | NASA Goddard Institute for Space Studies | 2.0 x 2.5 | Schmidt, G.A. et. al., 2006. |
| 9 | GISS-E2-R | NASA Goddard Institute for Space Studies | 2.0 x 2.5 | Schmidt, G.A. et. al., 2006 |
| 10 | HadGEM2- ES | Met Office Hadley Centre | 1.2414 x 1.875 | Collins, W.J.et. al.(2011) |
| 11 | IPSL-CM5A- LR | Institute Pierre-Simon Laplace | 1.875 x 3.75 | Dufresne, J.L.et. al., 2013 |
| 12 | IPSL-CM5A- MR | Institute Pierre-Simon Laplace | 1.2587 x 2.5 | Dufresne, J.L.et. al., 2013 |
| 13 | MIROC-ESM | Atmosphere and Ocean Research Institute (The University of Tokyo), National Institute for Environmental Studies, and Japan Agency for Marine- Earth Science and | 2.8125 x 2.8125 | Watanabe, S.et. al., 2011 |
| 16 | MRI-CGCM3 | Meteorological Research Institute | 1.125 x 1.125 | Yukimoto, S., 2012 |
| 17 | NorESM1-M | Norwegian Climate Centre | 1.875 x 2.5 | Kirkevag, A., Iversen, T., Seland, O., debernard,J.B., Storelvmo, T., Kristjansson, J.E.,2008 |

Source: IPCC, 2013.

3.7.1 Climate Change Scenarios

The new scenarios are called Representative Concentration Pathways (RCPs). There are four pathways: RCP8.5, RCP6, RCP4.5 and RCP2.6. According to van Vuuren (2011a)-

“Two important characteristics of RCPs are reflected in their names. The word “representative” signifies that each of the RCPs represents a larger set of scenarios in the literature. In fact, as a set, the RCPs should be compatible with the full range of emissions scenarios available in the current scientific literature, with and without climate policy. The words “concentration pathway” are meant to emphasize that these RCPs are not the final new, fully integrated scenarios (i.e. they are not a complete package of socio-economic, emission and climate projections), but instead are internally consistent sets of projections of the components of radiative forcing that are used in subsequent phases.

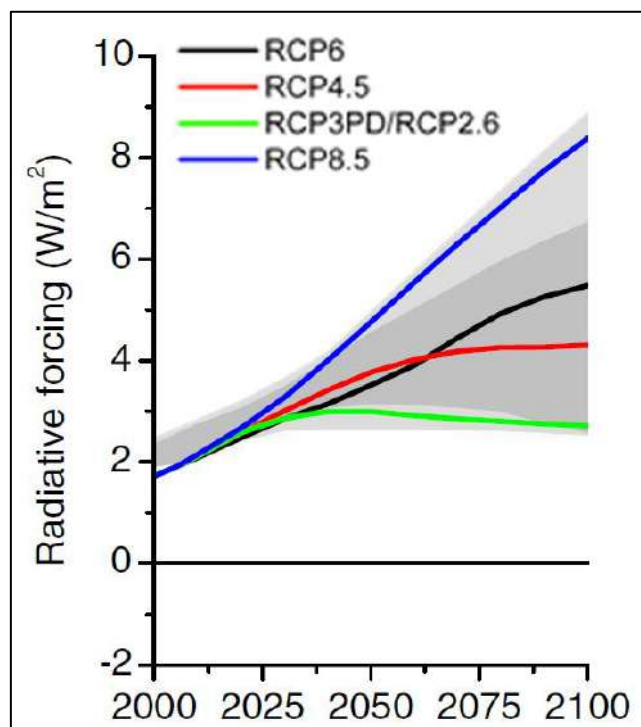


Figure 3.6: Total RF (anthropogenic plus natural) for RCPs and extended concentration pathways (ECP)—for RCP2.6, RCP4.5, and RCP6, RCP8.5 (Source: IPCC, 2013)

The use of the word “concentration” instead of “emissions” also emphasizes that concentrations are used as the primary product of the RCPs, designed as input to climate models. Coupled carbon-cycle climate models can then as well calculate associated emission levels (Hibbard et.al., 2007). In total, a set of four pathways were

produced that lead to radiative forcing levels of 8.5, 6, 4.5 and 2.6 W/m², by the end of the century. Each of the RCPs covers the 1850–2100 period.

Table 3.5: Overview of Representative Concentration Pathways (RCPs) adopted by IPCC AR5.

| RCP | Description | IA Model | Publication – IA Model |
|------------|---|-----------------|---|
| RCP 8.5 | Rising radiative forcing pathway leading to 8.5 W/m ² in 2100. | MESSAGE | Riahi et al. (2007), Rao & Riahi (2006) |
| RCP 6 | Stabilization without overshoot pathway to 6 W/m ² at stabilization after 2100 | AIM | Fujino et al. (2006), Hijioka et al. (2008) |
| RCP 4.5 | Stabilization without overshoot pathway to 4.5 W/m ² at stabilization after 2100 | GCAM (MiniCAM) | Smith and Wigley (2006), Clarke et al. (2007) |
| RCP 2.6 | Peak in radiative forcing at ~ 3 W/m ² before 2100 and decline | IMAGE | van Vuuren et al. (2006; 2007) |

Source: IPCC-AR5.

Emissions and concentrations, forcing and temperature anomalies Each Representative Concentration Pathway (RCP) defines a specific emissions trajectory and subsequent radiative forcing (a radiative forcing is a measure of the influence a factor has in altering the balance of incoming and outgoing energy in the Earth atmosphere system, measured in watts per square meter).

3.8 Summary

Theoretical background of a model has been very important for a research study. It is essential to gather knowledge about how the model simulation is done. It is also necessary to know about the background equation of the model. If the theoretical background is clear then the proper utilization of the model has done. In this chapter background theory of this study have been reviewed.

CHAPTER 4

STUDY AREA AND METHODOLOGY

4.1 General

In this chapter, methodology of this study had described in detail. In this study, the whole Ganges basin has been set up with SWAT hydrology model. For this purpose, SWAT model has been set up over the Ganges Basin using Digital Elevation Model (DEM), land use pattern, soil distribution, climate data and flow time series were collected to setup a hydrological model using SWAT. For proper planning and efficient utilization of the land and water resources, it is necessary to understand the hydrological cycle and estimate the hydrological parameters.

4.2 Methodology of the Study

Assessment of climate and land use change impact on the water flow any river basin using hydrological model involves several steps. Steps followed in the present research can be described as following:

Step 1-Data Collection: This includes DEM, land use pattern, soil distribution, climate data and flow time series.

Step 2-Model Setup: Model setup which includes watershed delineation, weather data setup, HRU definition and selection of calculation methods.

Step 3-Sensitivity Analysis, Calibration and validation of model: Sensitivity analysis of the calibration parameters, calibration using the selected parameters, validation of the model by comparing available observed discharge with simulated hydrograph at Hardinge Bridge transit (SW90) and evaluate the performance of hydrologic model.

Step 4-Scenario development: Selection of scenarios for climate change and land use change impact assessment.

Step 5- Climate and Land Use Change Impact Assessment: Run the model with GCMs data and analyzed the impact of climate change on the flow of Ganges River Basin. Assessment on flow due to changing pattern of land use (urbanization and deforestation) of Ganges River Basin.

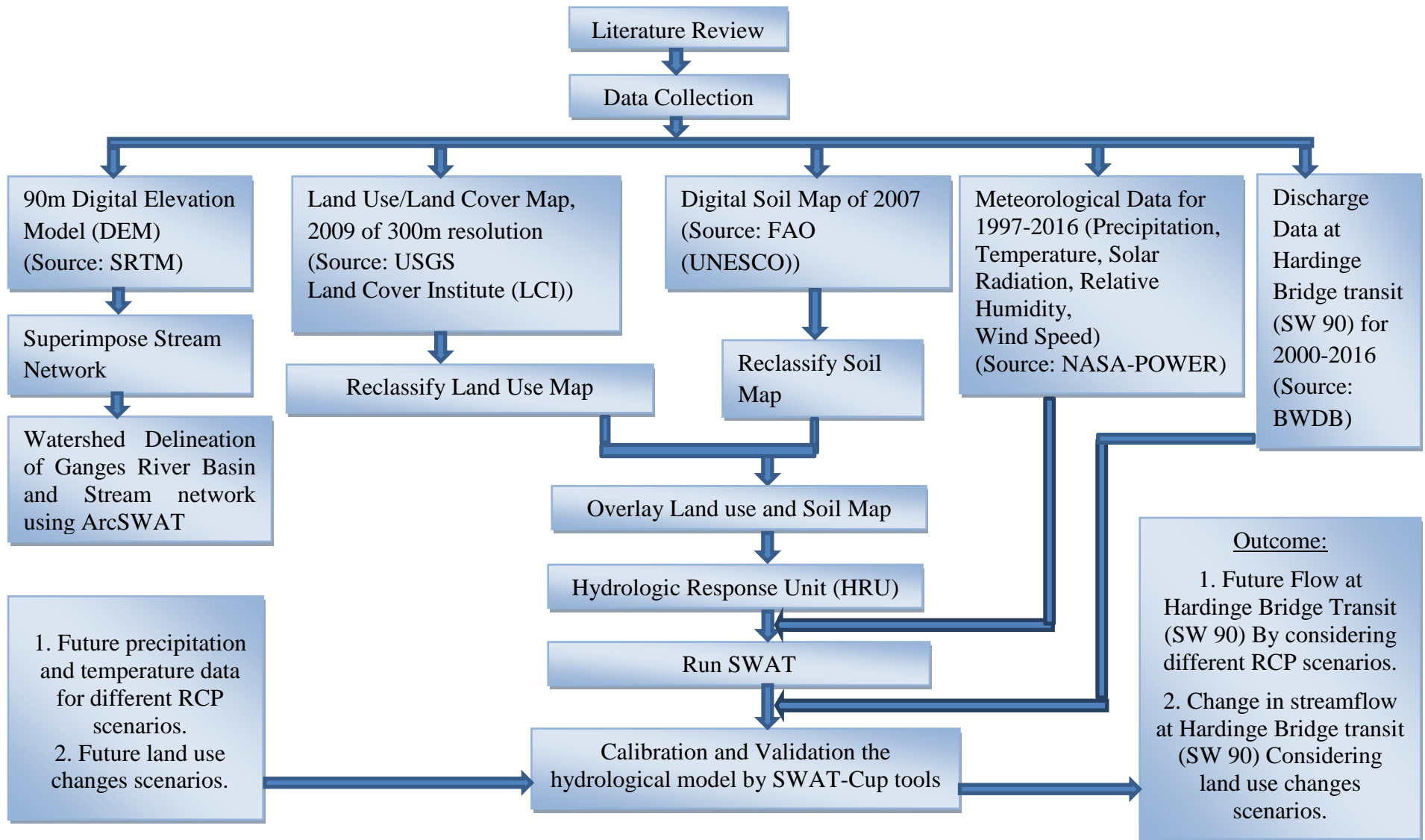


Figure 4.1: Methodology of the Study

4.3 Study Area

Ganges River originates at an elevation about 3892m above mean sea level (MSL) at Gangotri Glacier in the central Himalayas at Uttarakhand, India (Bhutiani, 2014). It traverses through 2,510 km in India and Bangladesh before draining into the Bay of Bengal. The total catchment area of the river is 1,086,000 sq. km (between 73° to 88° East and 22° to 32° North). 79% of the catchment area lies in India, 14% is in Nepal, 4% is in Bangladesh, and 3% is in China. (Gosain et. al., 2015).

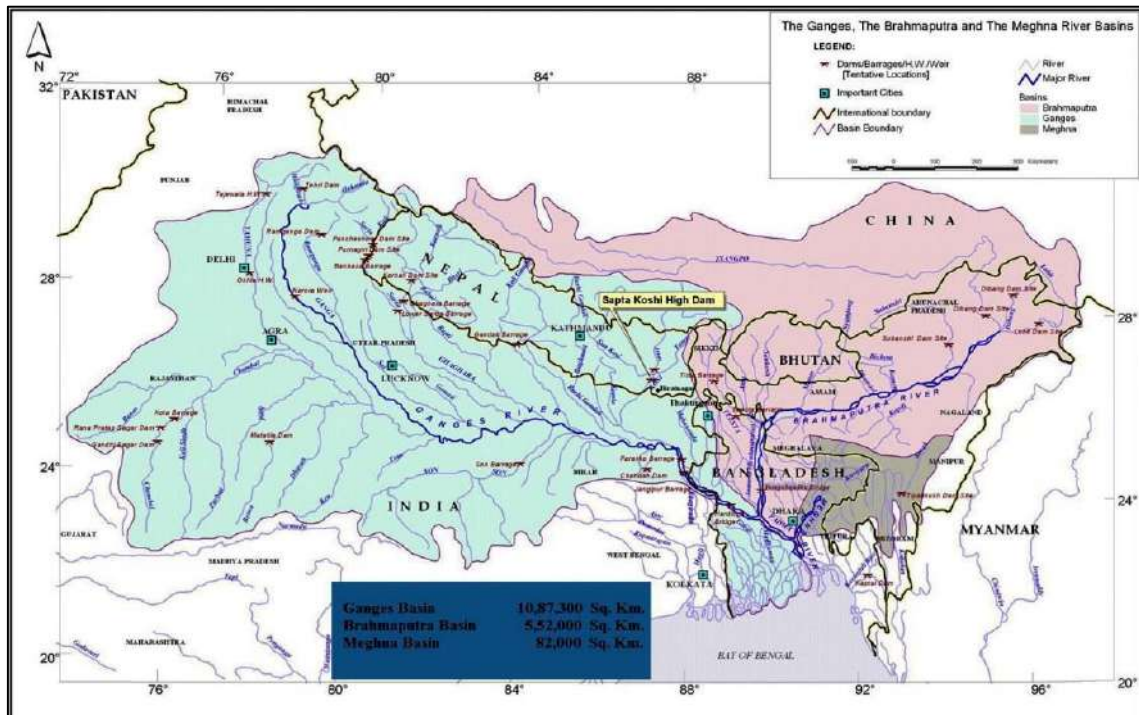


Figure 4.2: Ganges River Basin in GBM basins (JRCB, 2018)

The important tributaries of Ganges River are Yamuna, Ramganga, Gomti, Ghagra, Sone, Gandak, Burhi Gandak, Kosi, Mahananda and the important distributaries are Hugli, Gorai-Modhumati, Mathabhanga and Arial Khan river. The river divides into two arms namely the Ganges which flows through Bangladesh and the Hugli which flows through West Bengal at Farakka point in West Bengal. Farakka barrage is located roughly 16.5 km upstream from the border with Bangladesh near Chapai Nawabganj district. At Farakka barrage; a major diversion delivers water from the Ganges into the Hooghly River providing water to West Bengal and Kolkata. Approximately 50 percent of flows are diverted except during high flows ($>1133 \text{ m}^3/\text{s}$), (Begum, 1987) with the exact diversions varying depending on inflows and season. After passed through Farakka Barrage, Ganges River enters into Bangladesh and meet with Brahmaputra and Meghna River to fall into the Bay of Bengal.

4.3.1 Topography

The headwaters of the Ganges River begin high in the Himalayan Mountains where the Bhagirathi River flows out of the Gangotri Glacier in India's Uttarakhand state (Sandeep, 2018). The Ganges River proper begins farther downstream where the Bhagirathi and Alaknanda rivers join. In Uttar Pradesh the river Ganges flows over the fertile plains and receives the Ramganga before touching Allahabad (Sundariyal et al. 2007).



Figure 4.3: Topography of Ganges River Basin (Source: Riccardo, 2015)

At Allahabad, it is joined by the Yamuna on its right bank. The Chambal, the Betwa and the Ken are the principal streams flowing into the Yamuna and they drain considerable areas of Madhya Pradesh. After Allahabad, the river sweeps for another 245km to Vanarasi and receives the Tons from the south. The Gomti joins it immediately below Vanarasi. The total length of the Ganges River from its source to its outfall into the sea is measured along the Bhagirathi and the Hooghly is 2525 km of which 1450 km lie in Uttar Pradesh, 110 km along the U.P.-Bihar border, 445 km in Bihar and 520 km in West Bengal (Balasubramanian, 2017).

The Ganges flows approximately in the direction of north-west to south-east. The Ganges basin is roughly rectangular in shape, the width in the western end, where the Yamuna and the Chambal originate from the north and south respectively, being more. The plateau at the Central India forms the southern basin boundary. The width of the basin is narrowest at the Rajmahal Hills near Bihar-West Bengal border, where the Ganges River takes a turn towards south.

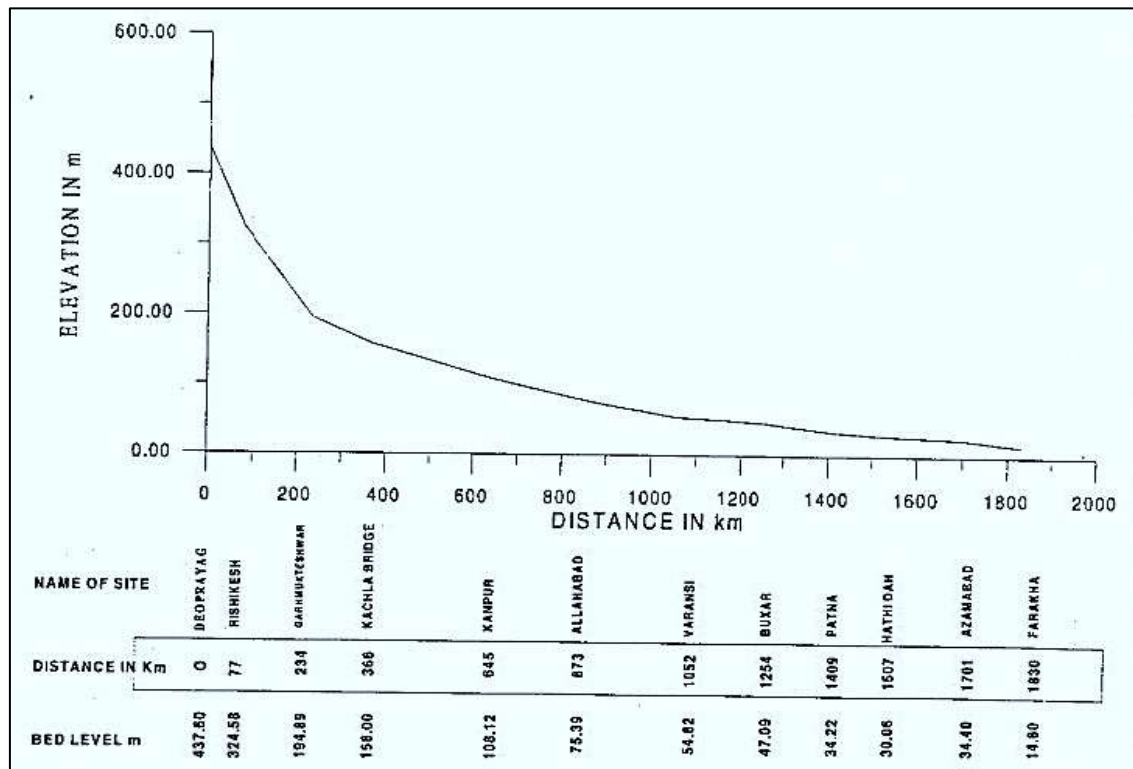


Figure 4.4: The longitudinal section of its course of flow upto Farakka (Source: Hydrological inventory of River basin by NIH 1998-1999)

The delta of the Ganges starts downstream of this turning, where the river bifurcates, one arm bearing the name of the Padma, flows through Bangladesh on its way to the sea and other bearing the name of the Bhagirathi flows through West Bengal to the sea. Once the Ganges River flows out of India and into Bangladesh, its main branch is known as the Padma River. The Padma River is joined downstream by large rivers like the Jamuna and Meghna rivers. After joining the Meghna, it takes on that name before flowing into the Bay of Bengal. A significant portion of the discharge from the Ganges comes from the Himalayan mountain system. Within the Himalaya, the Ganges basin spreads almost 1,200 km from the Yamuna-Satluj divide along the Simla ridge forming the boundary with the Indus basin in the west to the Singalila Ridge along the Nepal-Sikkim border forming the boundary with the Brahmaputra basin in the east (Krishnan S. V. et. al., 2020).

The Himalayan portion of the basin includes the south-eastern portion of the state of Himachal Pradesh, the entire state of Uttarakhand, the entire country of Nepal and the extreme north-western portion of the state of West Bengal. In the western reaches of the basin, tributaries flow south from the Himalaya and north from the Deccan Plateau to form the main stem of the Ganges. The Deccan Plateau in the south of the basin is generally low elevation with hills up to 1,200 meters punctuated by rocky outcrops. The eastern part of the basin is a flat delta characterized by the extensive and delicate Sundarbans mangrove systems. The total area of the basin is estimated at 1 million square kilometers, 4 covering all of Nepal, over a third of the land area of Bangladesh, and nearly half of India (Pandey, 2016).

4.3.2 Flow Regime

The Ganges River is primarily a meandering channel (Coleman, 1969). While in India, the Ganges bifurcates into two Distributaries: The Hooghly River, which flows south through Calcutta into the Bay of Bengal, and the Ganges River which flows east into Bangladesh and is considered the Continuation of the main Ganges channel (Islam et al., 1999).

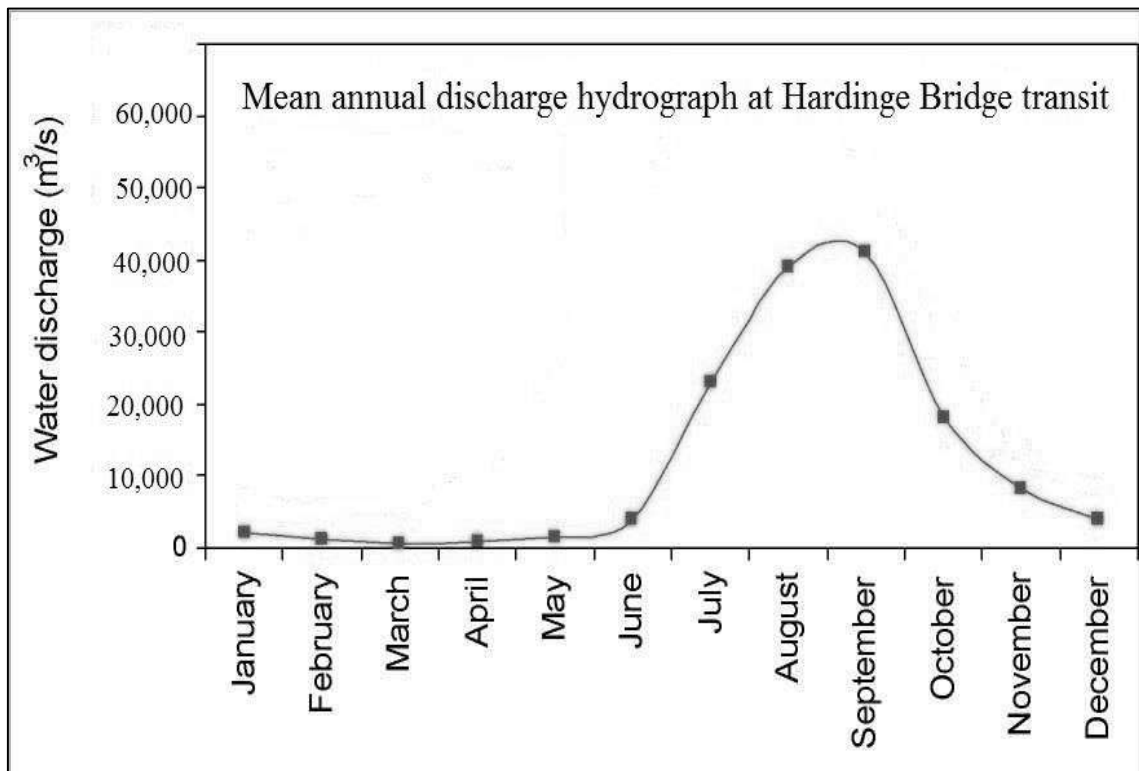


Figure 4.5: Mean annual discharge hydrograph of the Ganges River at Hardinge Bridge transit from 1990 to 2003 (Stephanie, 2007)

From source to sea, the Ganges flows approximately 2500 km and has a 34,188 km² drainage basin of total area lie within Bangladesh's borders (Islam et al., 1999). As shown in Figure 4.3, dry-season water discharge is approximately 5,000m³/s, while average maximum discharge is approximately 40,000m³/s (Coleman, 1969).

The rising stage occurs rapidly over the monsoon season, when the discharge increases from the yearly base-level in June to the yearly maximum in August. The maximum discharge in these rivers is observed during monsoon months (June to September). More than 75% of the annual rainfall occurs in monsoon months of June to September. The average annual discharge of the Ganges River is 16,650 m³/s. The average annual flow of Ganges River at Farraka is about 525×10⁵ Mm³. At Goalundo, the average annual flow of the Ganges River is 11,470 m³/s (Jain et al., 2009). The maximum and minimum flow at this site is 58,180 ft³/s and 32623 ft³/s (Mirza, 2014). The peak flow at Farakka in 1971 was estimated at 70,500 m³/s (Begum, 1987). The Figure 2.3 shows the mean annual hydrograph of the river at Hardinge bridge point which is prepared from the daily discharge data from 1990 to 2003 (Stephanie, 2007). Such a big variation of the discharge may be one of the causes of heavy dynamicity of the river.

4.3.3 Land Use Classes

Land use is a description of how people utilize the land and socio-economic activity. Land use is the physical material at the surface of the earth. Land covers include grass, asphalt, trees, bare ground, water, etc. This basin holds a variety of land use classes. The major part of basin is covered with agriculture accounting to 65.57% (Revenga et al., 1998). The states falling under Ganges River Basin are extensively cultivated, constituting approximately about 40% of the total area of the India. The land being the chief resources has been subject to misuses which have resulted into several land and associated problems. The overgrazing and deforestation in most areas have led to soil erosion and ravine formation on the one hand and have accentuated flooding on the other.

For example, the Yamunanagar district in Haryana has been subjected to severe ravine-formation, particularly by the Yamuna and the Chambal. Also land not available for cultivation and fallow land class covers a considerable area of the basin. This category of land consists of tracts which cannot be put to agricultural or silvicultural uses at an economic level due to their unproductive nature, as well all lands put to various other

economic uses, such as mineral exploitation or construction of human settlements, industrial structures, roads, railways, airports and other civil works needed for providing transport, communication and similar infrastructural facilities for human habitation.

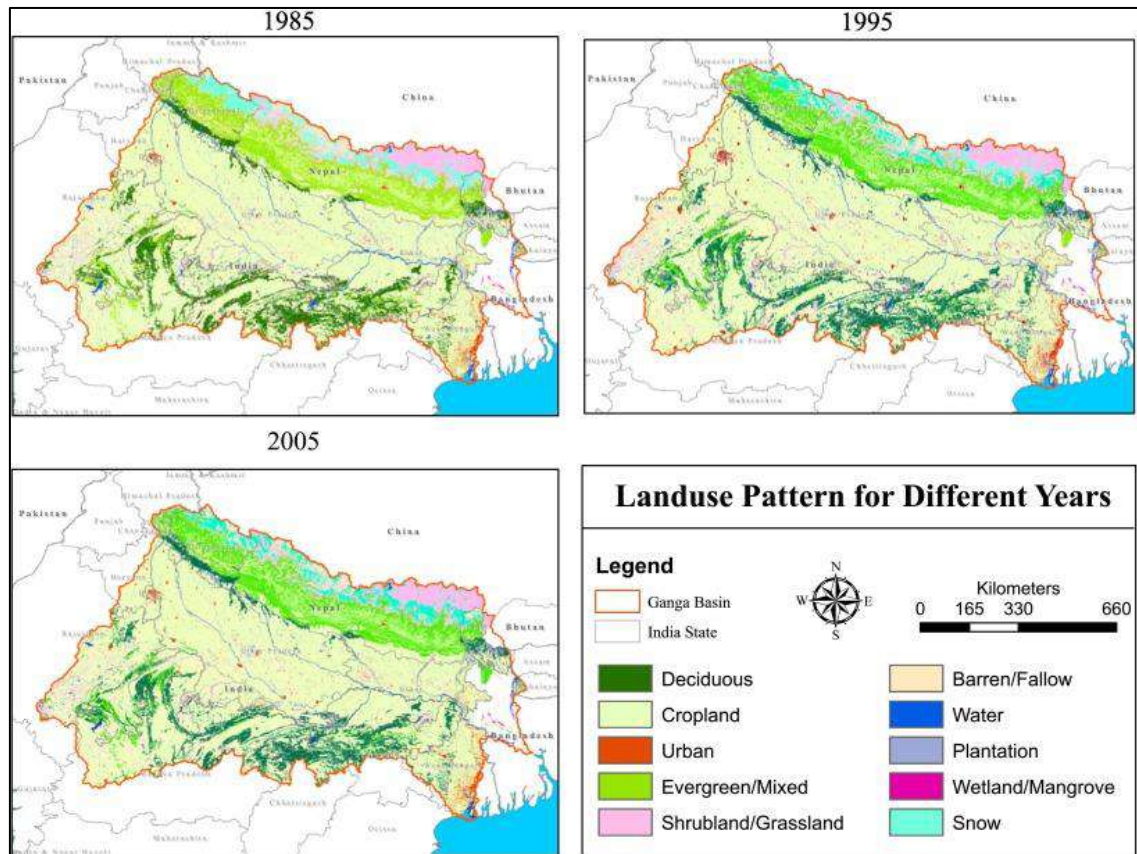


Figure 4.6: Landuse pattern for different years on Ganges River Basin (Source: Anand et al., 2018)

A proportion of the Ganges basin comprises of the non-arable land that is used in urbanization and in construction of homesteads in rural areas which is one of the thickly populated. The states falling under Ganges basin have only 16.6% of total land areas covered by forest, as compared to India as a whole which has 21.2% of land under forest cover (India-WRIS). In some states, especially Haryana, Delhi, Bihar, Uttar Pradesh, Rajasthan and West Bengal, the forest cover is as low as 0.1 to 13.2 percent of the geographical area. Most of forest tracts within the Ganges basin are severely degraded on account of over exploitation. As a result, the forest ecosystem in the Ganges basin is under severe stress. Even in the states of Uttarakhand (64.7 %), Madhya Pradesh (28.2 %) and Himachal Pradesh (19.8 %) where the forest cover is higher (Uppgupta S. et. al., 2015), the proportion of land actually under dense tree cover

within the government forest tracts is very low due to extensive clear felling of trees carried out in recent decades.

4.3.4 Climate of Ganges Basin

The Ganges basin receives nearly 1,000 mm of precipitation annually. The distribution of the average June through October precipitation climatology (mm/mon) shows a band of accumulated high precipitation over 250 mm/mon. The Eastern part of the Ganges basin up to 80°E experiences moderate precipitation between 100- and 250-mm/mon, while west of 80°E is generally semiarid to arid with less than 100 mm mon⁻¹ of June through October precipitation. The greatest amount of rain – 84% of the annual total – falls during the monsoon season. Of the remainder, 7% falls during the pre-monsoon season, 5% in the post-monsoon season, and 4% in winter. There are some differences in precipitation between the upper and lower Ganges basins. Although there is not much difference between the annual amount of precipitation in the lower and upper parts of the basin, the number of rainy days varies considerably. In the upper basin, there are 179 rainy days, whereas in the lower basin there are 152 rainy days.



Figure 4.7: Monthly average precipitation of Ganges River Basin for normal period (Source: Riccardo, 2015)

The monsoon season accounts for 75% of the rain in the upper basin and 85% of the rain in the lower basin. For both the upper and lower basins, the number of rainy days is increasing, but the occurrence of rainfall greater than 10 mm/day is decreasing. The monsoon season shows a slight decreasing trend across the basin (although the trend is statistically insignificant, the amount may be significant). There is also an increasing trend in the duration of the monsoon season, with more dry spells within each season.

During the winter season, there is an increasing trend in rainfall over most parts of the basin, and a decreasing trend in the central, southwest and extreme north of the basin. Over the past decades and across the Ganges basin, winters are getting warmer, but summer average temperatures have remained constant. Summer extremes are becoming more intense, while winter extremes are showing mixed trends across the basin. The average maximum temperature across the basin is 30.3°C in summer and 21.1°C in winter. The average minimum temperature across the basin is 21.5°C in summer and 6.4°C in winter. The pre-monsoon season is the hottest in the Ganges basin with an average temperature of 31.4°C, with June being the hottest month in the upper basin and May the hottest in the lower basin. The coldest month is January across the whole basin. Over the last decades, there has been no significant trend in terms of changes in maximum temperatures, but there has been an increase in minimum temperatures in every season across the Ganges basin, with as much as 0.7°C increase in winter minimum temperature. Night-time temperatures are also showing an increasing trend. Extreme high temperatures (highest maximum) are generally increasing across the basin. Extreme low temperatures are rising (getting warmer) in most parts of the basin with more severity over the central part of the basin, while in the northern-most part temperatures are decreasing (getting colder).

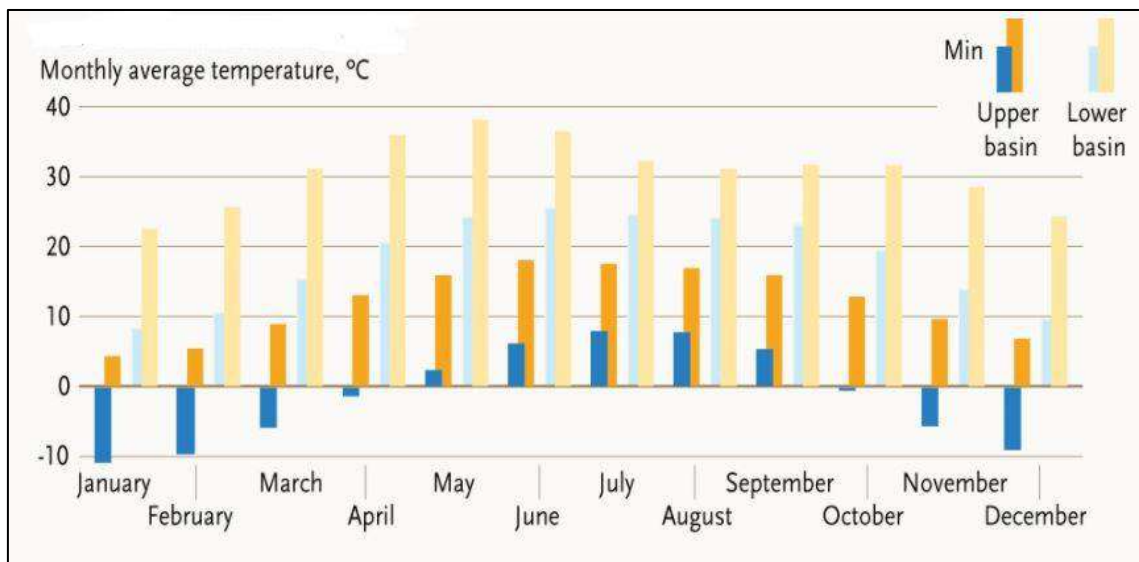


Figure 4.8: Monthly average temperature of Ganges River Basin for normal period (Source: Riccardo, 2015)

The water supply depends partly on the rains brought by the southwesterly monsoon winds from July to October as well as on the flow from melting Himalayan snows in the hot season from April to June. Precipitation in the river basin accompanies the

southwest monsoon winds, but it also comes with tropical cyclones that originate in the Bay of Bengal between June and October. Only a small amount of rainfall occurs in December and January. The delta region experiences strong cyclonic storms both before the commencement of the monsoon season, from March to May, and at the end of it, from September to October. The GBM river basin is unique in the world in terms of diversified climate. For example, the Ganges river basin is characterized by low precipitation in the northwest of its upper region and high precipitation in the areas along the coast. (Mirza et al., 2011).

During winter, rain first enters Nepal in the west and gradually moves eastward with diminishing intensity. Temperature increases from the high Himalayan region to the lowland terai (northern part of the Ganges plain). Extreme temperatures recorded are -14.6°C in 1987 in Lo Manthang (Mustang district), located at an elevation of 3705 m, and 44°C in 1987 in Dhangadhi (Kailali district), located at an elevation of 170 m. Precipitation falls as snow at elevations above 5 100 m in summer and above 3000 m in winter. Temperature is a constraint to crop production in the Himalayas and the mountain region where only a single crop per year can be grown. On the other hand, in the low land terai three crops per year are common where the water supply is adequate. Single rice cropping is possible up to elevations of 2300 m while double rice cropping is limited to areas below 800 m.

Bangladesh has a tropical monsoon climate with significant variations in rainfall and temperature throughout the country. There are four main seasons: i) the pre-monsoon during March-May, which has the highest temperatures and experiences the maximum intensity of cyclonic storms, especially in May; ii) the monsoon during June-September, when the bulk of rainfall occurs; iii) the post-monsoon during October-November which, like the pre-monsoon season, is marked by tropical cyclones on the coast; iv) the cool and sunny dry season during December-February. The country is regularly subjected to drought, floods and cyclones. Mean annual lake evaporation is 1040 mm, which is about 45 percent of the mean annual rainfall. Mean annual temperature is about 25°C, with extremes as low as 4°C and as high as 43°C. Humidity ranges between 60 percent in the dry season and 98 percent during the monsoon.

4.4 Data Collection

4.4.1 Digital Elevation Model (DEM)

DEM refers to the elevation contour map in digital form. Here, the elevation throughout a grid of particular size refers to as the resolution is averaged and many such grids are combined to form a map called DEM.

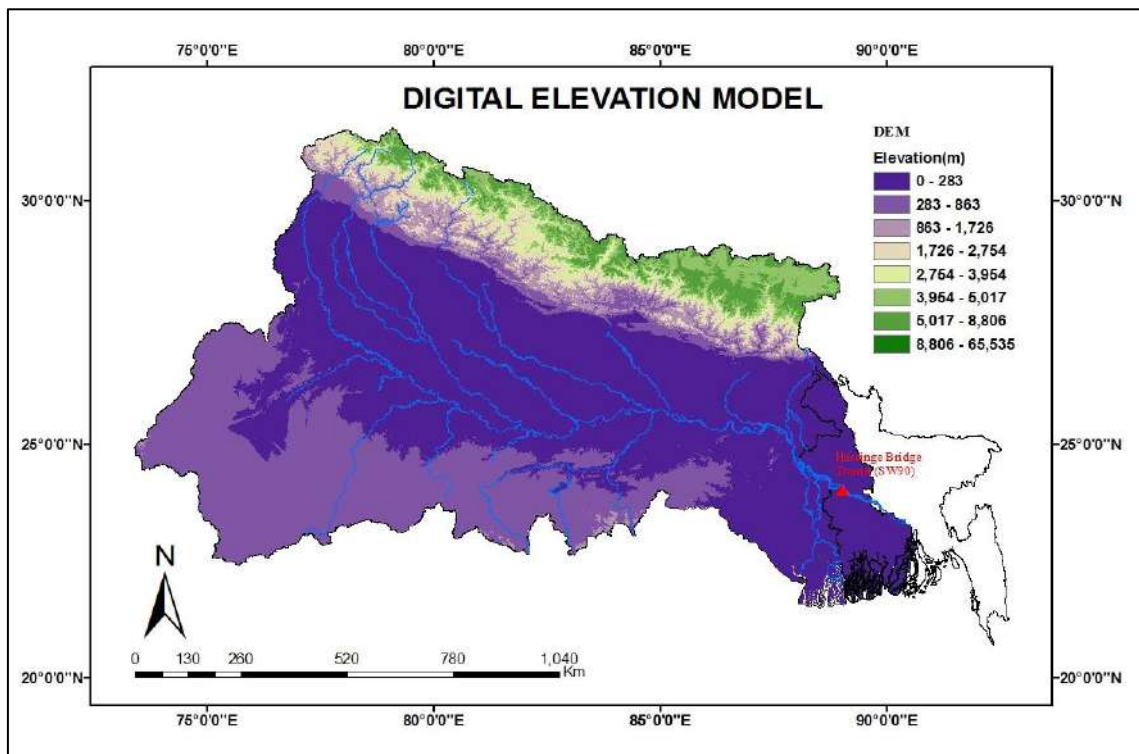


Figure 4.9: Digital Elevation Model (DEM) of Ganges River Basin

DEM data are required to provide the basic topographic information to the model. Using DEM, analysis such as flow accumulation and stream network, there are delineate many watershed and sub-basins which is created many HRUs which means hydrological response units are areas within a watershed that respond hydrological similarly to given input. The sub-basin parameters such as slope gradient, slope length of the terrain, and the stream network characteristics (channel slope, length and width) are derived from the DEM. For this study, a 90m resolution Digital Elevation Model (DEM) has been collected from Shuttle Radar Topography Mission (SRTM) website (<http://srtm.csi.cgiar.org>). DEM for the Ganges River Basin have masked for the SWAT model development. The DEM of the study area is shown in Figure 4.9.

4.4.2 River Network Data

River network helps the model identify the natural streams in the area so that it can set up its watershed based on the location and pattern of the natural streams. Although the model itself may be able to delineate the river network from the given DEM data, providing the river network data makes the catchment delineation process much more accurate. The River Network data was downloaded from USGS Hydrosheds.

4.4.3 Land use Data

Land use map is a map showing the land use and land cover classes of the area. This is also in digital format and the land use classes are denoted by polygons with various LU/LC characters. In the present study, a detailed classification of the land use classes is done. The digital map is linked to the database table containing the land use classes through a text format file known as the land use look-up table. Land use and land cover is one of the most important factors that affect runoff, surface erosion, and evapotranspiration in a watershed. Land use data allows the swat model characterize the initial parameters of the watersheds as well define the behavior of the catchment in case of precipitation. The presence of urban areas or forest area greatly changes the soil characteristics and the model will try to emulate the changing condition with the land use data type.

Land use classes for Ganges river basin is shown in Table 4.1. Land use classes have been parameterized based on existing SWAT land use classes. There are 13 types of land use data in Ganges basins. Land use classes have been found in the Ganges River basin which is shown in Figure 4.10.

Table 4.1: Land use distribution in Ganges River Basin

| Land Use | Area (%) |
|------------------------|-----------------|
| <i>Agricultural</i> | 65.57 |
| <i>Forest</i> | 16 |
| <i>Wetland</i> | 8.89 |
| <i>Built Up Land</i> | 4.28 |
| <i>Water bodies</i> | 3.47 |
| <i>Snow / Glaciers</i> | 0.94 |
| <i>Grassland</i> | 0.85 |
| <i>Total</i> | 100 |

(Source: India-WRIS, 2018)

In the present study, Land use map of 300m resolution for 2009 has been collected from USGS (United State Geological Survey) Land Cover Institute (LCI) website (Loveland et al., 2000). The required area is available from South Central Asia dataset. The data is available in geographic coordinate system - WGS84 datum. Land use map of other year has not collected because of avoiding model setup difficulties (Anand et al., 2018).

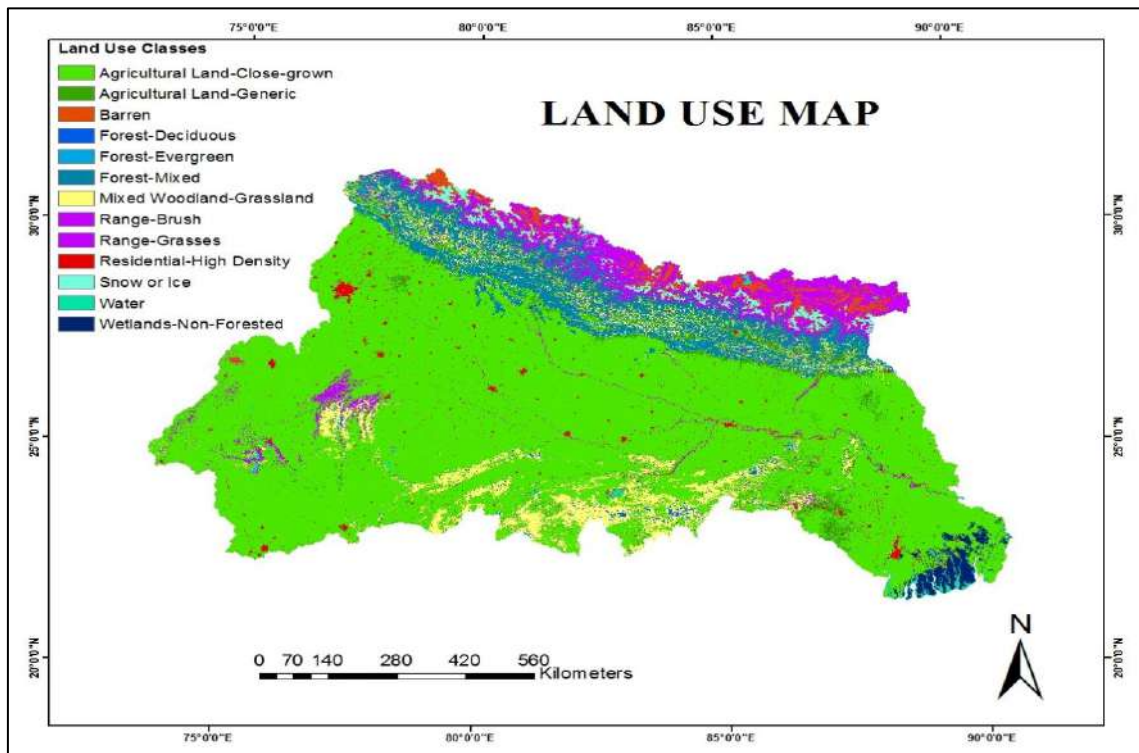


Figure 4.10: Land use map of Ganges River Basin

4.4.4 Soil Type Data

This is similar to the land use map but shows the soil distribution in the region. The SWAT model requires soil map and a database table of soil texture, available water content, hydraulic conductivity, bulk density and organic carbon content for different layers of each soil type. The soil map of the study catchment was clipped from the FAO digital soil map of the world (<http://www.fao.org/geonetwork/>). A “usersoil” database table was created for the study area from the SWAT2012 database has been shown in Table 4.2.

This map is at a scale of 1:5000000 and based on the compilation of available soil survey material and on field correlation. Figure 4.11 shows the extracted portion of the “Global soil Map” for the study area.

Table 4.2: Properties of soil used in SWAT setup for Ganges River basin.

| Soil name | Percentage of clay | Percentage of silt | Percentage of sand |
|------------|--------------------|--------------------|--------------------|
| Acrisols | 27 | 30 | 43 |
| Arenosols | 13 | 21 | 66 |
| Cambisols | 26 | 35 | 39 |
| Fluvisols | 25 | 37 | 38 |
| Gleysols | 30 | 29 | 41 |
| Histosols | 26 | 38 | 36 |
| LITHOSOLS | 29 | 31 | 40 |
| Luisols | 25 | 24 | 51 |
| Nitisols | 33 | 25 | 42 |
| Regosols | 24 | 28 | 48 |
| Solonchaks | 43 | 36 | 21 |
| Vertisols | 54 | 27 | 19 |
| Xerosols | 26 | 50 | 24 |
| Yermosols | 27 | 34 | 39 |

Source: SWAT 2012 database (link <http://swat.tamu.edu>)

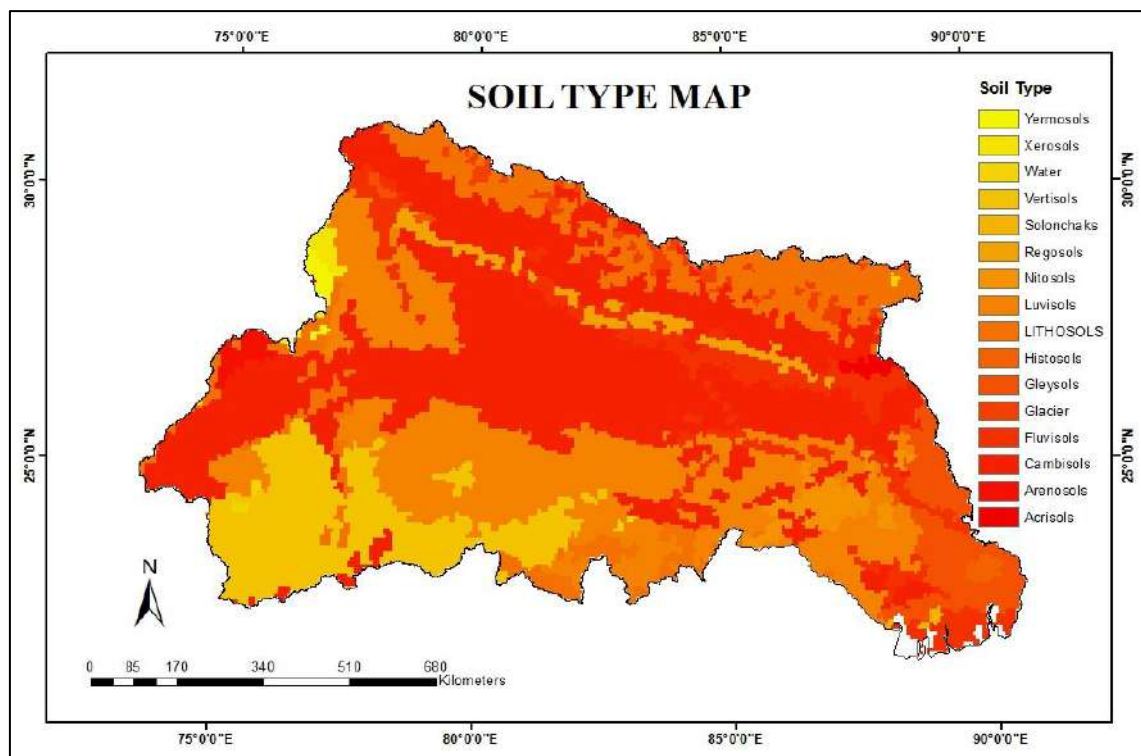


Figure 4.11: Soil type map of Ganges River Basin

It is worth mentioning that the along with the map, the “Global Soil Map” also provides a comprehensive data about its soil characteristics which can be incorporated in the model for better model output.

4.4.5 Weather and Discharge Data

The SWAT model requires daily values of precipitation, average temperature, solar radiation, relative humidity and wind speed. For this study, meteorological data for the Ganges River Basin have been collected from the NASA-Prediction of Worldwide Energy Resource (link <http://power.larc.nasa.gov>) for the climate normal period (1997 to 2016).

Discharge data at Hardinge Bridge Transit (SW 90) at Ishwardi, Pabna district for the year of 2000-2016 have been collected from Bangladesh Water Development Board (BWDB). Discharge data is required to calibrate and validate the model. The discharge generated by the model due to precipitation must be checked against a set of observed discharge data. Future precipitation and temperature data considering RCP scenario have been collected for climate model run for 2005-2099 time period. Table 4.3 shows basic data used in this study including their source, resolution and time period.

Table 4.3: Basic input data used in this study.

| Data Type | Resolution/ Location | Source | Time period |
|---|--------------------------------|---|-------------|
| Digital Elevation Model (DEM) | 90m | Shuttle Radar Topography Mission (SRTM) ^a | |
| River Network | | USGS Hydrosheds | |
| Precipitation, temperature and other climatic variables | Ganges River Basin | NASA-Prediction of Worldwide Energy Resource ^s | 1997-2016 |
| Land cover map | 300m | USGS Land Cover Institute (LCI) ^d | 2009 |
| Digital soil map | 1:5,000,000 | FAO (UNESCO) ^b | 2007 |
| Discharge | Hardinge Bridge transit (SW90) | BWDB | 2000-2016 |
| Future precipitation and temperature data | RCP 2.6, 4.5, 8.5 | All data are downloaded from ESGF Portal | 2005-2099 |

Source: ^aShuttle Rudder Topographic Mission. ^b FAO (UNESCO)

^cNASA Prediction of Power Worldwide Energy Resources

(<http://power.larc.nasa.gov/cgi-bin/cgiwrap/solar/hirestimeser.cgi?email=daily@larc.nasa.gov>).

^dUSGS Land Cover Institute (LCI). ^eEarth System Grid Federation (<http://pcmdi9.llnl.gov/esgf-web-fe/>)

4.5 Steps of SWAT Model Setup

Five sequential steps have been followed to set up the SWAT model, which are (1) watershed delineation, (2) HRU Analysis (3) Weather data definition, (4) Write inputs table, and (5) Streamflow simulation (both for present condition as well as in future) at different points which are basically outflow of different sub-catchments. In Figure 4.12 shows the flow chart of model setup in SWAT.

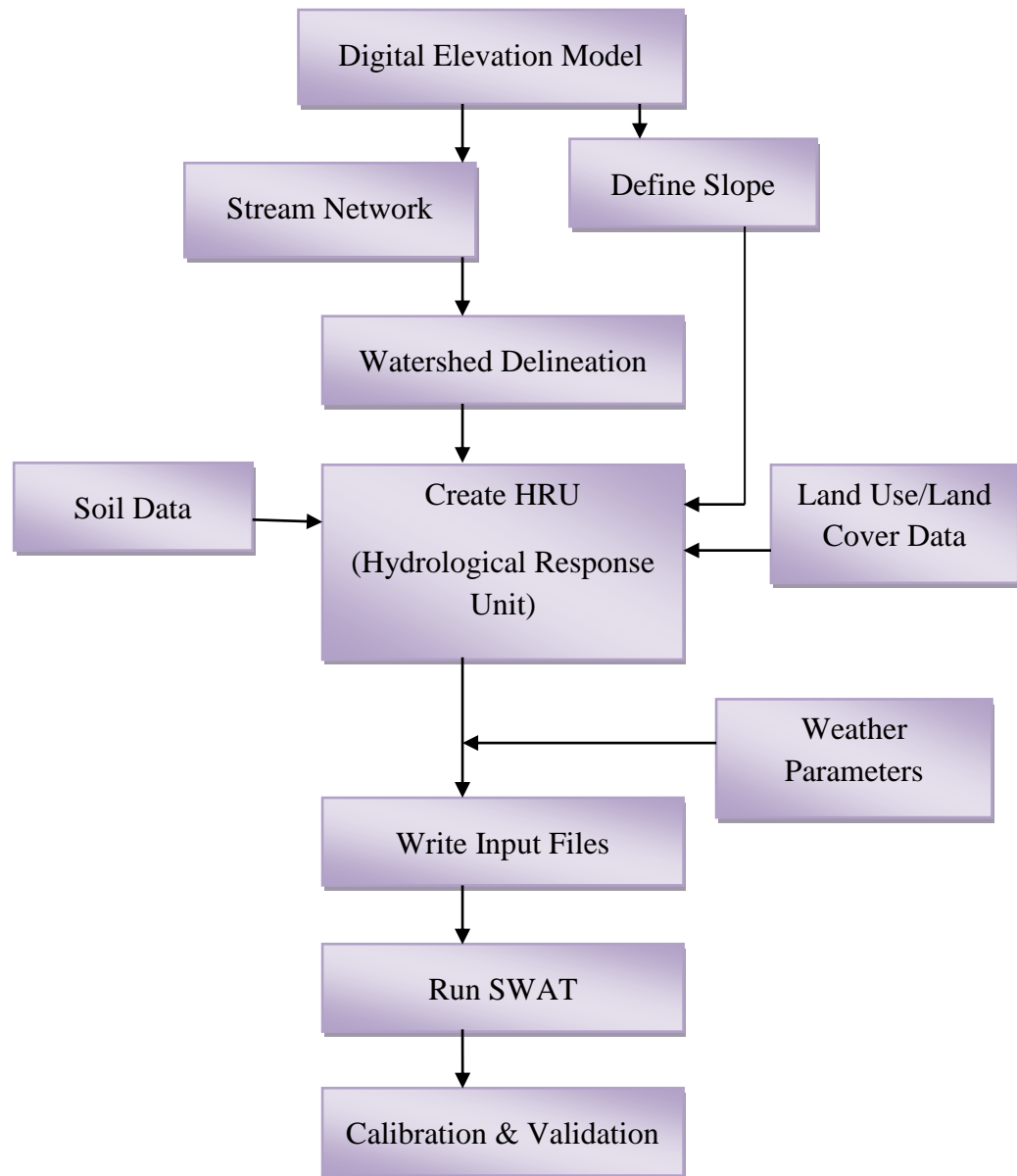


Figure 4.12: Flow chart of model setup in SWAT

4.6 Climate Model and Scenario Generation

There are lots of GCMs available at different resolution for projecting future climate scenarios. Moreover, it has very much difficult to work with all the GCMs at a time. So, selecting a model for assessing the hydrological impact of climate change is one of the most important tasks. All the projections were made by forcing the corresponding GCM with Representative Concentration Pathway - RCP (van Vuuren et al., 2011). For this study, precipitation obtained from different ensembles was average for three periods, viz. 2010-2039 (2020s), 2040-2069 (2050s) and 2070-2099 (2080s). For all the periods, changes of precipitations from the base period were analyzed separately. Finally, selection of GCM models was done based on the changes at the beginning, middle and end of 21st century which is represented by 2020s, 2050s and 2080s. The following steps are followed for selecting ensembles and scenarios. Gridded points all over the basin at which GCMs result are extracted and used for further analysis. An assessment on different GCMs for three scenarios (RCP 2.6, RCP 4.5 and RCP 8.5) according to IPCC AR5 (IPCC 5th Assessment Report) has been conducted to justify the use of specific GCM outputs.

Steps followed can be summarized as following:

Step 1: Annual average precipitation on Ganges River Basin was determined for three-time periods, viz. 2020s (2010-2039), 2050s (2040-2069) and 2080s (2070-2099). Annual average precipitation was also collected for base period (2000-2016).

Step 2: Percentage increase or decrease in precipitation for each model for these three different periods has been calculated.

Step 3: Model giving highest positive and negative change in precipitation were selected in future.

4.7 Climate and Land Use Change Impact Assessment

Temperature and precipitation data of 3 GCMs selected from ESGF (Earth System Grid Federation) database are used to estimate the range of potential impact of climate changes on flow of Ganges River basin (Raju, K. S. et al, 2017). The changes in flow at Hardinge Bridge transit (SW 90) are analyzed for 2020s, 2050s and 2080s in monthly and annual scale. After an additional increase in urbanization about 20%, 30% and 40% have been considered and deforestation about 10%, 15% and 20% have been also considered as land use changes to find out the impact on flow at Hardinge Bridge transit (SW 90).

4.8 Summary

Methodology are the backbone of any research work. If the methodology is well established and clear, then it has expected that the study result based on this methodology will also be as expected. So, in this chapter a brief description of each section of methodology have described. Further description and analysis based on this methodology has been discussed in the following chapter.

CHAPTER 5

RESULTS AND DISCUSSIONS

5.1 General

This chapter describes about the model development and the output of analysis of hydrological modelling outcome. After model setup and calibration/validation, analysis of model output was carried out in order to assess the impact of climate change and land use change on the flow for future scenarios. The hydrological model SWAT of Arnold and Allen (1996) selected for this study operates on daily time step and uses physiographical data such as elevation, soil use, land use, meteorological data and river discharge. Once the data is arranged in the required format, the model simulation takes a sufficiently high amount of time based on the basin size. As described earlier, the effects of variations in topography, land use, soil and other characteristics of watershed hydrology are incorporated by dividing a basin into several sub-basins based on drainage areas of tributaries and then the sub-basins are further divided into a number of Hydrological Response Units (HRUs) based on land cover and soils. Each HRU is assumed to be spatially uniform in terms of land use, soil, topography and climate.

Initially the basin water balance was discussed which quantifies water distribution throughout the basin. After quantified water balance of the basin, temperature and precipitation change obtained from several GCMs and RCPs were discussed based on which two climate scenarios were selected. Projected flow for high resolution precipitation and temperature of two selected scenarios were then analyzed to identify the impact of climate change on flow of Ganges River Basin.

This chapter also includes an analysis of the output and discusses the performance of the SWAT model. Visual observation and statistical measures were used to evaluate the performance of the model. In this study, NSE vales were calculated and reported to provide an indication of model performance relative to other studies. Judgment of goodness-of-fit of the model was primarily based upon statistical comparison of observed and predicted streamflow.

5.2 Steps of Model Setup

A hydrological model had been setup for Ganges River Basin by SWAT. A Model setup according to real condition is very important step for accurate output. In order to obtain output data from SWAT model, it is required to pass through different stages using relevant datasets.

The following steps were followed to set-up the model:

1. Watershed delineation
2. Hydrologic Response Units Analysis
3. Weather Data Definition
4. Creating the SWAT Input datasets
5. Simulation Method Selection
6. Sensitivity analysis
7. Calibration and Validation
8. Model Performance Evaluation

5.2.1 Watershed delineation

Automatic delineation of watersheds was done by using the DEM as input. The whole watershed outflow point is manually selected. The Ganges River basin has been delineated using 180,000 hectares as minimum stream threshold and has resulted in 388 sub-basins (Figure 5.1).

The standard methodology, based on the eight –pour algorithm (Jensen and Domingue, 1988) is applied for automatic delineation. First, the SWAT project set up was created. The watershed delineation process consists of five major steps, DEM setup, stream definition, outlet and inlet definition, watershed outlets selection and definition and calculation of sub basin parameters. Once, the DEM setup was completed and the location of outlet was specified on the DEM, the model automatically calculates the flow direction and flow accumulation. Subsequently, stream networks, sub watersheds, and topographic parameters were calculated using the respective tools. The stream definition and the size of sub basins were carefully determined by selecting threshold area or minimum drainage area required to form the origin of the streams.

The geographic information system interface – ArcSWAT (Winchell et al., 2010) – was used to parameterize the model for the Ganges River basin. The stream network of the basin was delineated from a 90-m DEM (Farr et al. 2007).

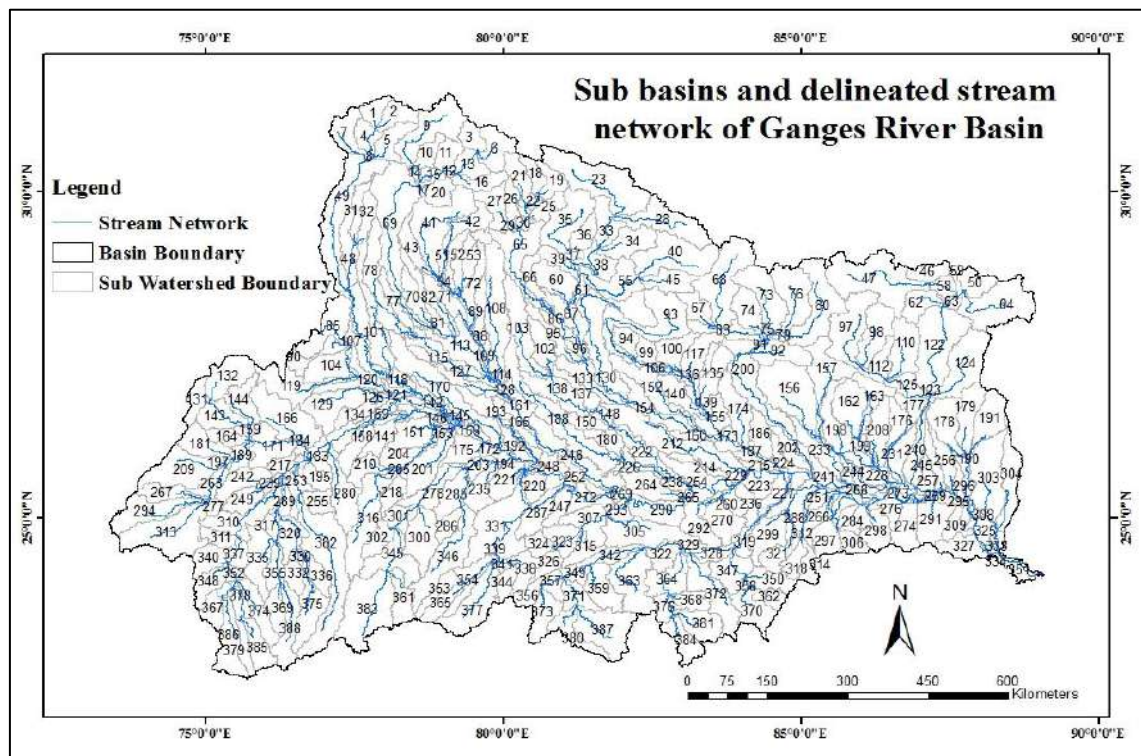


Figure 5.1: Sub basins and delineated stream network of Ganges River Basin

Relatively high resolution of elevation data (90m) allowed skipping the step on use of predefined streams and watershed. Resampled from the Hydrosheds (Hydrological data and maps based on Shuttle Elevation Derivatives at multiple scales) dataset (Lehner et al., 2008). Using a DEM of Ganges River Basin, the ArcSWAT watershed generating module was employed to identify the outlet point and watershed for the river basin. Hydrological datasets such as flow direction and flow accumulation were created in the process.

A watershed mask was created to define the extent of the study area. Including an additional outlet at Hardinge Bridge discharge gauge station, the basin was sub-divided into 388 sub-basins. The outlet at Hardinge Bridge station was considered to be the final outlet of the Ganges basin. Characterization of the stream reaches and subbasin geomorphology was done automatically by the interface.

Stream networks were delineated in SWAT with a minimum drainage area threshold of 1,80,000 hectares using the DEM of the basins.

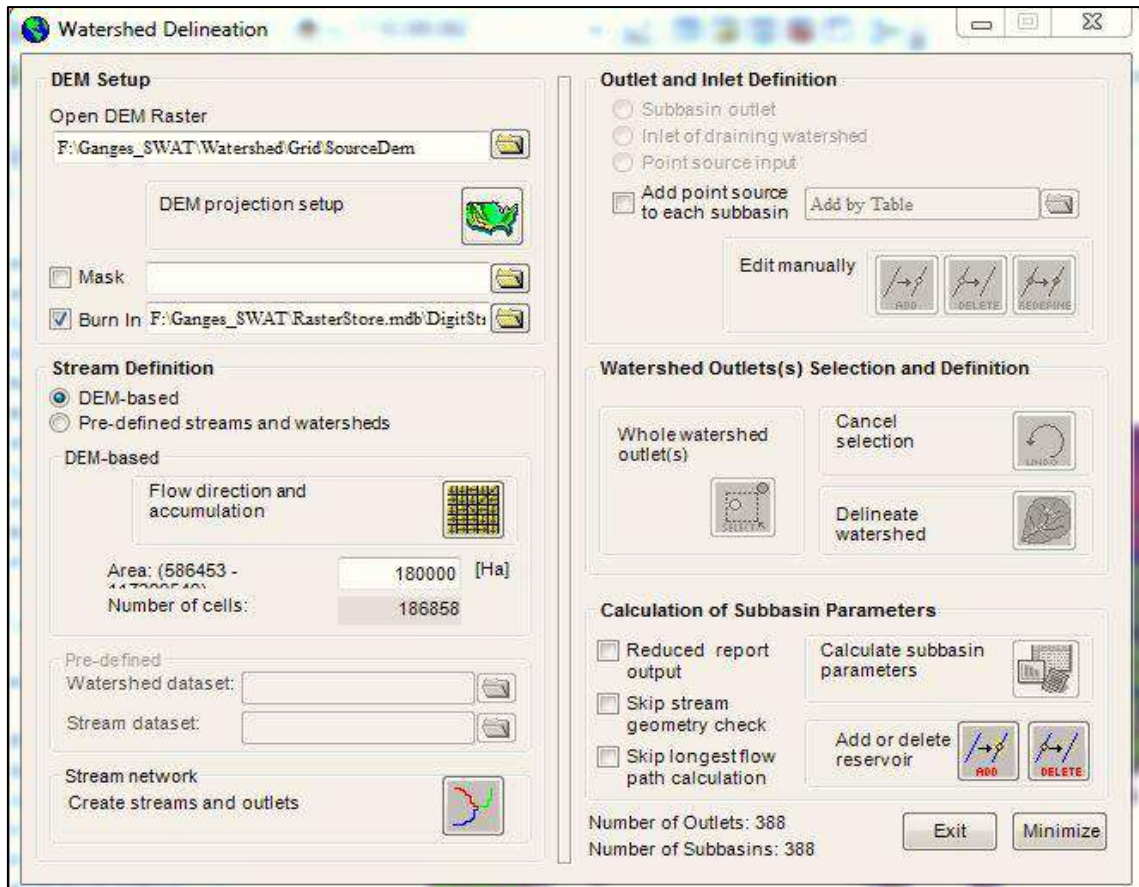


Figure 5.2: Automatic Watershed Delineation Dialogue box in SWAT

Later, the outlines of the complete basins were delineated by considering the basin outlets at Harding Bridge transit Ganges basins. The area of these delineated basins is approximately 10,70800 km² for this basin. The Ganges River basin contained 388 sub-basins.

To setup the hydrological model using SWAT, the first step would be to delineate the river basin. The “Automatic Watershed Delineation” tool of ArcSWAT was used for this purpose. This is accomplished using the automatic watershed delineation tool of ArcSWAT 2012.10.2.16 employing a 90m DEM for Ganges basin. The Mercator Auxiliary Sphere projection has been used for the DEM and all other GIS layers. All the watershed delineation steps such as filling sink, defining flow direction and accumulation have been done automatically through the user interface.

As an output of this step 4 layers were added to the map and displayed over the DEM layer grid: Reach drainage network (created on the basis of elevation data) and Monitoring point (respective stream junction points), watershed with all sub-basins, outlets (defined by SWAT and added by table) and Basin with full watershed boundary.

In order to define the border of watershed it was necessary to select the main outlet. Finally, calculation of sub-basin parameters containing elevation data has been derived with information on the stream geometry and longest flow path calculation.

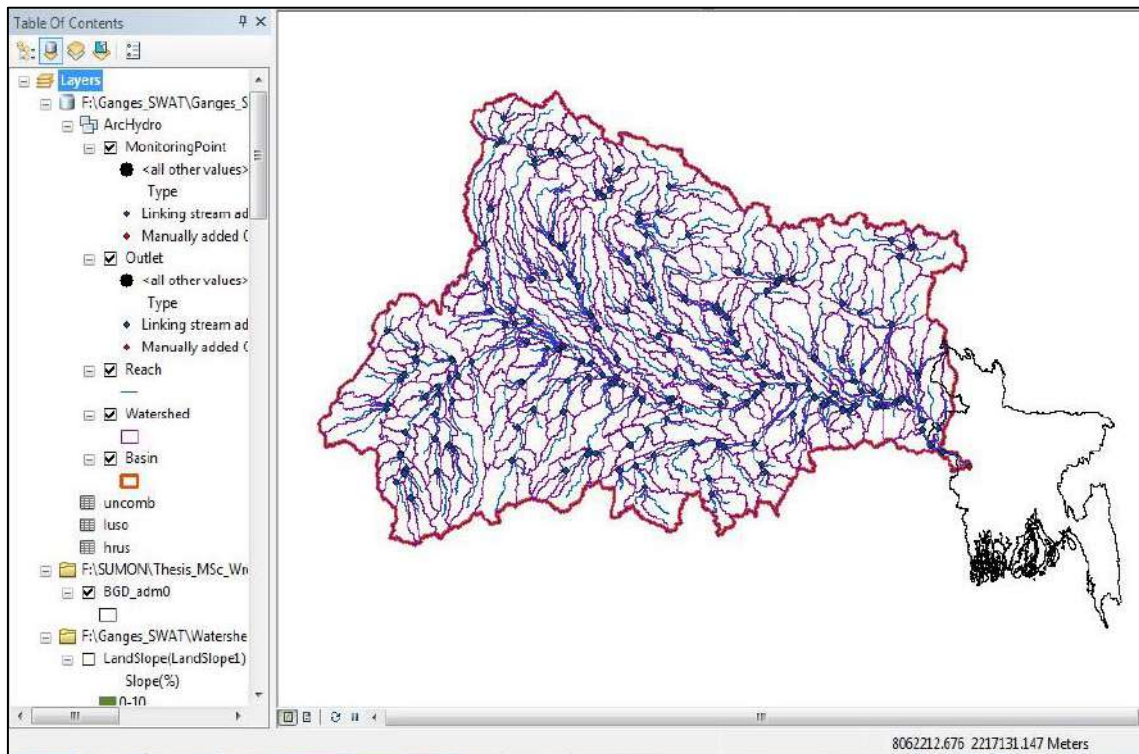


Figure 5.3: ArcSWAT window after Watershed Delineation

5.2.2 Hydrologic Response Units Analysis

SWAT requires soil properties and land cover information to simulate loads in the hydrological components. The soil map was obtained from the Food and Agriculture Organization of the United Nations (FAO, 1995). 69 soil types for the Ganges basin were differentiated, and soil properties for two layers (0-30 cm and 30-100 cm depth) were provided. Other soil properties such as particle-size distribution, bulk density, organic carbon content, available water capacity, and saturated hydraulic conductivity were obtained (Reynolds et al. 1999). Global soil dataset FAO has been used for soil layers (FAO IIASA 2012). The soil database with classes used in dataset was incorporated to the SWAT database file. In order to link this data to SWAT database it is necessary to formulate datasets in the required format and create lookup tables that will connect used datasets to the SWAT default database.

After completion of watershed delineation, it is required to define unique sub-watersheds, hydrologic response unit. The land area in a sub-basin was divided into

HRUs. The HRU analysis tool in ArcSWAT helped to load land use, soil layers and slope map to the project. The delineated watershed by ArcSWAT and the prepared land use and soil layers were overlaid 100%.

HRU analysis in ArcSWAT includes divisions of HRUs by slope classes in addition to land use and soils. The multiple slope option (an option which considers different slope classes for HRU definition) was selected. The land use / land cover, soil and slope map were reclassified in order to correspond with the parameters in the ArcSWAT database. After reclassifying the land use, soil and slope in ArcSWAT database, all these physical properties were made to be overlaid for HRU definition. For this thesis a 12% threshold value for land use, 10% for soil and 15% for slope were used (Frankenberger, J. et. al., 2015).

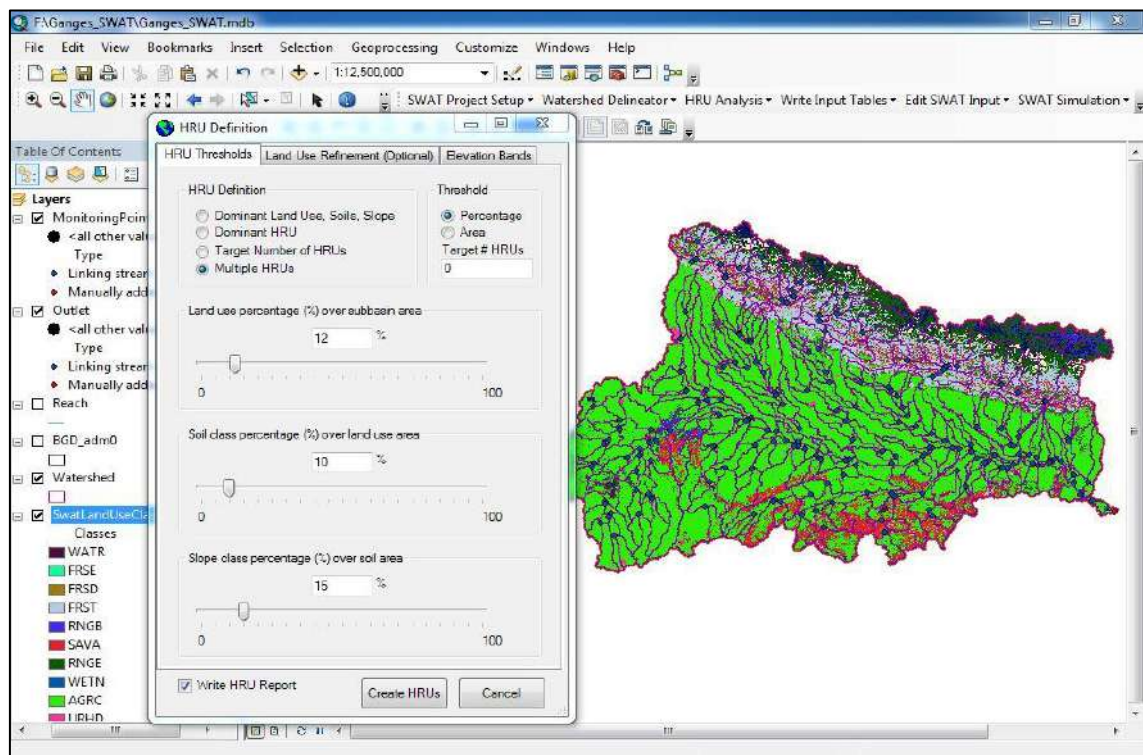


Figure 5.4: ArcSWAT window of HRU definition

In general, the threshold level used to eliminate minor land use and land covers in sub basin, minor soil with in a land use and land cover area and minor slope classes with in a soil on specific land use and land cover area (Setegn et al., 2008). Following minor elimination, the area of remaining land use and land covers, soils and slope classes are reapportioned so that 100% of their respective areas are modelled by SWAT. The HRU distribution in this study was determined by assigning multiple HRU to each sub-basin. To further characterize the subbasin for dominant land use and soil types, the multiple

Hydrological Response Unit (HRU) option in SWAT was implemented, which resulted in discretization of 1525 HRUs for the Ganges River Basin. The discretization of basin into HRUs allows a detailed simulation report of the hydrological processes (Chaubey et. al., 2015).

The report has been created with land use, soil and characteristics for the whole watershed and for each sub-watershed.

5.2.3 Weather Data Definition

The climatic variables required by SWAT consist of daily precipitation, maximum/minimum air temperature, solar radiation, wind speed and relative humidity. The model allows values for daily precipitation, maximum/minimum air temperatures, solar radiation, wind speed and relative humidity to be input from records of observed data using CFSR (Climate Forecast System Reanalysis) datasets (Fuka et.al., 2013). Sample CFSR dataset has given in Appendix A1. The daily weather data for the GBM basins have been used from NASA power without bias correction.

The data includes daily weather data (precipitation, minimum and maximum temperature) starting from 1997 to 2016 which is used for SWAT modeling calibration. Metrological or weather data are then loaded into the model in text (tab delimited) format.

After HRU definition weather data for the watershed should be loaded using Write Input tables command in SWAT. The meteorological stations locations assign climate data to the sub-watersheds, delineated through HRU analysis. The data is loaded through the Weather Data Definition menu.

In Figure 5.5, meteorological station grid has showed on Ganges River Basin. This menu contains sis. tabs: Weather Generator Data, which must be set, and five tabs with optional weather parameters, which ear be loaded based on measurement from specified stations.

It was required to create database with location of the stations used for weather generation and weather generator data, data on wind speed, humidity and solar radiation has been created for the whole watershed. Then for increasing effectiveness of simulation measured data on maximum and minimum temperature and daily precipitation has been loaded. However, some data required additional processing in

order to be read by SWAT program. After completion of weather database setup, the weather gaged were added to the Monitoring Point layer in the map.

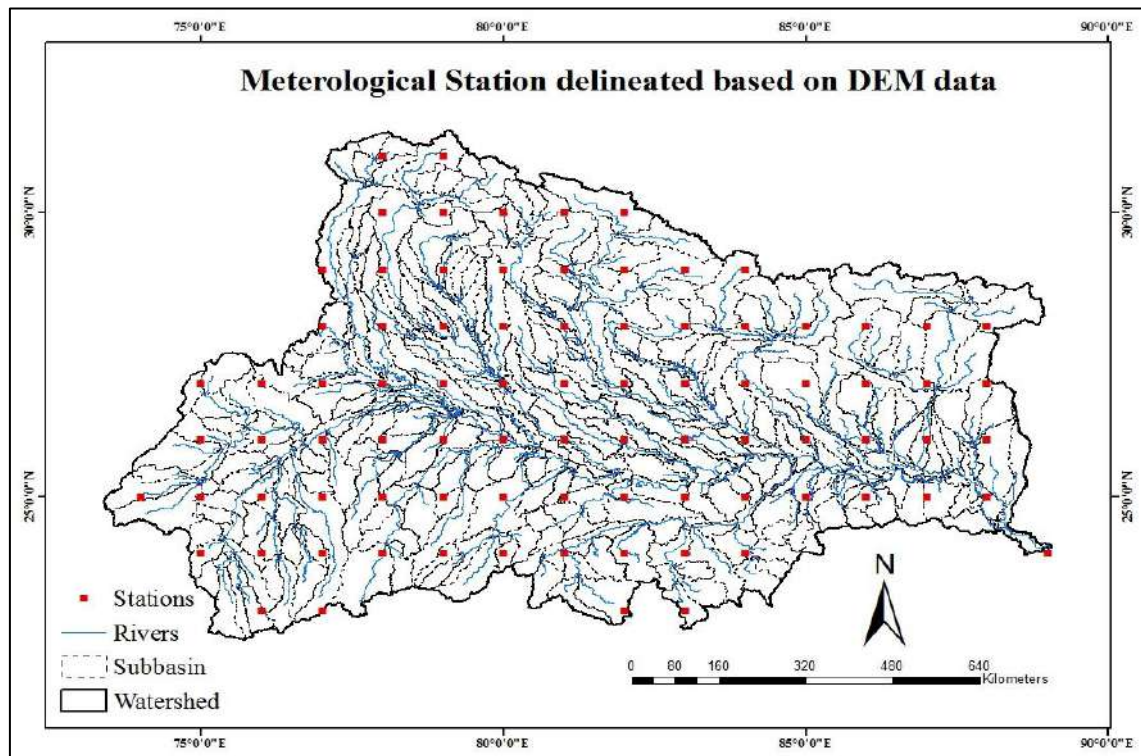


Figure 5.5: Meteorological Station grid of NASA-POWER on Watershed

5.2.4 Creating the SWAT Input datasets

After definition of weather data SWAT allows to build different database files containing the information needed to generate default input for SWAT. There are 2 options on building initial watershed input files, which are required for running the model: it can be done through the Write All command using default database of the SWAT or the individual Write commands. The first option, applying default data has been chosen. It was assumed that default value on Manning's roughness factor (0.14) is appropriate for the respective watershed (Winchell et al., 2010).

After generating all default input values, it is possible also to start editing default values using the Edit SWAT Input menu. However, it was assumed that there were no significant reservoirs in the watershed, water quality analysis has not been included in the research and Soil database was included in the default SWAT database, so finally input SWAT data was not edited.

5.2.5 Simulation Method Selection

In order to run the model, it is required to set up model running parameters using SWAT Simulation menu. The resulting dialogue box is shown in Figure 5.6. The dialogue box has preloaded time band based on the weather data and rainfall data entered previously. The period of simulation for 21 years from 1 January 1997 to 31 December 2016 has been chosen. 3-years of warm up period, which is required for better simulation performance, have been set up. Default options with skewed normal distribution of rainfall and monthly printout setting have been selected. Now, the SWAT setup is run and once this is successful, the SWAT run tab is available.

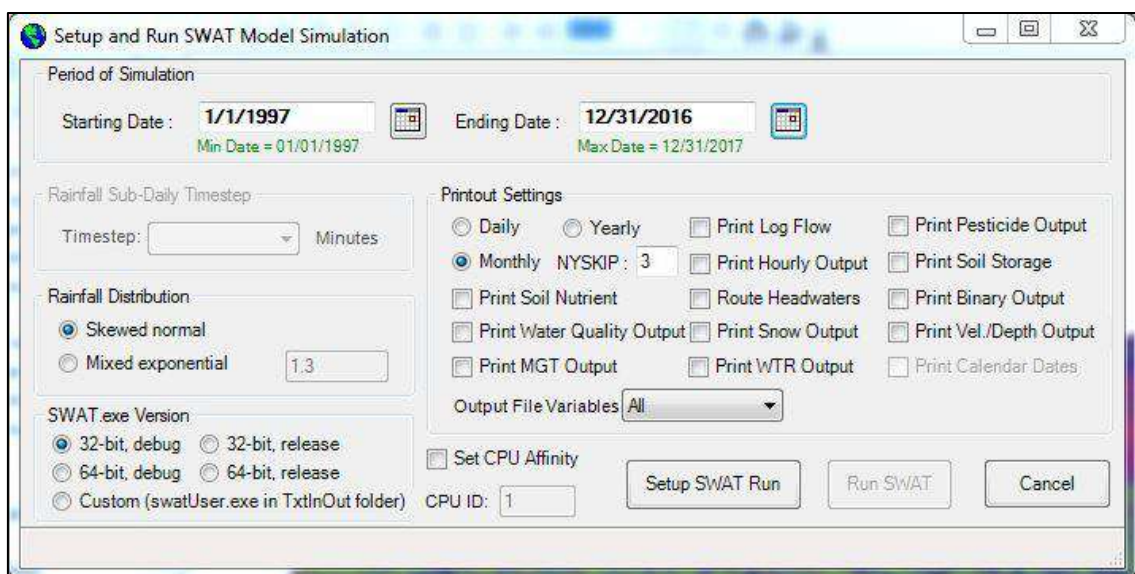


Figure 5.6: SWAT dialogue box to Run the Model

On choosing the run SWAT button, an MS-DOS window appears and starts calculating the flow parameters. SWAT calculates the flow account for each year for the entire period. This takes a long time based on the basin size. When the run is successful, the results are checked. The Read SWAT output dialogue is now chosen and the three output files with extensions. rch. sub. and hru. are selected and write input file tab is selected. The simulation can also be saved as a separated file for further database file reference with required name.

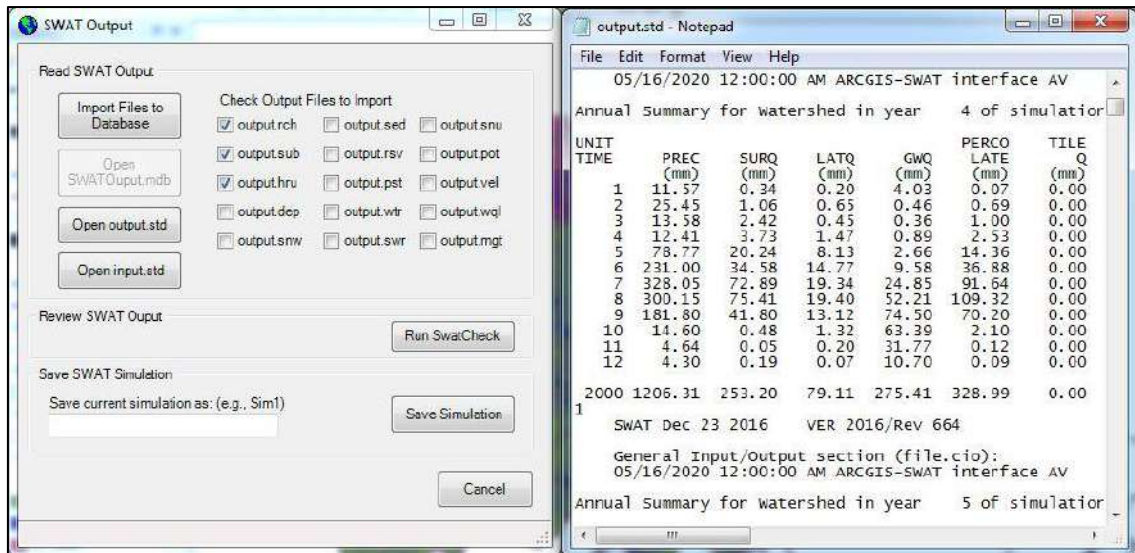


Figure 5.7: SWAT output dialog box and output.std file

The information on watershed statistic was provided through the output.std text file which shown in Figure 5.7 and MS Access database, where the monthly statistics on HRU, subbasins and reaches within the sub-catchment has been derived. Sample output table for the period of 2000 provided by SWAT model has given in Appendix A2.

5.2.6 Sensitivity Analysis

It is very important for Model users for determining which parameters to calibrate so that the model response mimics the actual field, subsurface, and channel conditions as closely as possible. When the number of parameters in a model is substantial as a result of either a large number of sub-processes being considered or because of the model structure itself, the calibration process becomes complex and computationally extensive (Rosso, 1994; Sorooshian and Gupta, 1995). In such cases, sensitivity analysis is helpful for identifying and ranking parameters that have a significant impact on specific model outputs of interests (Saltelli et.al., 2000).

Before running the calibration, analyzed the sensitivity of the parameters by using the Latin hypercube one-factor-at-a-time (LHOAT) method of SWAT (van Griensven et al., 2006). This approach combines the advantages of global and local sensitivity analysis methods and can efficiently provide a rank ordering of parameter importance (Sun and Ren, 2013). Based on the rank ordering, sensitive parameters (Table 5.1) were optimized using the SUFI2 algorithm in the SWAT-CUP.

Table 5.1: The Sequential Uncertainty Fitting (SUFI2) optimized value with optimization range of the SWAT model parameters included in the final calibration.

| Rank | Parameter | Description | Range | Fitted value |
|-------------|------------------|---|---------------|---------------------|
| 1 | CN_2 | SCS runoff curve number | -0.2 to 0.2 | -0.12 |
| 2 | ALPHA_BNK | Base flow alpha factor for bank storage | 0 to 1 | 0.26 |
| 3 | CH_K2 | Effective hydraulic conductivity in main channel alluvium | 0.025 to 3.35 | 2.14 |
| 4 | CH_N2 | Manning's n value for the main channel | 0.025 to 0.07 | 0.068 |
| 5 | HRU_SLP | Average slop steepness | -0.70 to 1 | -0.88 |
| 6 | SURLAG | Surface runoff lag time | -1.10 to 3.70 | 2.90 |
| 7 | GW_REVAP | Groundwater "revap" coefficient | 0.01 to 0.30 | 0.24 |
| 8 | ALPHA_BF | Baseflow alpha factor | 0 to 1 | 0.01 |
| 9 | EPCO | Plant uptake compensation factor | 0.1 to 0.9 | 0.21 |
| 10 | ESCO | Soil evaporation compensation factor | -0.1 to 0.7 | 0.63 |

“r__” means the existing parameter value is multiplied by (1+a given value), “v__” means the default parameter is replaced by the given value, and “a__” means the given parameter value is added to the existing parameter value.

In SUFI2 all uncertainties such as model input, model conceptualization, model parameters, and measured data are mapped onto the parameter ranges as the procedure tries to capture most of the measured data within the 95% prediction uncertainty (Abbaspour et al., 2009). Overall uncertainty in the output is quantified by the 95% prediction uncertainty (95PPU) calculated at the 2.5% and 97.5% levels of the cumulative distribution of an output variable obtained through Latin hypercube sampling. The goodness of calibration/uncertainty performance is quantified by *P*-factor, which is the percentage of data bracketed by the 95PPU band, and *R*-factor, which is the average width of the band divided by the standard deviation of the corresponding measured variable. Thus, SUFI2 seeks to bracket most of the measured data within the smallest possible uncertainty band (Abbaspour, 2007). During calibration, the target has to bracket most of the measured data including uncertainties within the 95PPU band, a *P*-factor close to 1, while having the narrowest band, an *R*-factor close to zero. For the present study, sensitivity analysis was performed using the Latin hypercube one-factor-at-a-time (LH-OAT) (Van Griensven et.al., 2002, 2005) method to rank the simulation parameters of the model for each sub basin. Sensitivity

analysis can be performed for many inputs such as for flow, sediment discharge, Organic Nitrogen, Phosphorus etc. In this study, sensitivity analysis is performed only for stream flow. Figure 4.9 shows the results and sensitivity of various parameters used in SWAT model calibration; this analysis was done by using SWAT-Cup tool. Total 10 parameters have been selected to find out their sensitivity on flow conditions. Most sensitive parameters and their fitted values are shown in Table 5.1.

5.3 Model Calibration and Validation

To calibrate the SWAT model at the basin level using observed river discharge at the Hardinge Bridge gauging station (SW 90). Calibration on upstream outlets could not be done because of lack of shearing data between countries. The observed discharge for the period 2000-2007 was used for the model calibration. Most part of Ganges basin area is located in India; the Ganges River has been under gone approximately 200 numbers of small to large hydraulic structures (dams, barrage and reservoirs etc.).

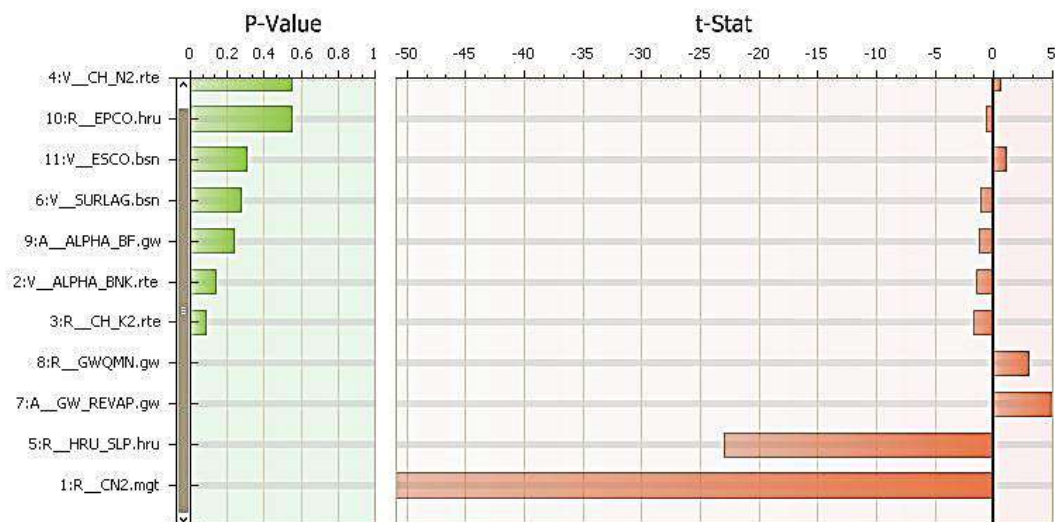


Figure 5.8: Global sensitivity analysis of calibration parameters

At monsoon season, all controlling devices of different types of hydraulic structures remain open so the river act like a natural stream without obstacle and the peak flow occurs depending on upstream rainfall, connectivity of rivers, land uses, soil type etc (Mohammed et al., 2018).

Before running the calibration, analysis of the sensitivity of the parameters by using the Latin hypercube one-factor-at-a-time (LHOAT) method of SWAT (van Griensven et al., 2006). For validation, keeping the optimized parameters constant. There are numerous parameters in hydrological models which can be classified as physical parameters (i.e., parameters that can be physically measurable from the properties of

watershed) and process parameters (i.e., parameters represent properties which are not directly measurable) (Sorooshian and Gupta, 1995). A sensitivity analysis of parameters was carried out by regressing Latin Hypercube generated parameters against objective function values (SWAT-CUP, 2012).

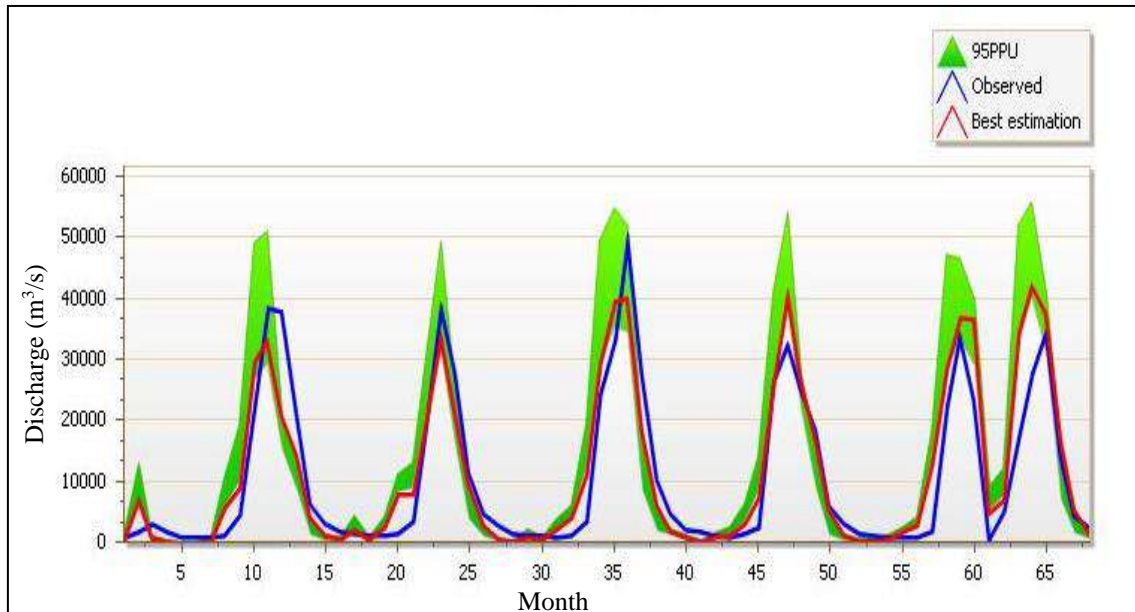


Figure 5.9: Output window of SWAT-CUP for Calibration

It was found that, out of 10 selected parameters, SCS runoff curve number, Base flow alpha factor for bank storage, Effective hydraulic conductivity in main channel alluvium, Manning's n value for the main channel, Average slope steepness, Surface runoff lag time, Groundwater "revap" coefficient, Baseflow alpha factor, Plant uptake compensation factor, Soil evaporation compensation factor parameter to which the flow has sensitivity shown in Figure 5.8.

In Figure 5.9 show the calibration output from SWAT-CUP after iteration. In, Figure 5.10 and 5.11 has showed the graphical representation of monthly observed and simulated flow for both calibration and validation period. It was found that the simulated flow is in great compliance with the observed discharge for both monsoon and dry season.

However, the curve number (CN2) was found to be the main sensitivity parameter for outlets. The model was calibrated from 2000 to 2007 and validated from 2008 to 2016 with monthly observed stream flow data at Hardinge Bridge station. It has more realistic if the calibration has done on some upstream outlets. But for the lack of discharge data from upstream basin's outlet that couldn't be done. In calibration and validation stage, model performance is evaluated based on statistically and graphically.

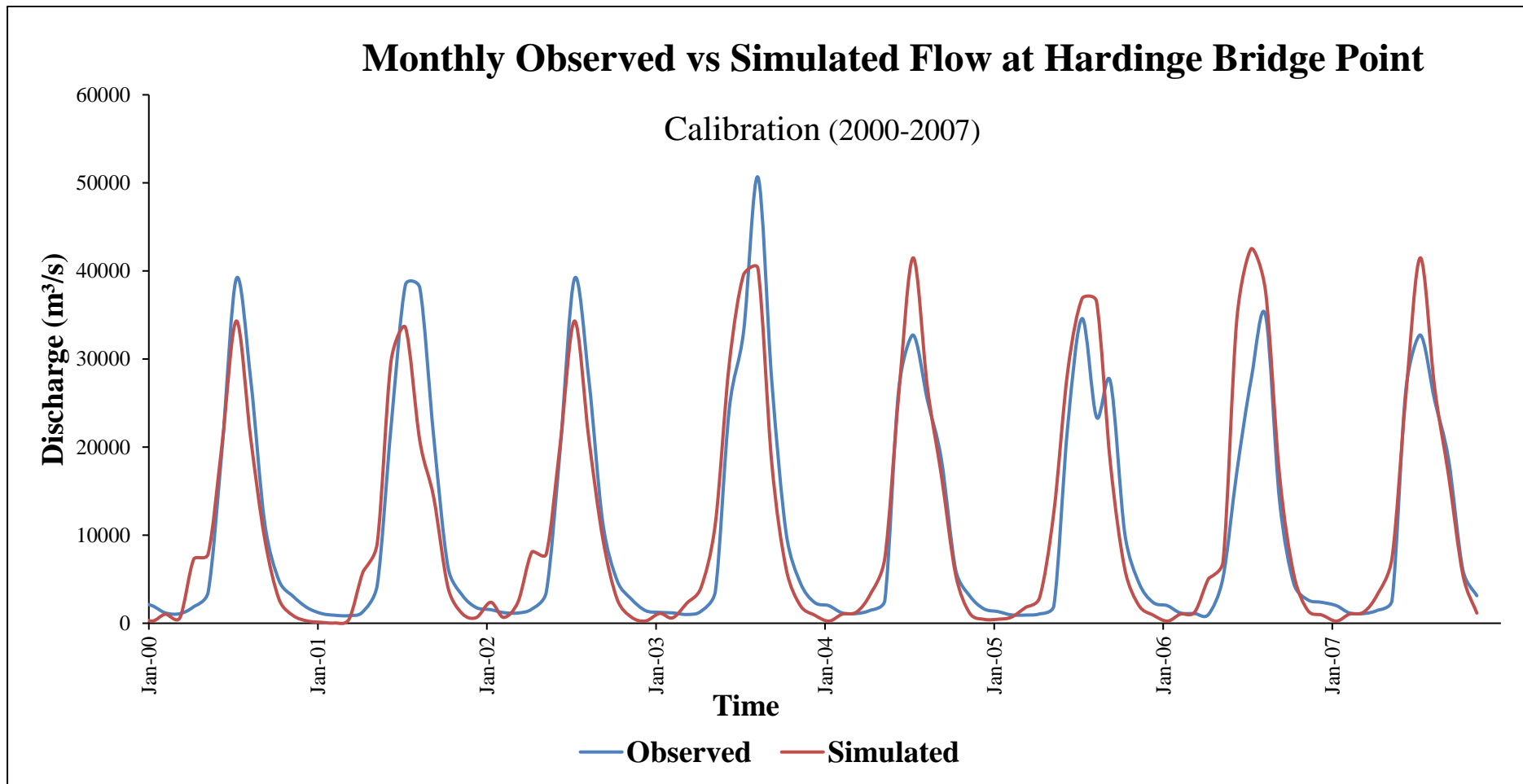


Figure 5.10: Monthly observed and simulated flows for the Calibration period of 2000 to 2007

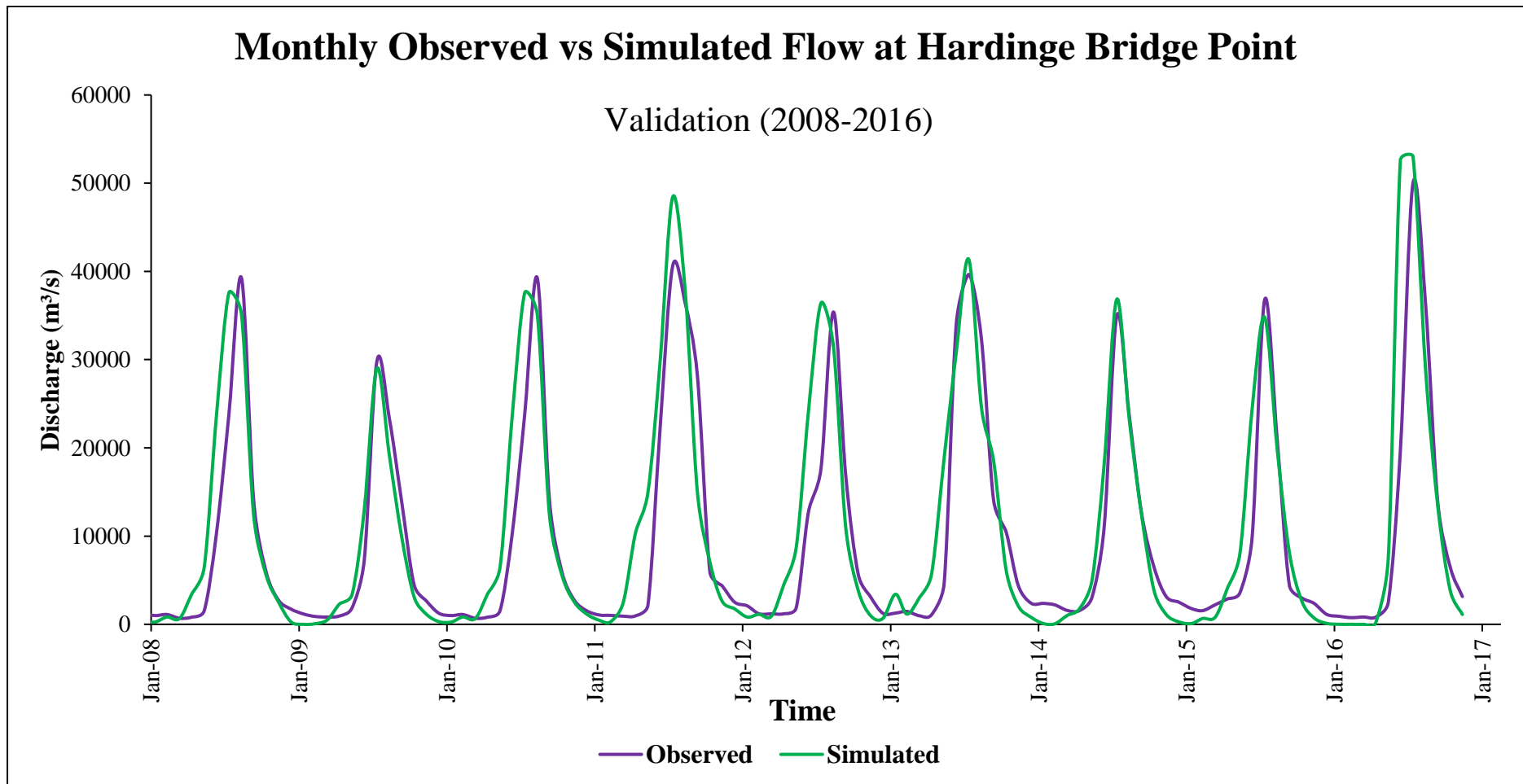


Figure 5.11: Monthly observed and simulated flows for the Validation period 2007 to 2008

In figure 5.10 has shown about the Model hydrographs for monthly (at Hardinge Bridge) for calibration period generated by NASA-POWER rainfall data products. It has been found that simulated monthly discharge are good correlate with the observed daily discharge. The results of calibration of simulated vs. observed during monthly in the figure 5.10. It has been found that simulated monthly avg. discharge assign 3% higher value from observed monthly discharge for the period of 2000-2007. The monsoon flow of simulated has been found as varies 6-12% from observed monsoon flow. In calibration period, peak flow of each year has not fully matched for grid-based precipitation used in this study. Because model could not take into account the extreme precipitation. Model consider the extreme precipitation as an average of grid precipitation. For this reason, peak flow would not match 100%. Another reason is the role of flood plain could not take into account by SWAT. In every climate model, peak rainfall has under estimated and the low rainfall has overestimated.

Table 5.2: Mean observed and simulated flow for calibration (2000-2007) and validation period (2008-2016) of the Ganges River basin.

| Period | Observed Mean (m³/s) | Simulated Mean (m³/s) |
|--------------------|--|---|
| Calibration | 10675.58 | 11008.75 |
| Validation | 9443.81 | 10751.01 |

During Validation period for NASA-POWER datasets has been shown in Figure 5.11. From this graph, it can be interpreted that base flow have shown low value from the observed discharge. It can also say that the simulated peak daily discharge is closely to observed discharge but in the flood year, simulated peak daily discharge over-estimate from the observed discharge. The model has been validated for monthly scale for the input of NASA-POWER datasets that is shown in 5.11. It has been found that monthly avg. simulated discharge is 13% higher from the observed monthly discharge.

5.4 Model Performance Evaluation

The performance of the model has been evaluated using the Nash– Sutcliffe Efficiency value (NSE), the coefficient of determination (proportion of the variance in the observations explained by the model, R^2), percent bias (PBIAS) and the ratio of the root mean square error between the simulated and observed values to the standard deviation of the observations (RSR).

Table 5.3: General Reported ratings for Nash-Sutcliffe efficiency (NSE), Mean relative bias (PBIAS), Root mean square error-standard deviation ratio (RSR) and Coefficient of determination (R^2) for calibration and validation process.

| Formula | Value | Rating |
|--|---|---|
| $NSE = 1 - \frac{\sum_{i=1}^n (Q_i - Q'_i)^2}{\sum_{i=1}^n (Q_i - \bar{Q}_i)^2}$ | >0.65 0.54 to 0.65 >0.50 | Very Good Adequate Satisfactory |
| $PBIAS = \frac{\sum_{i=1}^n (Q_i - Q'_i)^2}{\sum_{i=1}^n Q_i} * 100$ | < ± 10 ± 10 to ± 25 > ± 25% | Good Satisfactory Unsatisfactory |
| $RSR = \frac{RMSE}{STDEV_{obs}} = \frac{\sqrt{\sum_{i=1}^n (Q_i - Q'_i)^2 / n}}{\sqrt{\sum_{i=1}^n (Q_i - \bar{Q}_i)^2 / n}}$ | $0 \leq RSR \leq 0.5$ $0.5 \leq RSR \leq 0.6$ $0.6 \leq RSR \leq 0.7$ $RSR \geq 0.7$ | Very Good Good Satisfactory Unsatisfactory |
| $R^2 = \frac{[\sum_{i=1}^n (Q_i - \bar{Q}_i) \cdot (Q'_i - \bar{Q}'_i)]^2}{\sum_{i=1}^n (Q_i - \bar{Q}_i)^2 \cdot \sum_{i=1}^n (Q'_i - \bar{Q}'_i)^2}$ | 0 to 1 | 1 is optimum number |

Note: Q_i =observed flow, Q'_i = model/simulated flow
Source: (Rossi et al., 2008).

Table 5.4: Model performance statistics for calibration (2000-2007) and validation period (2008-2016) of the Ganges River basin.

| Period | Model Performance | | | | Rating |
|--------------------|-------------------|------|-------|------|-----------|
| | NSE | R2 | PBIAS | RSR | |
| Calibration | 0.82 | 0.84 | -7.60 | 0.42 | Very Good |
| Validation | 0.76 | 0.81 | -13.2 | 0.49 | Very Good |

The statistical model performance is given in Table 5.4. General reported rating of NSE, R^2 , PBIAS and RSR are given in Table 5.3.

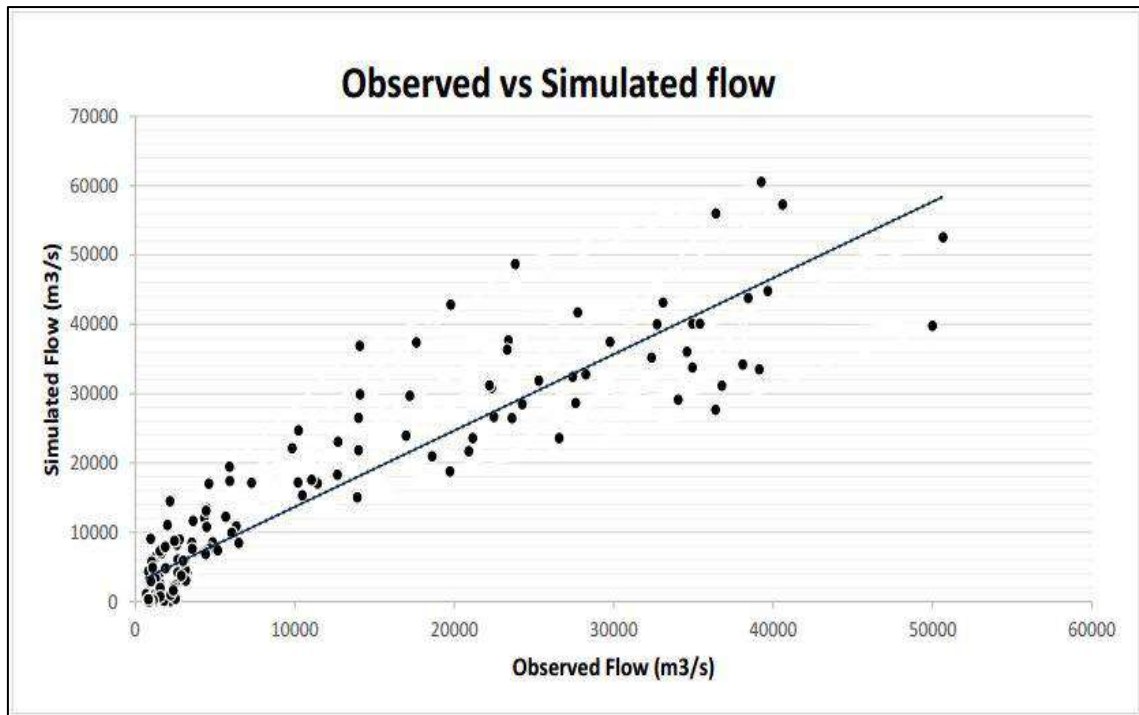


Figure 5.12: Scatter plot of observed vs simulated flow at Hardinge Bridge station for 2000-2016.

The NSE values are 0.82 and 0.76 for calibration and validation period respectively. The co-efficient of determination (R^2) values are 0.84 for calibration and 0.81 for validation period. The PBIAS and RSR values are found to be -7.60 and -13.2 in calibration stage and 0.42 and 0.49 in validation stage, respectively. These statistics indicates that SWAT generally performed well in both calibration and validation stages based on historical measured data for Ganges River Basin (Moriassi et.al., 2007), which establishes the basis for conducting climate change studies based on the simulations of SWAT, ‘unchanged. Scatter plot of observed vs simulated flow at Hardinge Bridge station for 2000-2016 has been plotted in Figure 5.12. Simulated flow shows good compliance with the observed flow at this station.

5.5 Water Balance of the Ganges River Basin

The computation includes all water receiving components (rainfall, snow fall.) within the hydrological system as well as water losses (evaporation, percolation, runoff etc.) from the hydrological system. The main principle of water balance is the difference between total incoming water and total losses equal to storage in the system. The water balance of the study area, the calibrated SWAT models have been simulated for the time period of 2000-2016 and the hydrological components have been analyzed to

compute average annual water balance. The simulation results of the annual water balance for the Ganges River Basin is given in Table 5.5.

Table 5.5: Annual average Water balance of Ganges River Basin (2000-2016).

| Water Balance Component | Amount(mm) |
|---|-------------------|
| Precipitation (PR) | 1257.5 |
| Snowfall (SF) | 48.41 |
| Surface runoff (SR) | 309.17 |
| Lateral soil flow contribution (LatQ) | 71.27 |
| Ground water contribution to streamflow (GWQ) | 275.56 |
| Revap or shallow aquifer recharges (SAR) | 38.64 |
| Deep Aquifer Recharges (DAR) | 16.48 |
| Total water yield/ flow (WY) | 666.82 |
| Percolation out of Soil (PER) | 329.57 |
| Actual Evapotranspiration (ET) | 547.8 |
| Potential Evapotranspiration (PET) | 798.99 |
| Change in soil water storage (SW) | 82.85 |

*Change in water storage, $SW=PR+SF-SR-LatQ-GWQ-SAR-DAR-ET$

The water balance in SWAT considers precipitation and snow fall as inflow to the sub-basin (the basic modeling unit in SWAT), evapotranspiration and deep percolation as loss and surface runoff and lateral flow as the outflow. From the output of model, it has observed that the average annual basin precipitation over the Ganges River Basin is about 1257.5 mm.

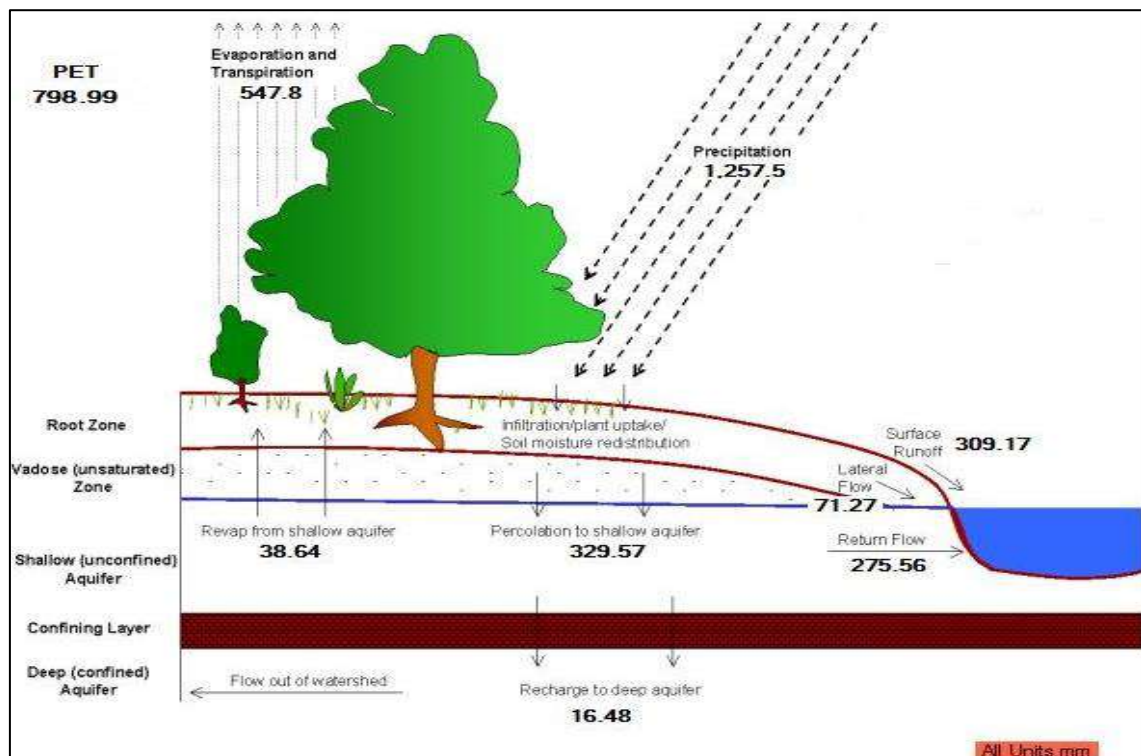


Figure 5.13 : Schematic figure of water balance of Ganges River Basin (SWAT-Check)

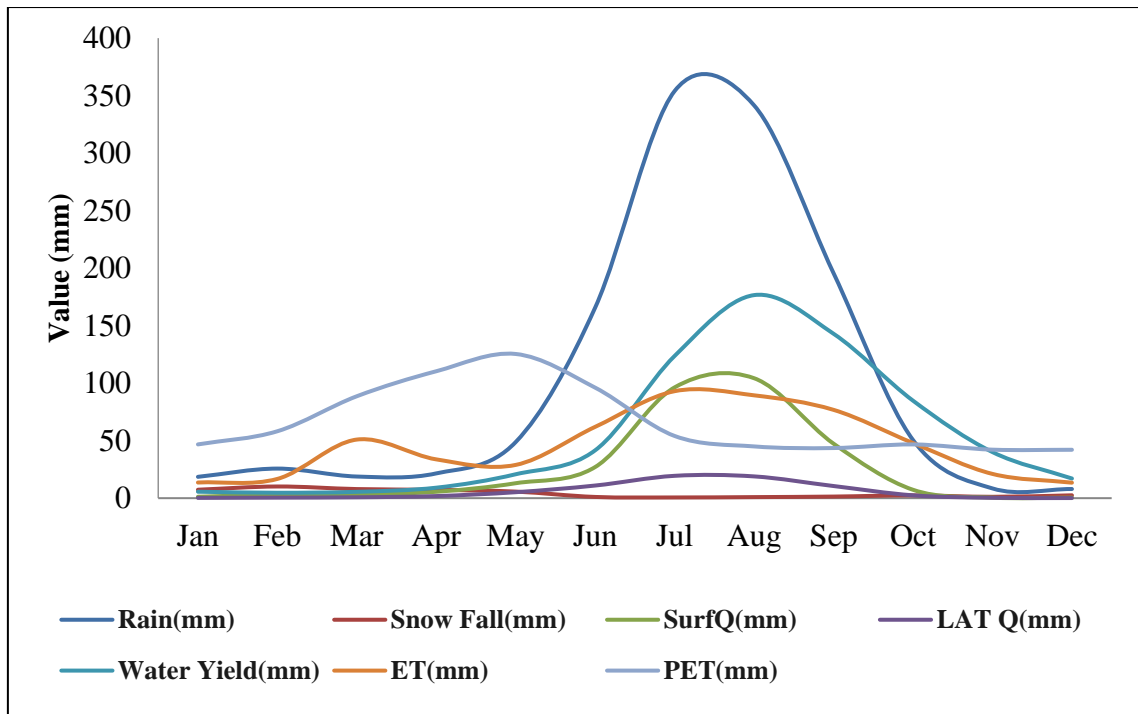


Figure 5.14: Average (2000-2016) monthly water availability of Ganges River Basin (all in mm)

The annual evapotranspiration loss is 547.68 mm, which is 42% of annual inflow for Ganges River Basins. Annual percolation in the Ganges River basin is 329.57 mm which is 25% of annual inflow. After the losses, the remaining water contributes to stream flow as surface runoff and lateral flow. A schematic figure of water balance in Ganges has been shown in Figure 5.13. In, Figure 5.14 Average (2000-2016) monthly water availability of Ganges River Basin has shown.

Table 5.6: Average monthly water availability of Ganges River Basin.

| Mon | Rain (mm) | Snow Fall (mm) | SurfQ (mm) | LAT Q (mm) | Water Yield (mm) | ET (mm) | PET (mm) |
|-----|-----------|----------------|------------|------------|------------------|---------|----------|
| Jan | 18.56 | 7.34 | 1.24 | 0.26 | 5.6 | 13.62 | 46.748 |
| Feb | 25.71 | 10.16 | 2.98 | 0.49 | 4.71 | 16.74 | 58.196 |
| Mar | 18.8 | 7.91 | 3.07 | 0.75 | 5.51 | 50.95 | 88.632 |
| Apr | 21.55 | 7.22 | 5.56 | 1.82 | 9.12 | 33.71 | 110.368 |
| May | 48.84 | 5.7 | 13.01 | 5.18 | 20.79 | 28.93 | 125.372 |
| Jun | 165.75 | 1.06 | 27.08 | 10.98 | 41.62 | 62.03 | 96.076 |
| Jul | 354.05 | 0.62 | 96.35 | 19.43 | 123.69 | 93.03 | 54.056 |
| Aug | 341.5 | 0.93 | 104.28 | 18.92 | 176.57 | 89.41 | 44.984 |
| Sep | 195.56 | 1.39 | 47.37 | 10.55 | 142.92 | 76.78 | 43.58 |
| Oct | 50.55 | 2.42 | 7.27 | 2.46 | 84.75 | 47.94 | 46.74 |
| Nov | 8.46 | 1.18 | 0.45 | 0.32 | 40.05 | 21.07 | 42.164 |
| Dec | 7.96 | 2.48 | 0.47 | 0.11 | 17.09 | 13.47 | 42.076 |

Monthly water availability of the base scenario has been analyzed and given in Table 5.6. Flows are mainly concentrated in the wet period (June to November). For Ganges basin peak flow occurs during July.

5.6 Selection of Climate Change Scenarios

The IPCC scenarios provide a mechanism to assess the potential impacts on climate change. Global emission scenarios were first developed by the IPCC in 1992 and were used in global general circulation models (GCMs) to provide estimates for the full suite of greenhouse gases and their potential impacts on climate change. Since then, there has been greater understanding of possible future greenhouse gas emissions and climate change as well as considerable improvements in the general circulation models. Many GCMs such as GFDL-ESM2M, MIROC, IPSL-CM5A-LR are available at different resolution for projecting future climate scenarios. There exist great variations in their output values from one GCM to another GCM. Some tend to give high changes in temperature and precipitation, whereas some provide moderate changes. Moreover, it is very much complex to work with all the GCMs at the same time. So, selecting a model for assessing the hydrological impact of climate change is one of the most important tasks. In the present study an attempt has been made to identify the warmest, coolest, wettest and driest scenarios for the Ganges River Basin. The selection of the ensemble member is based on the availability in the database at the time and also based on some literature about GCMs of South Asia of the study (Kamworapan, S. et al, 2019). All the projections were made by forcing the corresponding GCM with Representative Concentration Pathway – RCP 2.6, RCP 4.5 and RCP 8.5 (van Vuuren et al., 2011).

This scenario represents no change in current trend of greenhouse gas emission, i.e. business as usual. So far, the actual trend in emission is found to follow this pathway (Piontek et al., 2013; Friedlingstein et al., 2014). RCPs are four greenhouse gas trajectories adopted by the IPCC for its fifth Assessment Report (AR5). The four RCPs; RCP 2.6, RCP 4.5, RCP 6, and RCP 8.5, are named after a possible range of radiative forcing values in the year 2100. In this study, analysis have conducted with 3 RCP scenarios named RCP 2.6, RCP 4.5 and RCP 8.5 which depended on available data.

5.6.1 Analyzing the GCM Climate data

The extracted downscaled GCM data has been analyzed for the Ganges River Basin to find the wettest, driest, coolest and warmest model scenarios for each of the RCPs. The precipitation data have been analyzed for the relevant grids falling in the Ganges river Basin (Figure 5.15) for the different time periods with Baseline period of 2000 - 2016. Bias correction of this gridded data is not done because the study had focus on obtain change in streamflow. So present bias had not valid for future change in streamflow.

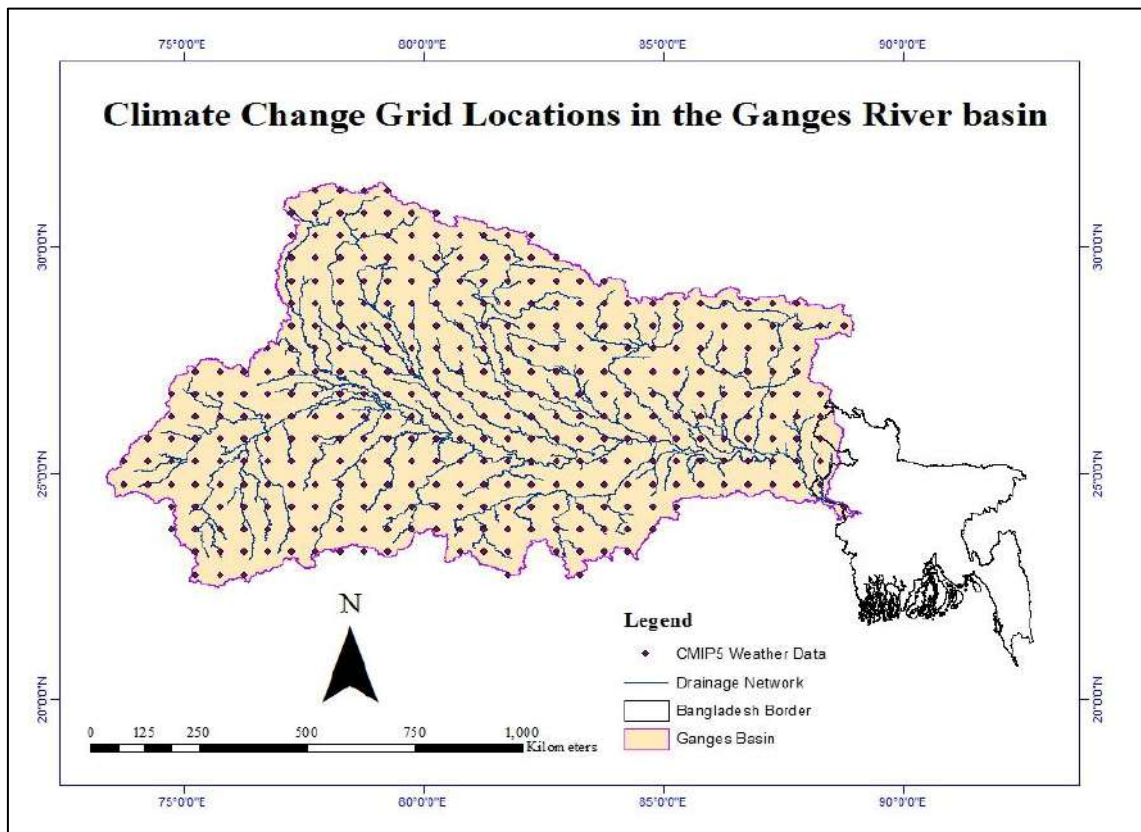


Figure 5.15: Climate Change Grid Locations in the Ganges River Basin

RCP 2.6 Scenario

The change of temperature and precipitation for three GCMs are analyzed for RCP 2.6. The results are separated for three periods; viz. 2010-2039 (2020s), 2040-2069 (2050s) and 2070-2099 (2080s). Monthly precipitation/temperature data for each GCM was averaged and compared with the base period data (2000-2016). Table 5.7 shows the changes in precipitation (%) for RCP 2.6.

$$\Delta P = \frac{P_{rcp} - P_{Base}}{P_{Base}} \times 100 \dots\dots\dots (5.1)$$

Here the change is denoted with ΔP which is the difference between model simulated and base data divided by base data and represented in percent. So,

Table 5.7: Precipitation change (%) for RCP 2.6.

| Model | 2020s | 2050s | 2080s |
|---------------------|--------------|--------------|--------------|
| BCC-CSM 1.1 | 7.36 | 14.36 | 19.20 |
| HadGEM-2 ES | -9.21 | -6.42 | -2.76 |
| IPSL-CM5A-LR | 6.33 | 10.77 | 11.89 |

From the Table 5.7, found that the changes in precipitation varies from -9.21% to 19.20%. For all model the precipitation has increased throughout 2020s, 2050s and 2080s while the maximum precipitation has increased for BCC-CSM 1.1 throughout 21th the century.

The temperature changes for RCP 2.6 is shown in Table 5.8. From the table, it had been seen that the temperature for all models increases to about 2^oC by the end of the century.

Here the change is denoted with ΔT which is the difference between model simulated and base data.

$$\Delta T = T_{\text{rcp}} - P_{\text{Base}} \dots \dots \dots (5.2)$$

Table 5.8: Temperature increase (°C) for RCP 2.6.

| Model | 2020s | 2050s | 2080s |
|---------------------|--------------|--------------|--------------|
| BCC-CSM 1.1 | 0.86 | 1.16 | 1.96 |
| HadGEM-2 ES | 1.29 | 1.92 | 1.97 |
| IPSL-CM5A-LR | 0.79 | 1.86 | 1.95 |

RCP 4.5 Scenario

Precipitation changes for RCP 4.5 is shown in Table 5.9. From the tables, it had seen that precipitation increases for GCMs due to RCP 4.5. Maximum increase in precipitation occurs in BCC-CSM 1.1 in the 2080s while the minimum increase in precipitation occurs in HadGEM-2 ES in the 2020s.

Table 5.9: Precipitation change (%) for RCP 4.5.

| Model | 2020s | 2050s | 2080s |
|---------------------|--------------|--------------|--------------|
| BCC-CSM 1.1 | 12.08 | 17.57 | 15.91 |
| HadGEM-2 ES | 0.57 | 3.02 | 3.82 |
| IPSL-CM5A-LR | 2.50 | 4.21 | 10.22 |

The increase in temperature for RCP 4.5 had shown in Table 5.10. Here, temperature increase varies from 0.86⁰C to 3.14⁰C increase in 2020s and 2080s respectively in the Ganges River Basin. Maximum increases for HadGEM-2 ES Model and minimum increases occurs in BCC-CSM 1.1.

Table 5.10: Temperature increase (°C) for RCP 4.5.

| Model | 2020s | 2050s | 2080s |
|---------------------|--------------|--------------|--------------|
| BCC-CSM 1.1 | 0.86 | 1.52 | 2.11 |
| HadGEM-2 ES | 1.31 | 2.22 | 3.14 |
| IPSL-CM5A-LR | 0.94 | 1.91 | 2.08 |

RCP 8.5 Scenario

Precipitation changes for RCP 8.5 had shown in Table 5.11. From the table, found that the precipitation increases for HadGEM-2 ES, IPSL-CM5A-LR and BCC-CSM 1.1 GCMs due to RCP 8.5. Maximum increase in precipitation occurs in BCC-CSM 1.1 in the 2080s while the maximum decrease in precipitation occurs in HadGEM - 2 ES in the 2020s.

Table 5.11: Precipitation change (%) for RCP 8.5.

| Model | 2020s | 2050s | 2080s |
|---------------------|--------------|--------------|--------------|
| BCC-CSM 1.1 | 12.30 | 18.61 | 21.08 |
| HadGEM-2 ES | -8.67 | -6.01 | -2.06 |
| IPSL-CM5A-LR | 6.70 | 11.57 | 19.10 |

The increase in temperature for RCP 8.5 had shown in Table 5.12. As for the temperature increase varies from 0.85⁰C to 5.84⁰C increase in 2020s and 2080s respectively in the Ganges River Basin. Maximum increases for HadGEM-2 ES Model and minimum increases occurs in BCC-CSM 1.1.

Table 5.12: Temperature increase (°C) for RCP 8.5.

| Model | 2020s | 2050s | 2080s |
|---------------------|--------------|--------------|--------------|
| BCC-CSM 1.1 | 0.85 | 1.90 | 2.42 |
| HadGEM-2 ES | 1.33 | 3.02 | 5.84 |
| IPSL-CM5A-LR | 1.04 | 3.00 | 5.45 |

5.6.2 Selection of Scenarios for Climate Change Analysis

Spatial distribution of temperature and precipitation of different GCMs had plotted for each of the scenarios and time periods (2020s, 2050s and 2080s). All distributions have been shown for selected scenarios had given in Appendix-C. All the GCM data had compared to obtain the warmest, coolest, driest, wettest, scenarios for the Ganges River Basin. From the analyzed GCMs climate data, Figure 5.16, Figure 5.17 and Figure 5.18 has been produced which shows ΔT vs ΔP Plot for 2020s, 2050s and 2080s respectively.

From Figure 5.16, it had found that temperature increases for HadGEM-2 ES of its RCP 8.5 scenario is maximum which is 1.33°C for the period of 2020s. This scenario considered as warmest condition. While the maximum precipitation increase occurs for BCC-CSM 1.1 of its RCP 8.5 scenario which is 12.30%. This scenario considered as wettest condition. And minimum increase of temperature occurs for IPSL-CM5A LR model for its RCP 2.6 scenario.

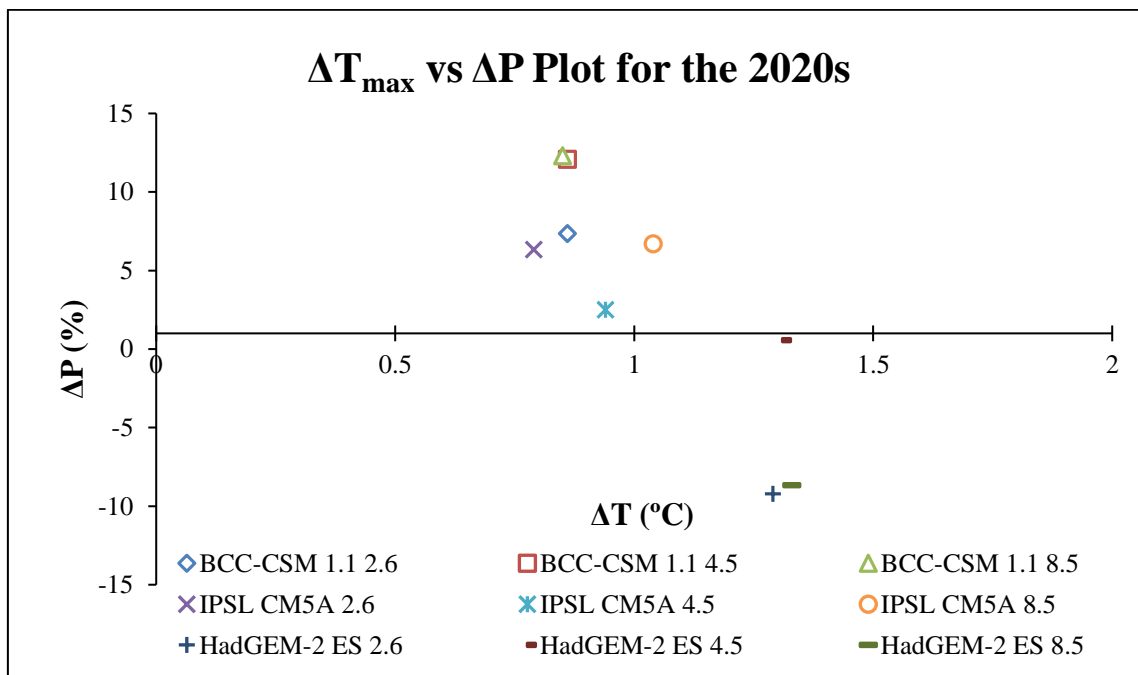


Figure 5.16: ΔT vs ΔP Plot for 2020s

Minimum change of precipitation for the period of 2020s is occurred at HadGEM-2 ES RCP 2.6 scenario. The value of Minimum change of precipitation is -9.21%. So HadGEM-2 ES RCP 2.6 scenario considered as driest scenario. Minimum increase in temperature had found in IPSL-CM5A LR RCP 2.6 scenario. Minimum temperature increase value for the period of 2020s is 0.79°C which is considered as coolest

condition. From Figure 5.17, it had found that temperature increases for HadGEM-2 ES RCP 8.5 scenario has maximum which is 3.02°C for the period of 2050s. This scenario considered as warmest condition. While the maximum precipitation increase occurs for BCC-CSM 1.1 RCP 8.5 scenario which is 18.61%.

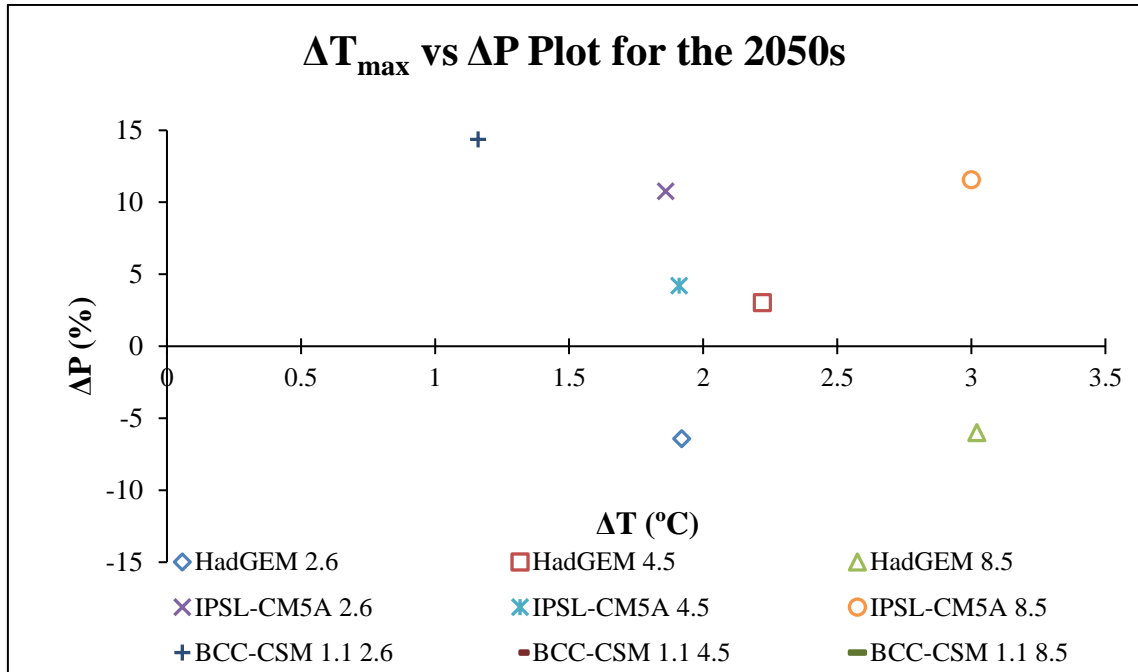


Figure 5.17: ΔT vs ΔP Plot for 2050s

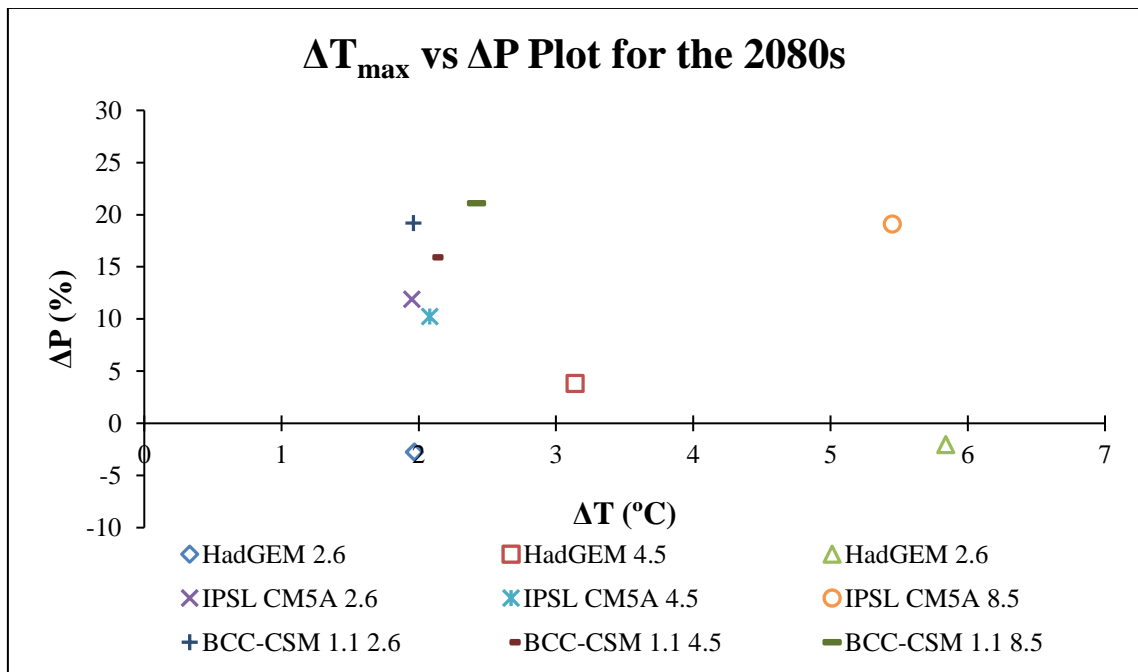


Figure 5.18 : ΔT vs ΔP Plot for the 2080s

This scenario considered as wettest condition. And minimum increase of temperature occurs for IPSL-CM5A LR RCP 2.6 scenario. Minimum change of precipitation for the period of 2080s is occurred at HadGEM-2 ES RCP 2.6 scenario which scenario

considered as driest scenario. Minimum increase in temperature had found in IPSL-CM5A LR RCP 2.6 scenario.

Minimum temperature increase value for the period of 2080s has 1.87°C which is considered as coolest condition.

In HadGEM-2ES RCP 2.6 scenario precipitation decreases comparing to base condition. From Figure 5.18, it had found that temperature increases for HadGEM-2 ES RCP 8.5 scenario is maximum which is 5.84°C for the period of 2080s. This scenario considered as warmest condition. While the maximum precipitation increase occurs for BCC-CSM 1.1 RCP 8.5 scenario which is 21.08%. This scenario considered as wettest condition.

And minimum increase of temperature occurs for IPSL-CM5A LR model for its RCP 2.6 scenario. Minimum change of precipitation for the period of 2080s is occurred at HadGEM-2 ES RCP 2.6 scenario which scenario considered as driest scenario. Minimum increase in temperature had found in IPSL-CM5A LR RCP 2.6 scenario. Minimum temperature increase value for the period of 2080s is 1.95°C which is considered as coolest condition. These selected scenarios had been shown in Table 5.13, Table 5.14 and Table 5.15 for 2020s, 2050s and 2080s respectively.

Table 5.13: Selected Scenarios for 2020s.

| <i>Scenario</i> | <i>Model</i> | <i>RCP</i> | <i>Δ Value</i> |
|-----------------|--------------|------------|--|
| <i>Wettest</i> | BCC-CSM 1.1 | 8.5 | $\Delta P = 12.30 \%$ |
| <i>Driest</i> | HadGEM-2 ES | 2.6 | $\Delta P = -9.21 \%$ |
| <i>Warmest</i> | HadGEM-2 ES | 8.5 | $\Delta T = 1.33 \text{ }^\circ\text{C}$ |
| <i>Coolest</i> | IPSL-CM5A-LR | 2.6 | $\Delta T = 0.79 \text{ }^\circ\text{C}$ |

Table 5.14: Selected Scenarios for 2050s.

| <i>Scenario</i> | <i>Model</i> | <i>RCP</i> | <i>Δ Value</i> |
|-----------------|--------------|------------|--|
| <i>Wettest</i> | BCC-CSM 1.1 | 8.5 | $\Delta P = 18.61 \%$ |
| <i>Driest</i> | HadGEM-2 ES | 2.6 | $\Delta P = -6.42 \%$ |
| <i>Warmest</i> | HadGEM-2 ES | 8.5 | $\Delta T = 3.02 \text{ }^\circ\text{C}$ |
| <i>Coolest</i> | IPSL-CM5A-LR | 2.6 | $\Delta T = 1.86 \text{ }^\circ\text{C}$ |

Table 5.15: Selected Scenarios for 2080s.

| <i>Scenario</i> | <i>Model</i> | <i>RCP</i> | <i>Δ Value</i> |
|-----------------|--------------|------------|--|
| <i>Wettest</i> | BCC-CSM 1.1 | 8.5 | $\Delta P = 21.08 \%$ |
| <i>Driest</i> | HadGEM-2 ES | 2.6 | $\Delta P = -2.76 \%$ |
| <i>Warmest</i> | HadGEM-2 ES | 8.5 | $\Delta T = 5.84 \text{ }^\circ\text{C}$ |
| <i>Coolest</i> | IPSL-CM5A-LR | 2.6 | $\Delta T = 1.95 \text{ }^\circ\text{C}$ |

5.7 Climate Change Impact Analysis on Flow of Ganges River Basin

After calibrations and validation of model (Article 5.3), the GCMs has been chosen. Then four different climate change scenarios such as Wettest, Driest, Warmest, Coolest (mentioned in Article 5.6) has been selected from the analysis of precipitation and temperature data of GCMs. To capture the change of flow for Wettest, Driest, Warmest, Coolest scenarios for the period of 2020s, 2050s, and 2080s the model has been simulated by 12 time. The water flow of each of the model analyzed and compared later.

Compared to the climate normal, the average annual temperature of the Ganges River Basin is projected to increase by 0.79 to 1.33°C, 1.86 to 3.02°C, and 1.95 to 5.84°C in 2020s, 2050s, and 2080s, respectively while precipitation is projected to change between -9.21% to 12.30% by 2020s, -6.42% to 18.61% by 2050s, and -2.76% to 21.08% by 2080s, respectively. In response to these projected changes to the primary climatic factors, SWAT simulated the mean annual streamflow for four projected climate change scenarios which are Wettest (BCC-CSM 1.1 RCP 8.5) Driest (HadGEM-2 ES 2.6), Warmest (HadGEM-2ES 8.5) and Coolest (IPSL-CM5A-LR 2.6) for 2020s, 2050s, and 2080s, with respect to that of the climate for normal period were analyzed.

It was found that the discharge of Ganges River Basin is increasing in all of the cases over the 21st century. The average annual flow volume of three time slices for four different scenarios shows that annual flow volume increases 24% by 2020s, 32% by 2050s and 37% by 2080s. The enhanced precipitation usually causes an increase in discharge while the enhanced temperature causes decrease in discharge by increasing evaporative losses.

5.7.1 Change of Monthly Flow for 2020s projection

In Figure 5.19 shows monthly mean discharge hydrograph at Hardinge Bridge station for 2020s projections. It is observed that flow hydrographs have a rising trend for 2020s with respect to base period, though the flow from December to February decreases for the future scenarios. In Figure 5.20 shows the Box and Whisker plot about future change of flow from baseline at Hardinge Bridge transit (SW 90) which is outlet of Ganges River Basin. The maximum change of avg. monthly flow for July, August and September might increase 22%, 29% and 40% respectively. Change monthly flow for

May, June has been found greater than February, March. The difference of maximum and minimum range for November and December are greater than January and October. In May flow is change of flow is decreasing. Future monthly flow (m^3/s) at SW 90 for 2020s for different Climate Change scenarios has given in Appendix B1.

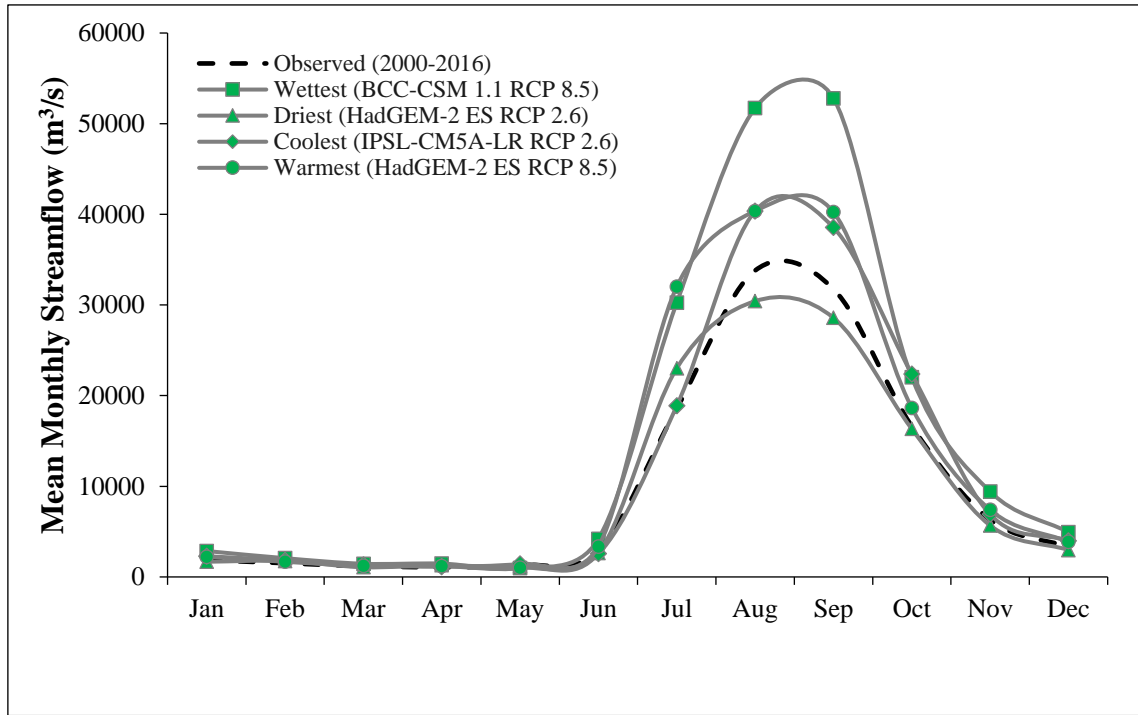


Figure 5.19: Mean monthly discharge (m^3/s) for 2020s at Hardinge Bridge station for Ganges River Basin

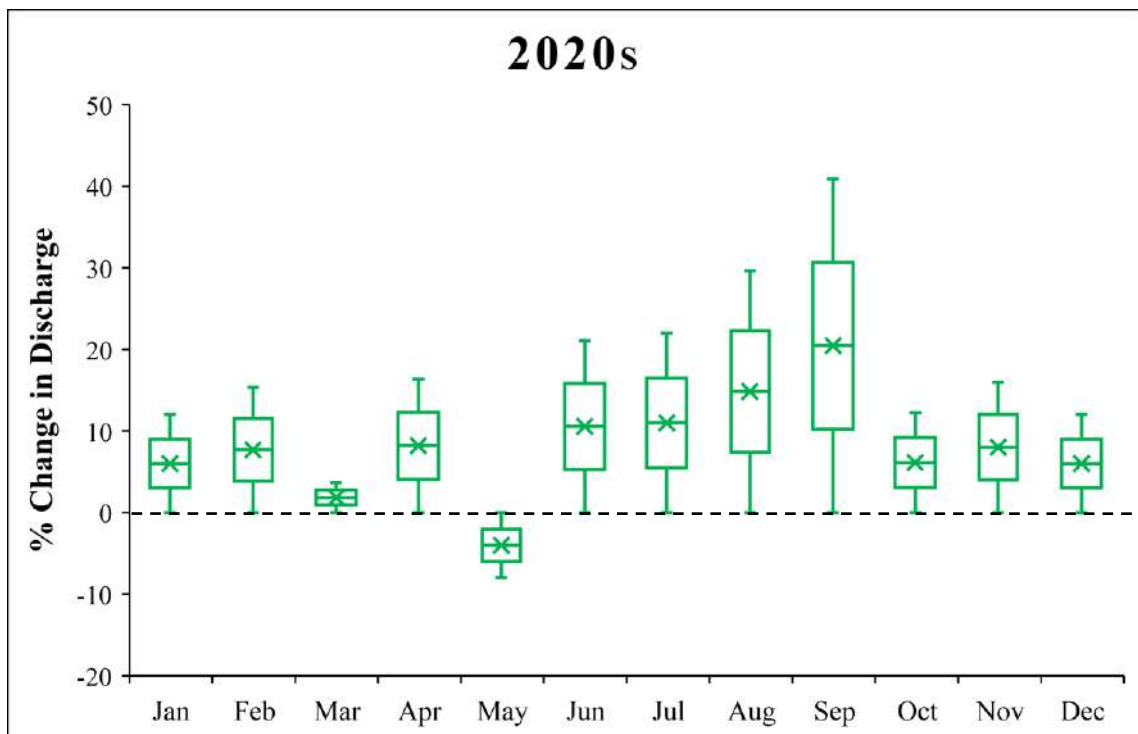


Figure 5.20: Change in monthly flow of the Ganges Basin at Hardinge Bridge for 2020s

The highest discharge values may occur in the month of September and it is within 28,000 m³/s to 55,000 m³/s.

5.7.2 Change of Monthly Flow for 2050s projection

Figure 5.21 shows monthly mean discharge hydrograph at Hardinge Bridge station for 2050s projection. It is observed that flow hydrographs have a rising trend for 2050s with respect to base period, though the flow from December to February decreases for the future scenarios. In the Figure 5.21 shows the volume of monthly flow for 2050s projections and Figure 5.22 shows the Box and Whisker plot about future change of flow from baseline at Hardinge Bridge transit (SW 90) which is outlet of Ganges River Basin.

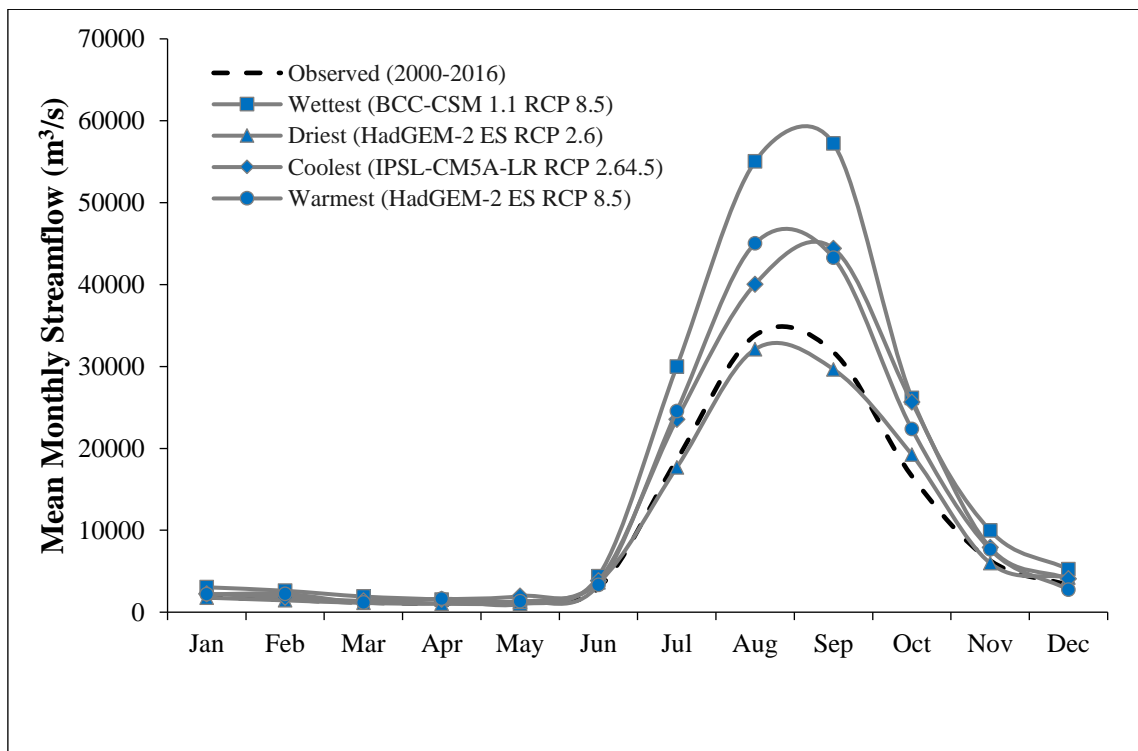


Figure 5.21: Mean monthly discharge (m³/s) for 2050s at Hardinge Bridge station for Ganges River Basin

The maximum change of monthly flow for September might increase 54%. Change monthly flow for July, August has been found greater than November, December. The difference of maximum and minimum range for November and December are greater than January and March, so there might be uncertainty in the change of monthly flow for November and December. In May flow is change of flow is decreasing. Future monthly flow (m³/s) at SW 90 for 2050s for different Climate Change scenarios has

given in Appendix B2. The highest discharge values may occur in the month of September and it is within 29,000 m³/s to 57,000 m³/s.

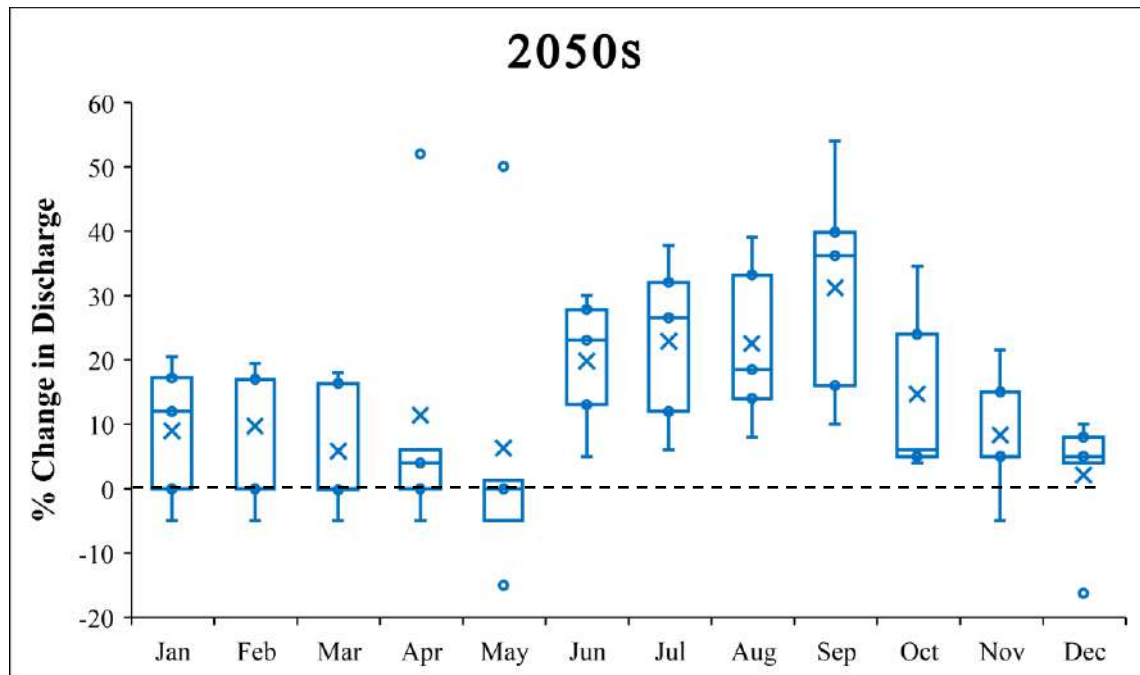


Figure 5.22: Change in monthly flow of the Ganges Basin at Hardinge Bridge for 2050s

5.7.3 Change of Monthly Flow for 2080s projection

Figure 5.23 shows monthly mean discharge hydrograph at Hardinge Bridge station for 2080s projection. It is observed that flow hydrographs have a rising trend for 2080s with respect to base period, though the flow from December to February decreases for the future scenarios. In the Figure 5.23 shows the volume of monthly flow for 2080s projections and Figure 5.24 shows the Box and Whisker plot about future change of flow from baseline at Hardinge Bridge transit (SW 90) which is outlet of Ganges River Basin. The maximum change of monthly flow for April, May and September might increase 102%, 85% and 55% respectively. Change monthly flow for May, June has been found less than February, March. So, there might be uncertainty in the change of monthly flow for November and December.

Future monthly flow (m³/s) at SW 90 for 2080s for different Climate Change scenarios has given in Appendix B3. The highest discharge values may occur in the month of September and it is within 32,000 m³/s to 74,000 m³/s.

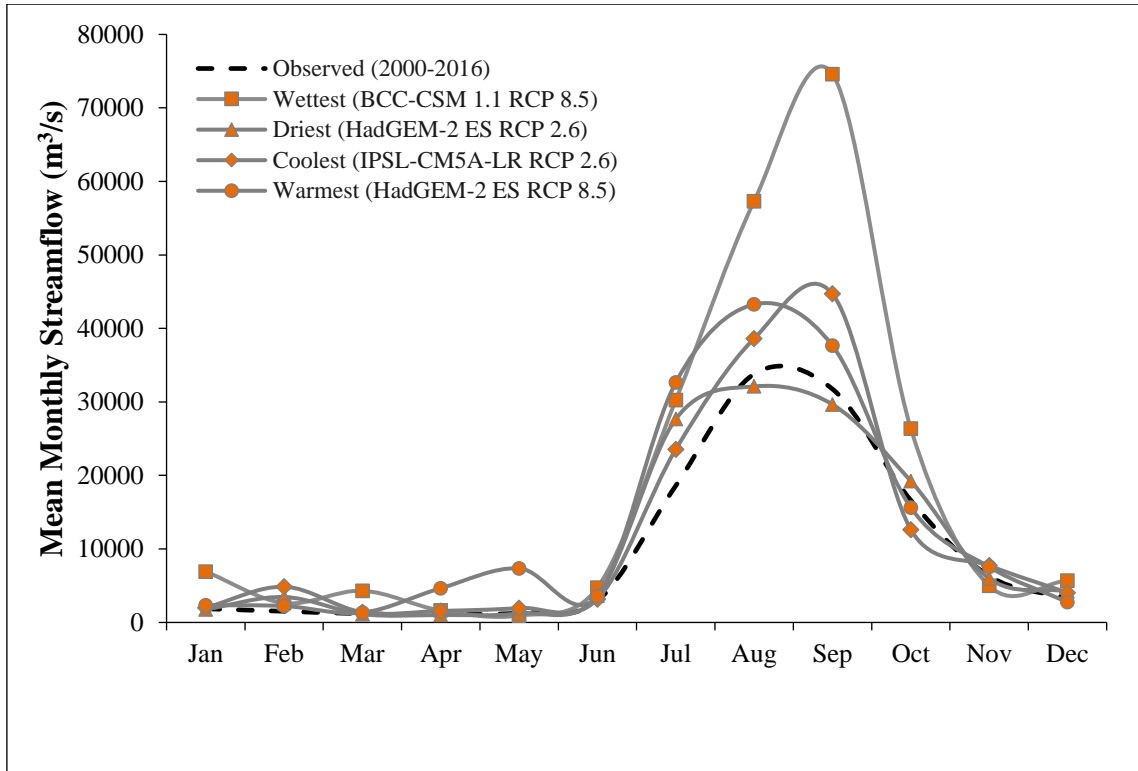


Figure 5.23: Mean monthly discharge (m³/s) for 2080s at Hardinge Bridge station for Ganges River Basin

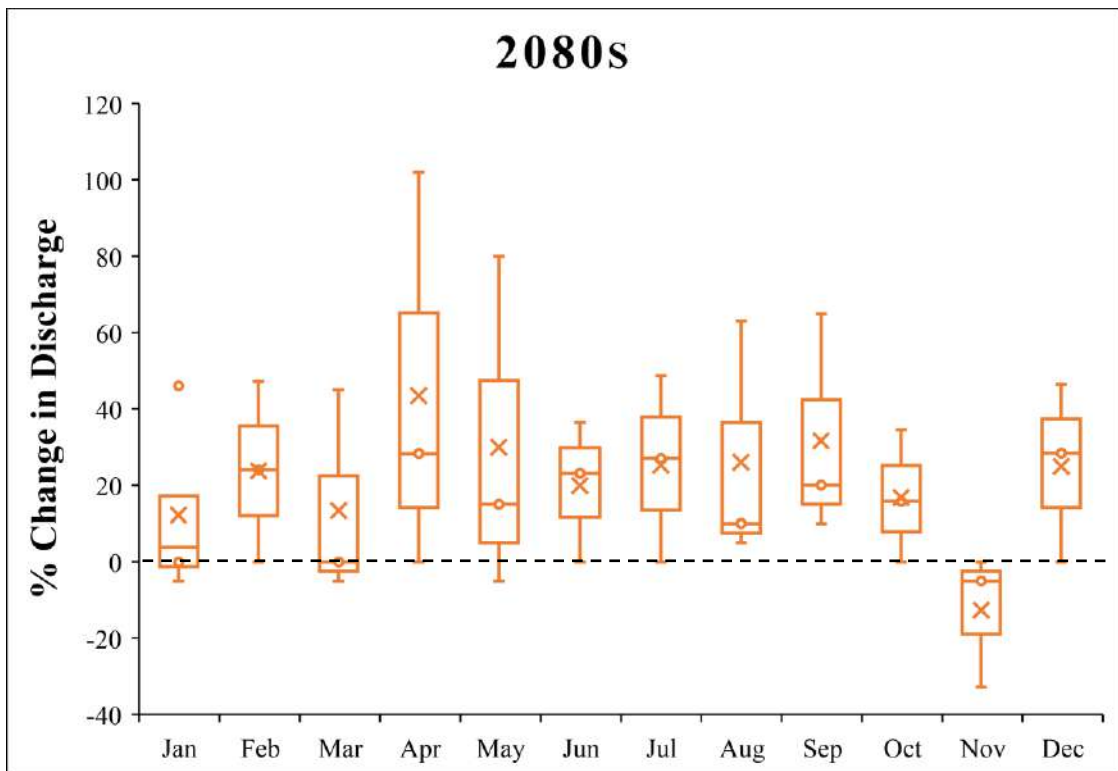


Figure 5.24: Change in monthly flow of the Ganges Basin at Hardinge Bridge for 2080s

5.7.4 Change of Monthly Flow for different Period for different scenarios

In figure 5.25 average monthly flow for different period with respect to base period for wettest scenario had showed. An increasing trend of flow had found in this figure. Mean monthly flow had increased with the time passing. Highest mean monthly flow had occurred at 2080s with respect to base or observed flow.

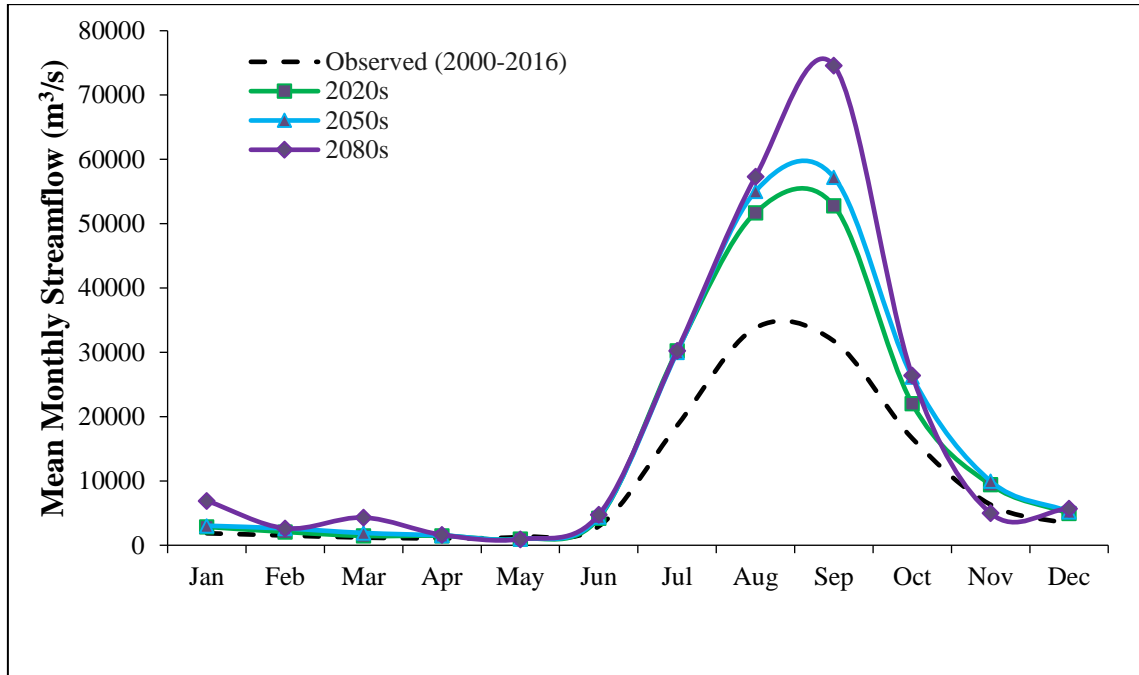


Figure 5.25: Average monthly discharge (m^3/s) of Wettest Scenario for 2020s, 2050s and 2080s

Flow for Driest Scenario

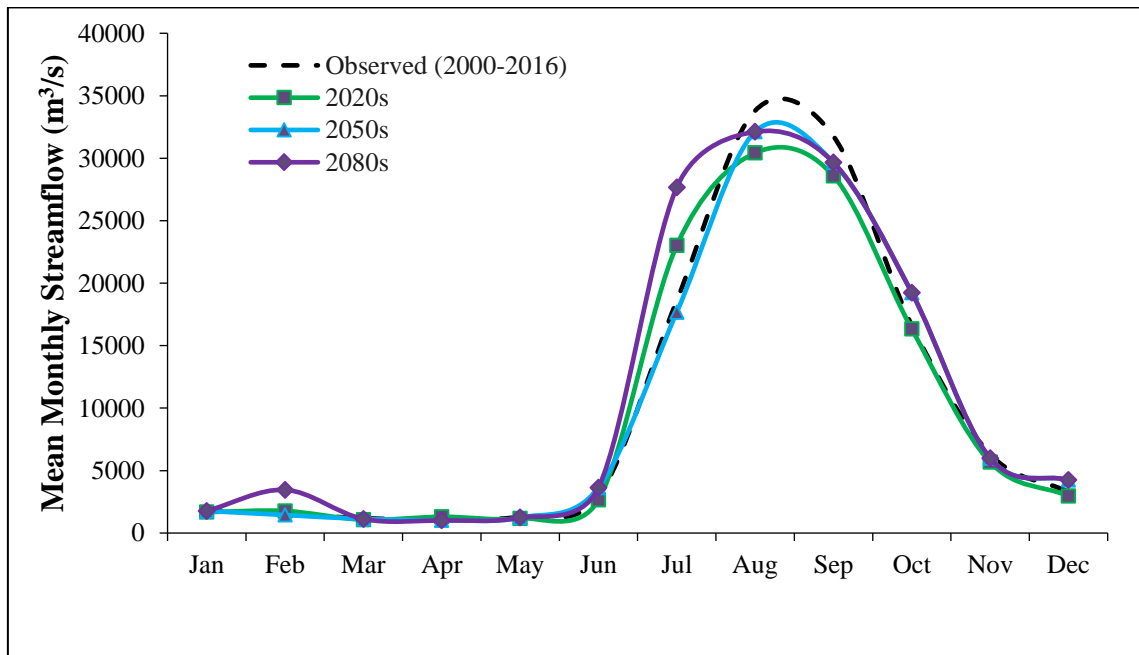


Figure 5.26: Average monthly discharge (m^3/s) of Driest Scenario for 2020s, 2050s and 2080s

In figure 5.26 average monthly flow for different period with respect to base period for driest scenario had showed. A decreasing trend of flow had found in this figure. Mean monthly flow had decreased with the time passing. Maximum decreasing of mean monthly flow had occurred at 2020s with respect to base or observed flow.

Flow for Coolest Scenario

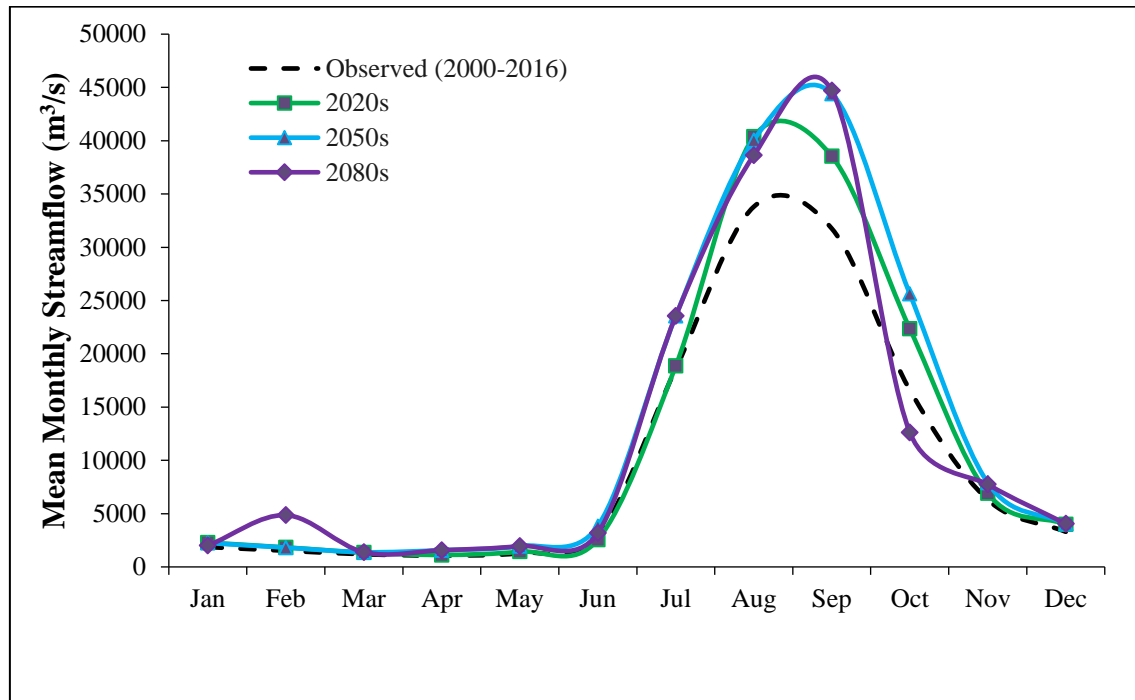


Figure 5.27: Average monthly discharge (m³/s) of Coolest Scenario for 2020s, 2050s and 2080s

In figure 5.27 average monthly flow for different period with respect to base period for coolest scenario had showed. An increasing trend of flow had found in this figure. Mean monthly flow had decreased with the time passing. Maximum increasing of mean monthly flow had occurred at 2080s with respect to base or observed flow.

Flow for Warmest Scenario

In figure 5.28 average monthly flow for different period with respect to base period for warmest scenario had showed. An increasing trend of flow had found in this figure. Mean monthly flow had increased with the time passing. Maximum increasing of mean monthly flow had occurred at 2050s with respect to base or observed flow.

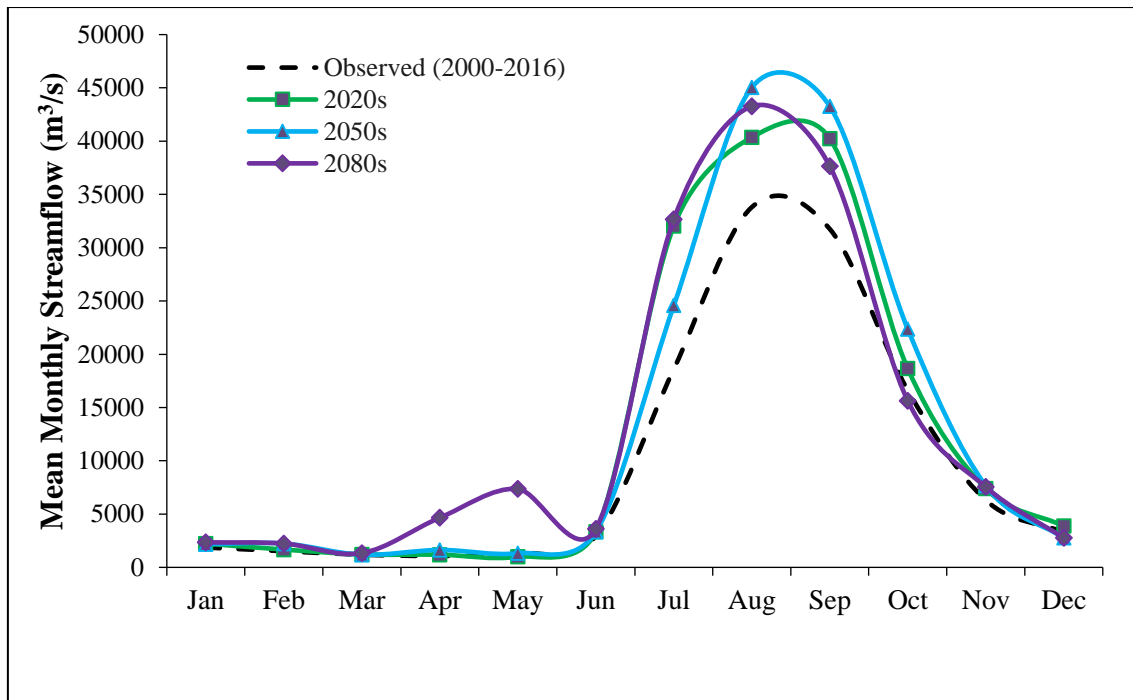


Figure 5.28: Average monthly discharge (m^3/s) of Warmest Scenario for 2020s, 2050s and 2080s

5.7.5 Change of Future Seasonal Flow of Ganges River Basin

Dry Period Flow Analysis for 2020s

Average dry season (Dec-May) flow had changed significantly for all the scenarios in 2020s (Table 5.16). Maximum projected increase in discharge was found for BCC-CSM 1.1 RCP 8.5 with 29.11% and minimum change in projected discharge was -0.44% which had found in HadGEM-2 ES (RCP 2.6) All other scenarios, viz. IPSL-CM5A-LR RCP 2.6 as coolest condition had given 15.24% increase in discharge and HadGEM-2 ES (RCP 8.5) as warmest condition had given an increased projected discharge with 6.16%.

Wet Period Flow Analysis for 2020s

Average wet season (Jun-Nov) flow had increase for almost all the scenarios (Table 5.16). Highest increase in projected flow was found for BCC-CSM 1.1 RCP 8.5 with 51.10% change which had considered as a wettest condition. In this condition, the discharge had increased as expected because of increase in precipitation. Minimum change in discharge in wet period had occurred in HadGEM-2 ES (RCP 2.6) with -3.00% which is considered as driest condition. All other scenarios viz; IPSL-CM5A-

LR (RCP 2.6) and HadGEM-2 ES (RCP 8.5) gave change in flow with 12.26% and 26.95% change consecutively for the wet period of 2020s compared to the base flow.

Table 5.16: Change in Discharge (%) for all the four scenarios for 2020s.

| | Wettest (BCC-CSM 1.1 RCP 8.5) | Driest (HadGEM-2 ES RCP 2.6) | Coollest (IPSL-CM5A- LR RCP 2.6) | Warmest (HadGEM-2 ES RCP 8.5) |
|---|--|---|---|--|
| Mean Dry Season (Dec to May) | 29.11 | -0.44 | 15.24 | 6.16 |
| Mean Wet Season (Jun to Nov) | 51.10 | -3.00 | 12.26 | 26.95 |

Dry Period Flow Analysis for 2050s

Average dry season (Dec-May) flow had increased for all the scenarios in 2050s (Table 5.17). Maximum projected increase in discharge was found for BCC-CSM 1.1 RCP 8.5 with 45.34% and minimum change in projected discharge was 0.57% which was obtained for HadGEM-2 ES RCP 2.6. In this condition discharge changes minimum as expected because in driest condition precipitation had occurred in minimum rate. All other scenarios, viz. IPSL-CM5A-LR RCP 2.6 as coolest condition had given 29.25% increase in discharge and HadGEM-2 ES (RCP 8.5) as warmest condition had given an increased projected discharge with 16.90% consecutively.

Table 5.17: Change in Discharge (%) for all the four scenarios for 2050s.

| | Wettest (BCC-CSM 1.1 RCP 8.5) | Driest (HadGEM-2 ES RCP 2.6) | Coollest (IPSL-CM5A- LR RCP 2.6) | Warmest (HadGEM-2 ES RCP 8.5) |
|---|--|---|---|--|
| Mean Dry Season (Dec to May) | 45.34 | 0.57 | 29.25 | 16.90 |
| Mean Wet Season (Jun to Nov) | 61.55 | 2.87 | 32.38 | 28.45 |

Wet Period Flow Analysis for 2050s

Average wet season (Jun-Nov) flow was found to increase for almost all the scenarios (Table 5.17). Highest increase in projected flow had found for BCC-CSM 1.1 RCP 8.5 with 61.55% change which had considered as a wettest condition. In this condition, the discharge had increased because of increase in precipitation. Minimum change in discharge in wet period had occurred in HadGEM-2 ES (RCP 2.6) with 2.87% which is

considered as driest condition. All other scenarios viz; IPSL-CM5A-LR (RCP 2.6) and HadGEM-2 ES (RCP 8.5) showed change in flow with 32.38% and 28.45% change consecutively for the wet period of 2050s compared to the base flow.

Dry Period Flow Analysis for 2080s

Average dry season (Dec-May) flow had increase for all the scenarios in 2080s (Table 5.18). Maximum projected increase in discharge was found for HadGEM-2 ES RCP 8.5 with 144.37% and minimum change in projected discharge was 22.66% which had found in HadGEM-2 ES RCP 2.6. In this condition discharge decrease as expected because in driest condition precipitation had occurred in minimum rate. All other scenarios, viz. IPSL-CM5A-LR RCP 2.6 as coolest condition had given 60.49% change in discharge and BCC-CSM 1.1 RCP 8.5 as wettest condition had given an increased projected discharge with 117.25% consecutively.

Table 5.18: Change in Discharge (%) for all the four scenarios for 2080s.

| | Wettest (BCC-CSM 1.1 RCP 8.5) | Driest (HadGEM-2 ES RCP 2.6) | Coolest (IPSL-CM5A- LR RCP 2.6) | Warmest (HadGEM-2 ES RCP 8.5) |
|---|--|---|--|--|
| Mean Dry Season (Dec to May) | 117.25 | 22.66 | 60.49 | 144.37 |
| Mean Wet Season (Jun to Nov) | 61.02 | 11.83 | 14.74 | 26.38 |

Wet Period Flow Analysis for 2080s

Average wet season (Jun-Nov) flow had increased for all the scenarios (Table 5.18). Highest increase in projected flow had found for BCC-CSM 1.1 RCP 8.5 with 61.02% change which had considered as a wettest condition. In this condition, the discharge had increased as expected because of increase in precipitation. Minimum change in discharge in wet period had occurred in HadGEM-2 ES (RCP 2.6) with 11.83% which had considered as driest condition. All other scenarios viz; IPSL-CM5A-LR (RCP 2.6) and HadGEM-2 ES (RCP 8.5) gave change in flow with 14.74% and 26.38% change consecutively for the wet period of 2080s compared to the base flow.

5.7.6 Change of Mean Annual Flow of Ganges River Basin at Hardinge Bridge

The model simulated percentage changes in the mean annual streamflow from the climate normal (2000-2016) with respect to climate change scenarios. Figure 5.29 shows Box and Whisker plots of differences in the average annual average discharge simulated by the selected GCMs with respect to the climate normal period. A gradual increase in annual average flow is found from 2020s to 2080s. The percentage changes of model simulated average annual discharge from the climate base period with respect to different climate change scenarios has been plotted in Figure 5.30. The percentage changes in average annual flow from baseline period for 2020s, 2050s and 2080s are 24%, 32% and 37% respectively. A gradual increase in annual average flow is found from 2020s to 2080s.

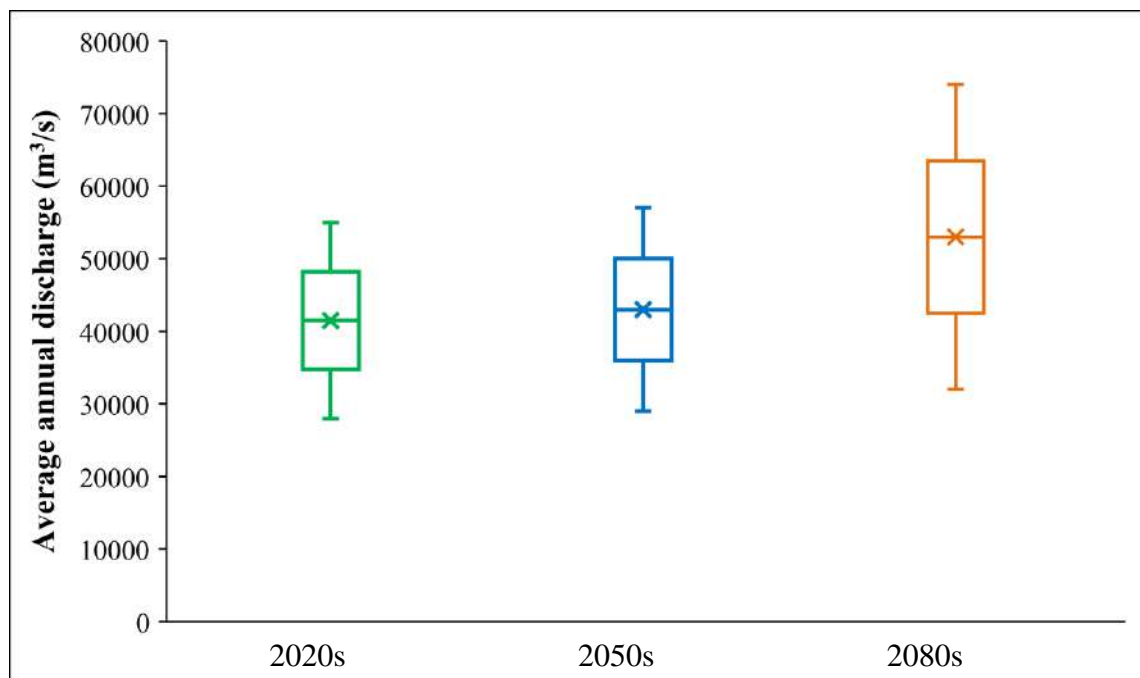


Figure 5.29: Box-plot of Average annual discharge (m^3/s) of all the scenarios for 2020s, 2050s and 2080s

In 2020s, mean annual streamflow is found to increase in all the scenarios. Highest discharge value in 2020s had varied from 28,000 m^3/s to 55,000 m^3/s . In 2050s, highest streamflow occurs in September and it had varied from 29,000 m^3/s to 57,000 m^3/s . And in 2050s increasing trend of discharge is also noticed. In 2080s highest discharge had found for 21st century which is 74,000 m^3/s . In this time period discharge also showed increasing trend.

From figure 5.30 percentage change in average annual discharge has been showed. The percentage changes in average annual flow from baseline period for 2020s, 2050s and

2080s are 24%, 32% and 37% respectively. It has been noticed that the average annual discharge had in increasing trend throughout at the end of the 21st century.

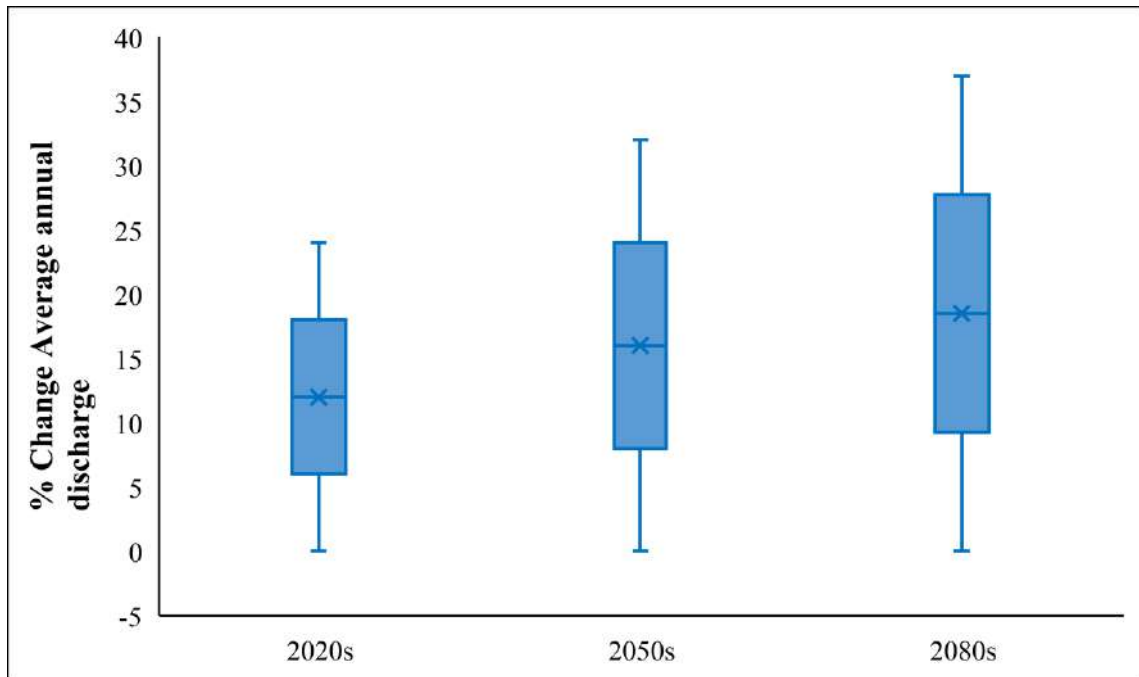


Figure 5.30: Box-plot of % Change of Average annual discharge of all the scenarios for 2020s, 2050s and 2080s

Percentage change of Q_{90} (High Flow) compared with the baseline period

To serve as an indicator of the future flood events Q_{90} flows had been calculated. And the changes in the magnitude of Q_{90} flows gradually increasing trend can be observed throughout the 21st century.

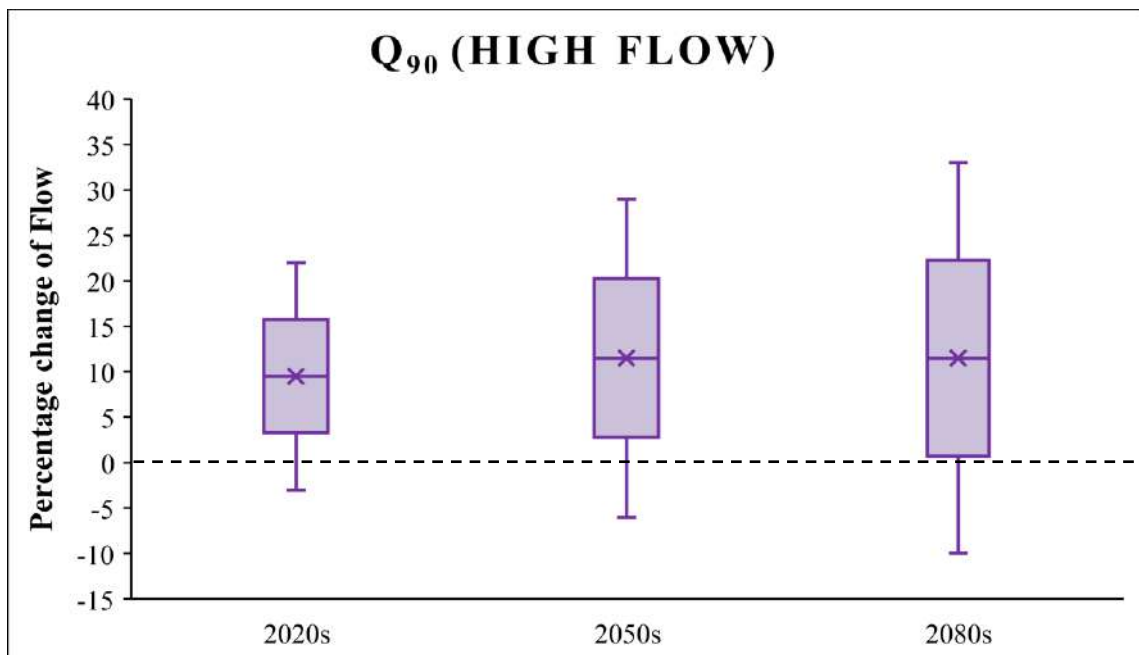


Figure 5.31: Percentage change of Q_{90} (High Flow) compared with the baseline period

5.8 Impact of Land Use changes on Flow of Ganges River Basin

In recent years, pressure has increased on the river canals to maintain flows during the dry season, due to the introduction of high-water-intensity crops, agricultural expansion and population growth (Sapkota et al., 2013). The urban area notably increased in the upstream area of Ganges River Basin by converting agricultural area into impervious area (Bhagat R. B. 2011). Similar trend continued in the following years, where the development of urban areas expanded in the catchment at the expense of agricultural area and forest area resulting in major loss in the green area.

To evaluate the effects of land use changes, the SWAT model calibrated and validated for streamflow discharge was used to simulate different land use scenarios. To analyze the impact on land use changes, according to a study of Anand J. et. al, 2018, an additional 20% 30% and 40% area of Ganges River Basin has been considered as urbanized for 2020s, 2050s and 2080s respectively. And also, additional 10% 15% and 20% area of Ganges River Basin has been considered as deforested for 2020s, 2050s and 2080s respectively which had showed in Table 5.19.

Table 5.19: Percentage of Area cover for different land use scenarios.

| Land Use Type | Area Cover (%) | Scenario-1 (40% Urbanization Increase) | Scenario-2 (20% Deforestation increase) |
|---------------------------|----------------|--|---|
| Water body | 3.47% | 3.47% | 3.47% |
| Forest | 16% | 15.28% | 12.8% |
| Permanent Wetland | 7.87% | 7.34% | 7.87% |
| Urban and Built-Up | 4.28% | 6.00% | 6.00% |
| Grasslands and Barren | 1.87% | 1.67% | 3.35% |
| Agriculture and Croplands | 65.57% | 65.27% | 65.57% |
| Snow and Ice | 0.94% | 0.94% | 0.94% |

5.8.1 Changes on Flow due to Urbanization

After simulation of SWAT model with the land use scenarios, in Figure 5.32 shows monthly mean discharge hydrograph at Hardinge Bridge station for 20%, 30% and 40% area increase of urbanization. Future monthly flow (m^3/s) at SW 90 for different Land Use scenarios has given in Appendix B4.

From the result it was found that, Streamflow had decreased on avg. by 5%, 11% and 16% during the pre-monsoon months of February to April for 2020s, 2050s and 2080s. In contrast, compared to the baseline scenario, streamflow was projected to increase by

7%, 34% and 46% during monsoon period of August to October for 2020s, 2050s and 2080s respectively. The maximum differences were predicted to occur during the peak monsoon months of July and August. July streamflow was predicted to decrease and August streamflow was predicted to increase under all the scenarios, compared to the baseline.

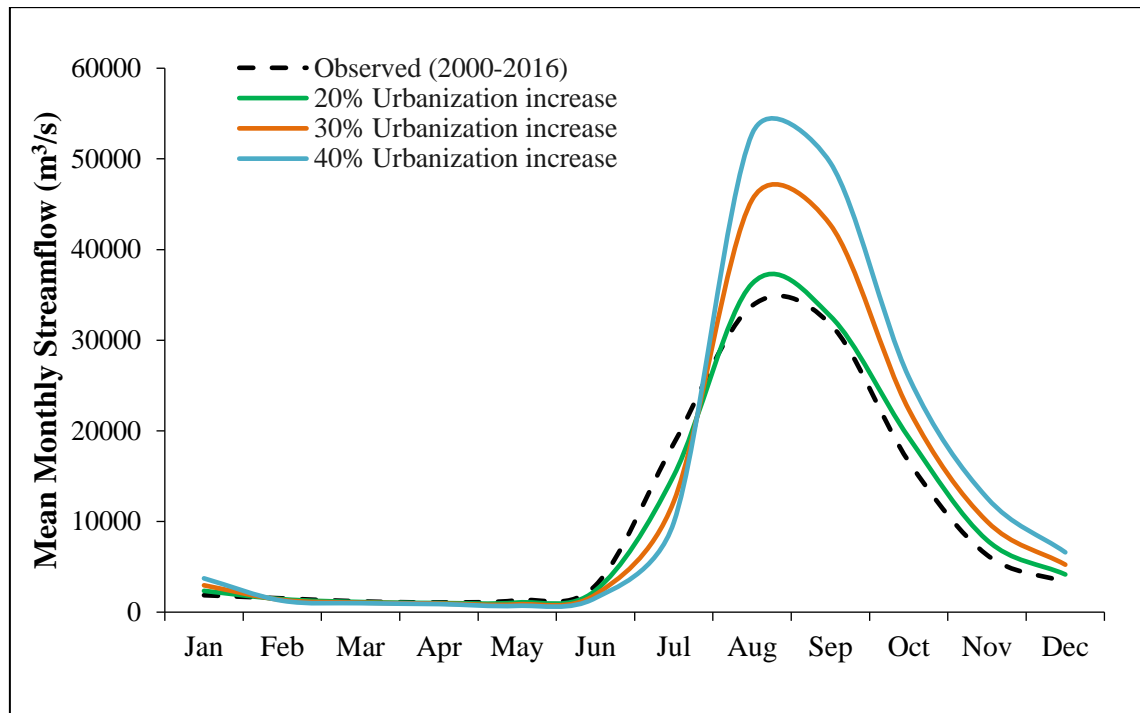


Figure 5.32: Average annual discharge for different urbanization scenarios

So, for 2020s is not significant from base line, for 2050s, percentage change of average annual discharge is about 21%, and the maximum percentage change of average annual discharge occurred 36% for 40% urbanization increasing scenario.

5.8.2 Changes on Flow due to Deforestation

After simulation of SWAT model with the land use scenarios, in Figure 5.33 shows monthly mean discharge hydrograph at Hardinge Bridge station for 10%, 15% and 20% area increase of deforestation.

From the result it was found that, Streamflow had decreased on avg. by 11%, 17% and 15% during the pre-monsoon months of February to April for 2020s, 2050s and 2080s. In contrast, compared to the baseline scenario, streamflow was projected to increase by 6%, 28% and 40% during monsoon period of August to October for 2020s, 2050s and 2080s respectively. The maximum differences were predicted to occur during the peak

monsoon months of July and August. July streamflow was predicted to decrease and August streamflow was predicted to increase under all the scenarios, compared to the baseline.

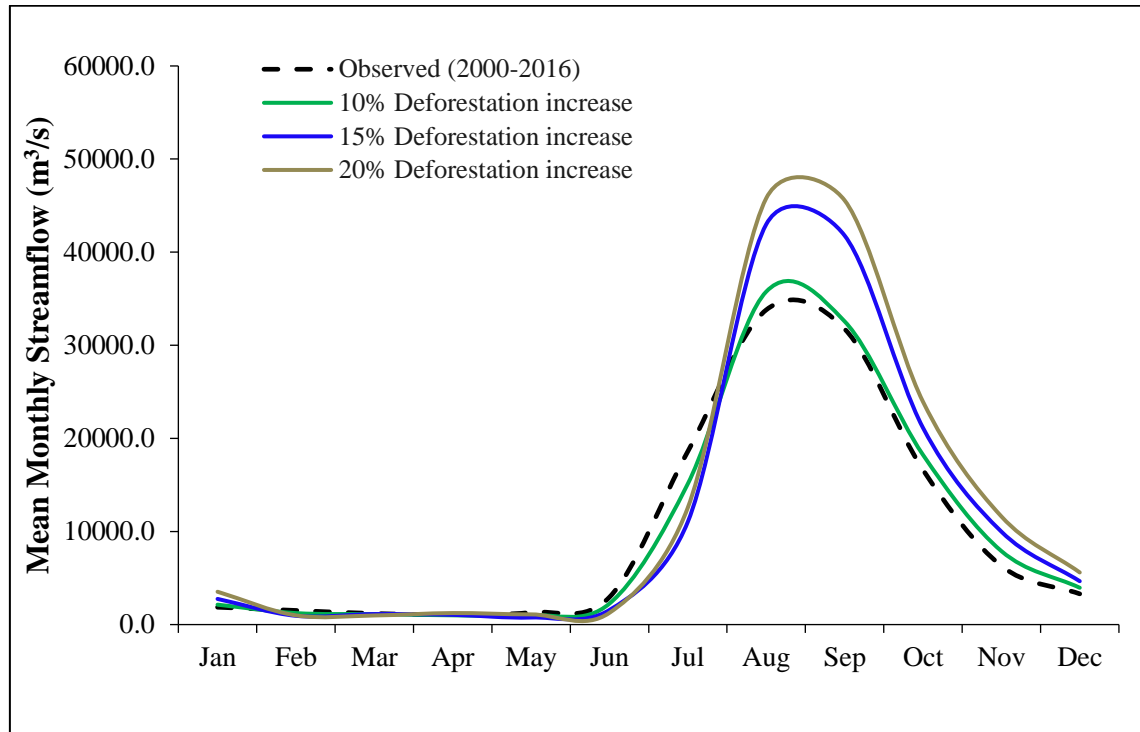


Figure 5.33: Average annual discharge for different deforestation scenarios

So, for 2020s is not significant from base line, for 2050s, percentage change of average annual discharge is about 16%, and the maximum percentage change of average annual discharge occurred 25% for 20% deforestation increasing scenario.

5.9 Comparison between previous study and this study

The main focuses of this study have been developing a hydrological model of Ganges River Basin using SWAT model to estimate present and future discharge considering climate and land use change scenarios in future.

The results of this study indicate that the discharge will decrease during dry period and increase during monsoon. The average annual flow volume increases 24%, 32% and 37% for 2020s, 2050s and 2080s. An increase in urbanization area, about 20% to 40% for all over Ganges River Basin, have been done to analyze the changes of discharge. Simulation results showed that land use changes have resulted for 2020s is not significant from base line. For 2050s and 2080s percentage change of average annual discharge is about 21% and 36 % respectively. For additional increase in deforestation

in Ganges River Basin area, annual average water flow at Hardinge Bridge transit increase about 16% to 25%.

In recent years, a number of studies have assessed the impact of climate change and land use change on water resources in Ganges River Basin.

Tsarouchi (2018) found the changes in the near-future (years 2030–2035) hydrologic fluxes arise under future land-cover and climate change scenarios pointing in Ganges River Basin towards a severe increase in high extremes of flow: the multi-model means of the 95th percentile of streamflow is projected to increase by 63% under the combined land-use and climate change high emissions scenario (RCP 8.5). The changes in all examined hydrological components are greater in the combined land-use and climate change experiment.

Aminul (2017) has been found that the average annual temperature will increase by 1.3 to 1.8°C for the Ganges River Basin. It has been also found that the basin-wise annual precipitation will increase by 6-10% for the Ganges. Finally, it has been found that there is an increase of flow during wet season and a decrease in the dry season.

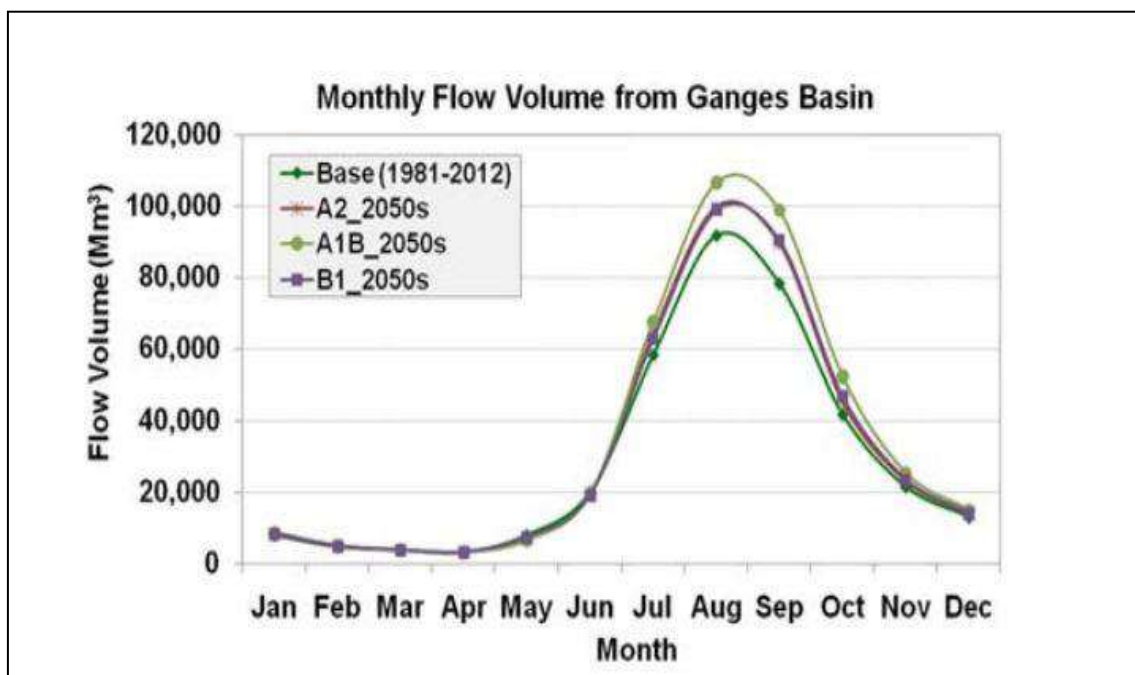


Figure 5.34: Comparison of climate change scenarios with base for the Ganges basin (Source: Islam, M. A. et al., 2017)

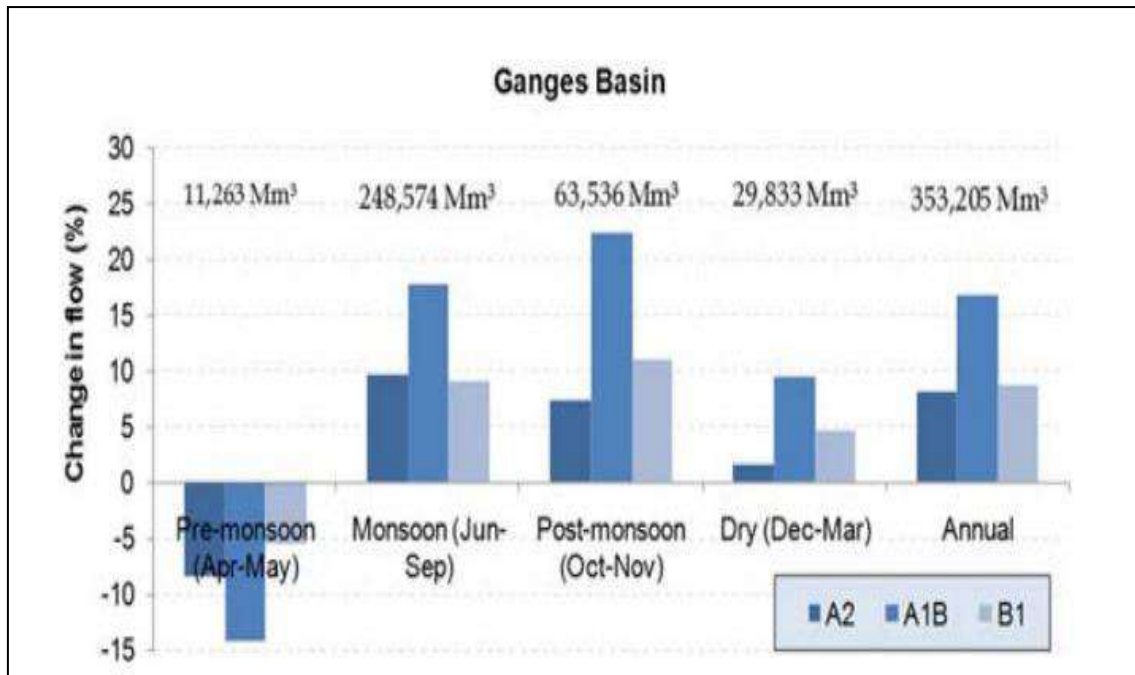


Figure 5.35: Change in seasonal and annual flow against different climate change scenario for the Ganges basin (Source: Islam, M. A. et al., 2017)

For the Ganges basin, the average annual flow increases by 17%, 8%, and 9% for high-emission, medium emission and low-emission climate change scenarios.

Tanvir (2015) assessed climate change impacts on water availability in the Ganges River Basin by developing a Hydrological model by SWAT. Result has been showed that the average annual flow volume increases 22% by 2030, 26% by 2050 and 19% by 2080 for high emission scenario. And a similar situation is observed for low emission scenario also.

Table 5.20: Monthly flow volume change of climate scenarios with respect to base scenario for the Ganges basin at Hardinge Bridge.

| Month | Discharge (Mm ³) | Percentage change of monthly flow | | | | | |
|-----------|------------------------------|-----------------------------------|---------|----------|---------|----------|---------|
| | | A1B_2030 | A2_2030 | A1B_2050 | A2_2050 | A1B_2080 | A2_2080 |
| January | 8,047 | 19.56 | 22.53 | 17.22 | 20.50 | 20.20 | 6.13 |
| February | 4,832 | 10.04 | 20.56 | 7.34 | 19.49 | 17.38 | 18.48 |
| March | 3,960 | 2.42 | 13.06 | -0.15 | 16.34 | 9.63 | 13.18 |
| April | 3,394 | 10.70 | 4.97 | -6.95 | 16.27 | 3.04 | 14.04 |
| May | 8,559 | -23.35 | 9.31 | -40.68 | 11.26 | -37.96 | -15.97 |
| June | 21,019 | 13.79 | -12.71 | 13.03 | 30.03 | 17.37 | 6.36 |
| July | 58,988 | 37.40 | 1.46 | 32.08 | 26.59 | 26.93 | 21.29 |
| August | 92,335 | 19.39 | 19.43 | 33.23 | 18.50 | 15.99 | 17.74 |
| September | 80,072 | 26.74 | 21.37 | 31.34 | 39.85 | 27.90 | 32.60 |
| October | 44,598 | 22.08 | 10.67 | 24.30 | 22.19 | 16.47 | 18.72 |
| November | 22,431 | 17.37 | 9.41 | 21.53 | 25.08 | 15.26 | 18.27 |
| December | 13,357 | 17.56 | 21.02 | 14.97 | 22.98 | 18.28 | 18.36 |

Source: Ahmed, T. et al., 2015

5.10 Summary

The GBM basin holds the world's largest reserve of fresh and annually replenished ground and surface water and needs timely attention to maintain this resource and reap the benefit for people at large through an integrated basin-wide approach to follow water management principles (Islam S. L. et. al, 2017). By the 21st century, this scenario will be changed, as the problem of dry season water scarcity and monsoon flooding will further aggravate and create much larger sufferings for people. Climate-induced change in water regime associated with the rapid urbanization will affect the water flow.

The model performance suggested that the SWAT model calibration and validation was satisfactory at the monthly scale. In this study, the objectives here was to assess long-term impacts of climate change assessment, so the well calibrated and validated model at a monthly scale could be considered acceptable to assess basin wide long-term impacts of climate and land use change (Wu et al., 2012b). The flow of Ganges River Basin was more sensitive to changes in precipitation. The impacts of climate and land use change were predicted to be more pronounced for the seasonal variation and annual also. When nearly all regions of the world were expected to experience a net negative impact of climate change on water resources (Parry, 2007). An increase in average seasonal streamflow is most likely to increase the number of extreme discharges, because there is a strong relationship between average monthly discharge and maximum monthly discharge (Immerzeel, 2008). The results of the model indicate that the discharge will decrease during dry period and increase during monsoon. The average annual flow volume increases 24% by 2020s, 32% by 2050s and 37% by 2080s. for all the scenarios.

CHAPTER 6

CONCLUSIONS AND RECOMMENDATIONS

6.1 General

In this study, potential impacts of climate change and land use change on the future streamflow of Ganges River Basin has been assessed by using SWAT hydrological model on the basis of climate change scenarios projected by multiple GCMs forced by several RCP scenarios of IPCC 5th Assessment (AR5) report for 2020s, 2050s, and 2080s of the 21st century.

6.2 Conclusions of the Study

1. In Sensitivity analysis, SCS runoff curve number and Soil evaporation compensation factor is the most and least sensitive parameter have been found for Ganges River Basin which provide a good assistance during calibration process.
2. NSE, R², PBIAS and RSR values are 0.82, 0.84, -7.60 and 0.42 for calibration and 0.76, 0.81, -13.2 and 0.49 for validation period of hydrological model respectively. These co-efficient has shown a satisfactory correlation between simulated and observed discharge.
3. Based on data analysis, BCC-CSM 1.1 (RCP 8.5), HadGEM-2 ES (RCP 2.6), IPSL-CM5A-LR (RCP 2.6) and HadGEM-2 ES (RCP 8.5) are found as the wettest, driest, coolest and warmest scenario of the Ganges River Basin in 2020s, 2050s and 2080s, respectively.
4. The average annual flow was in increasing trend for all of the scenarios through the century. The monsoon may see as much as 57% increase in surface runoff (wettest scenario) while the dry season might see a 3.9% increase in discharge (driest scenario).
5. For land use change, average monthly flow from Ganges River Basin area increases linearly. For increase in urbanization in Ganges River Basin area, annual average water flow increases about 21% to 36%. Due to urbanization, increase in impervious area will increase overland flow contribution at Hardinge Bridge transit which will provide more water flow of river. For additional increase in deforestation in Ganges River Basin area, annual average water flow at Hardinge Bridge transit increase about 16% to 25%.

6.3 Recommendations for Future Studies

Based on the results and the experience gained during the study, the following recommendations are made.

- In this study, SWAT model was calibrated and validated for flow. Future studies should be considered sediment, water quality and chemical calibration and validation. Also recommended to calibrate and validate the model after including dam and reservoirs data on this basin area. It may give more better estimation of parameters.
- In the present research three GCMs had taken into consideration from CMIP5 based on the literature review of GCMs output for selecting scenarios. In order to minimize uncertainties associated with streamflow projection for future period, it is recommended to select the scenarios comparing outputs of more GCMs from further CMIP for more dynamic and realistic result.
- Finally, it would be beneficial to develop a web portal consisting of science, information, and data on the hydrological responses of climate and land use and land cover change for Ganges River Basin.

Reference

- Abbaspour, K., 2007. User manual for SWAT-CUP, SWAT calibration and uncertainty analysis programs. Eawag: Swiss Federal Institute of Aquatic Science and Technology, Duebendorf, Switzerland.
- Abbaspour, K., Johnson, C. and Van Genuchten, M.T., 2004. Estimating uncertain flow and transport parameters using a sequential uncertainty fitting procedure. *Vadose Zone Journal*, 3(4), 1340-1352.
- Abbaspour, K.C., Faramarzi, M., Ghasemi, S.S. and Yang, H., 2009. Assessing the impact of climate change on water resources in Iran. *Water Resources Research*, 45(10), W10434.
- Alam, S. 2015 “Impact of climate change on future flow of Brahmaputra river basin using swat model”, M.Sc. Engg. Thesis, Department of Water Resources Engineering, Bangladesh University of Engineering and Technology.
- Allen, M.R. and Ingram, W.J., 2002. Constraints on future changes in climate and the hydrologic cycle. *Nature*, 419(6903), 224-232.
- Arnold, J.G., Srinivasan, R., Muttiah, R.S. and Williams, J.R., 1998. Large area hydrologic modeling and assessment part I: Model development1. *JAWRA Journal of the American Water Resources Association*, 34(1), 73-89.
- Arora, V.K. and Boer, G.J., 2001. Effects of simulated climate change on the hydrology of major river basins. *Journal of Geophysical Research: Atmospheres*, 106(D4), 3335-3348.
- Bárdossy, A., 1997. Downscaling from GCMs to local climate through stochastic linkages. *Journal of Environmental Management*, 49(1), 7-17.
- Betts, R.A., Cox, P.M., Lee, S.E. and Woodward, F.I., 1997. Contrasting physiological and structural vegetation feedbacks in climate change simulations. *Nature*, 387, 796- 799.

- Bharati, L., Gurung, P. and Jayakody, P., 2012. Hydrologic characterization of the Koshi Basin and the impact of climate change. *Hydro Nepal: Journal of Water, Energy and Environment*, 11(1), 18-22.
- Bharati, L., Lacombe, G., Gurung, P., Jayakody, P., Hoanh, C.T. and Smakhtin, V., 2011. The Impacts of water infrastructure and climate change on the hydrology of the upper Ganges River basin. *International Water Management Institute Research Reports Series* (142).
- Bingner R. L. 1996. “Runoff simulated from Goodwin Creek watershed using SWAT”. *Trans. ASAE* 39(1): 85-90.
- Brown S., and Nicholls R. J. 2015. “Subsidence and human influences in mega deltas: The case of the Ganges-Brahmaputra-Meghna.” *Sci. Total Environ.* 527–528: 362–374.
- Caesar J., Janes T., Lindsay A., and Bhaskaran B. 2015. “Temperature and precipitation projections over Bangladesh and the upstream Ganges, Brahmaputra and Meghna systems.” *Environ. Sci.: Processes Impacts*, 17 (6): 1047–1056.
- Chen, S.T., Yu, P.S. and Tang, Y.H., 2010. Statistical downscaling of daily precipitation using support vector machines and multivariate analysis. *Journal of Hydrology*, 385(1-4), 13-22.
- Chien, H., Yeh, P. J. F. and Knouft, J. H. (2013), “Modeling the potential impacts of climate change on streamflow in agricultural watersheds of the Midwestern United States”. *Journal of Hydrology*, Vol. 491, pp. 73-88.
- Chiew F.H.S., Whetton P.H., McMahon T.A. and Pittock A.B., 1995. “Simulation of the impacts of climate change on runoff and soil moisture in Australian catchments.” *Journal of Hydrology*, V-167, P: 121–147.
- Chowdhury M. R. and Ward N., 2004 “Hydro-Meteorological Variability in the Greater Ganges Brahmaputra–Meghna Basins”, *International Journal of Climatology*, vol. 24, pp.1495–1508.

- Chowdhury, J. U., Haque, A., Datta, A.R., and Hassan, A., “Impact of Climate Change on Surface Water Flow in Bangladesh”, Institute of Water and Flood management, BUET, Dhaka, Tech. Rep. Classic, February 2008.
- Chowdhury, M. D. and Ward, N. (2004). Hydro- meteorological variability in the greater Ganges–Brahmaputra–Meghna basins. *International Journal of Climatology*, 24(12), 1495-1508.
- Chowdhury, M.R. and Ward, M.N., 2004. Hydro-meteorological variability in the greater Ganges-Brahmaputra-Meghna basins. *Int. J. Climatol.*, 24(12), 1495-1508.
- Cibin, R., Sudheer, K. and Chaubey, I., 2010. Sensitivity and identifiability of stream flow generation parameters of the SWAT model. *Hydrological processes*, 24(9), 1133- 1148.
- Combalicer, E.A., Cruz, R.V.O., Lee, S. and Im, S., 2010. Assessing climate change impacts on water balance in the Mount Makiling forest, Philippines. *J. Earth Syst. Sci.*, 119(3), 265-283.
- David, M., 2007. *Water for food, water for life: A comprehensive assessment of water management in agriculture*. London: Earthscan, and Colombo: International Water Management Institute
- Davies, a. S., 2004. Urban water management vs. Climate change, impacts on cold region wastewater inflows. *Climatic Change*, 64, 103-126.
- De Roo, A.P.J., Wesseling, C.G. and Van Deursen, W.P.A., 2000. Physically based river basin modelling within a GIS, The LISFLOOD model. *Hydrological Processes*, 14, 1981-1992
- Dhar, O. N. and Nandargi, S. (2000). “A study of floods in the Brahmaputra basin in India”. *International journal of climatology*, Vol. 20(7), pp. 771-781.
- Dibike, Y.B., Gachon, P., St-Hilaire, A., Ouarda, T.B.M.J. and Nguyen, V.T.V., 2008. Uncertainty analysis of statistically downscaled temperature and precipitation regimes in Northern Canada. *Theor. Appl. Climatol.*, 91(1-4), 149-170.

- Elshamy, M.E., Seierstad, I.A. and Sorteberg, A., 2009. Impacts of climate change on Blue Nile flows using bias-corrected GCM scenarios. *Hydrology & Earth System Sciences*, 13(5).
- Environmental Modeling Center, 2010. NCEP Climate Forecast System Reanalysis (CFSR) Monthly Products, January 1979 to December 2010. Boulder, CO.
- Escurra, J. J., Vazquez, V., Cestti, R., De Nys, E. and Srinivasan, R., “Climate change impact on countrywide water balance in Bolivia”. *Regional Environmental Change*, Vol. 534, pp. 1-16, (2002).
- FAO, 1995. The digital soil map of the world and derived soil properties. FAO, Rome.
- Feyereisen G. W., Strickland T. C., Bosch D. D. and Sullivan D. G. 2007. “Evaluation of Swat manual calibration and input parameter sensitivity in the little river watershed”. Vol. 50(3): 843–855 2007 American Society of Agricultural and Biological Engineers ISSN 0001–2351
- Ficklin, D. L., Stewart, I. T. and Maurer, E. P., “Climate Change Impacts on Streamflow and Subbasin-Scale Hydrology in the Upper Colorado River Basin”. *PloS one*, Vol. 8(8), e71297, (2013).
- Ficklin, D.L., Luo, Y., Luedeling, E. and Zhang, M., 2009. Climate change sensitivity assessment of a highly agricultural watershed using SWAT. *Journal of Hydrology*, 374(1), 16-29.
- Fontaine, T.A., Cruickshank, T.S., Arnold, J.G. and Hotchkiss, R.H., 2002. Development of a snowfall-snowmelt routine for mountainous terrain for the soil water assessment tool (SWAT). *Journal of Hydrology*, 262(1-4), 209-223.
- Fowler, A., 1999. Potential climate change impacts on water resources in the Auckland Region (New Zealand). *Clim. Res.*, 11, 221-245.
- Fujino, J., Nair, R., Kainuma, M., Masui, T. and Matsuoka, Y. (2006) Multi-gas mitigation analysis on stabilization scenarios using aim global model. *The Energy Journal Special issue*, 3,343-354.

- Gain, A. K. and Wada, Y., “Assessment of Future Water Scarcity at Different Spatial and Temporal Scales of the Brahmaputra River Basin.” *Water Resources Management*, pp.1-14, (2014).
- Gain, A. K., Immerzeel, W. W., Sperna-Weiland, F. C. and Bierkens, M. F. P., “Impact of climate change on the stream flow of lower Brahmaputra: trends in high and low flows based on discharge-weighted ensemble modeling”. *Hydrology and Earth System Sciences Discussions*, Vol. 8(1), pp. 365-390, (2011).
- Garg, K.K., Bharati, L., Gaur, A., George, B., Acharya, S., Jella, K. and Narasimhan, B., 2012. Spatial mapping of agricultural water productivity using the SWAT model in Upper Bhima Catchment, India. *Irrigation and drainage*, 61(1), 60-79.
- Ghaffari, G., Keesstra, S., Ghodousi, J. and Ahmadi, H., 2010. SWAT-simulated hydrological impact of land-use change in the Zanjanrood basin, Northwest Iran. *Hydrological Processes*, 24(7), 892-903.
- Ghosh, S. and Dutta, S. (2012). Impact of climate change on flood characteristics in Brahmaputra basin using a macro-scale distributed hydrological model. *Journal of earth system science*, 121(3), 637-657.
- Giorgi F, 2008. A simple equation for regional climate change and associated uncertainty. *J Clim* 21(7),1589-1604.
- Githui, F., Gitau, W., Mutua, F. and Bauwens, W., 2009. Climate Change Impact on SWAT Simulated Streamflow in Western Kenya. *Int. J. Climatol*, 29, 1823-1834.
- Gosain, A., Rao, S. and Basuray, D., 2006. Climate change impact assessment on hydrology of Indian river basins. *Current Science*, 90(3), 346-353.
- Gosain, A.K., Mani, A. and Dwivedi, C., 2009. Hydrological modelling literature review, Report No.1. Indo-Norwegian Institutional Cooperation Program 2009-2011.
- Goswami, B.N., 1998. Interannual Variations of Indian Summer Monsoon in a GCM: External Conditions versus Internal Feedbacks. *J. Clim.*, 11(4), 501-522.

- Government of the People's Republic of Bangladesh. 2018, "Bangladesh Delta Plan 2100". Bangladesh Planning Commission, General Economics Division.
- Grayson, R.B., More, I.D. and McMahon, T.A., 1992. Physically based hydrological modelling, A terrain-based model for investigative purposes. *Water Resour. Res.*, 28(10), 2639-2658.
- Hessami, M., Gachon, P., Ouarda, T.B. and St-Hilaire, A., 2008. Automated regression based statistical downscaling tool. *Environmental Modelling & Software*, 23(6), 813-834.
- Heuvelmans, G., Muys, B. and Feyen, J., 1999. Analysis of the spatial variation in the parameters of the SWAT model with application in Flanders, Northern Belgium. *Hydrology and Earth System Sciences*, 8(5), 931-939.
- Hijmans, R.J., Cameron, S.E., Parra, J.L., Jones, P.G. and Jarvis, A., 2005. Very high-resolution interpolated climate surfaces for global land areas. *International Journal of Climatology*, 25(15), 1965-1978.
- Hofer, T. and Messerli, B., 2006. *Floods in Bangladesh: history, dynamics and rethinking the role of the Himalayas*. United Nations University Press, New York
- Hossain, M.A., 2012.
- Hulme, M., T. Jiang, and T.M.L. Wigley, 1995a, SCENGEN, A Climate Change SCENario GENERator, Software User Manual, Version 1.0. Climatic Research Unit, University of East Anglia, Norwich,38.
- Huntington, T.G., 2006. Evidence for intensification of the global water cycle: review and synthesis. *Journal of Hydrology*, 319(1), 83-95.
- Huth, R. 2002. Statistical downscaling of daily temperature in Central Europe. *Journal of Climate* 15, 1731-1742.
- Immerzeel, W. W., van Beek, L. P. and Bierkens, M. F. "Climate change will affect the Asian water towers". *Science*, Vol. 328(5984), pp. 1382-1385, (2010).

- Immerzeel, W., 2008. Historical trends and future predictions of climate variability in the Brahmaputra basin, *International Journal of Climatology*, Int. J. Climatol., 28, 243-254.
- IPCC Expert Meeting Report, 2007. Towards New Scenarios for Analysis of Emissions, Climate Change, Impacts, and Response Strategie, 19-21.
- IPCC, “Climate change Synthesis report contribution of working groups I, II and III to the fourth assessment report of the Intergovernmental panel on climate change”, Geneva, (2007).
- IPCC, 2014. Climate change 2014: Impacts, adaptation, and vulnerability: Contribution of Working Group II to the Fifth Assessment Report of the Intergovernmental Panel on Climate Change. IPCC.
- IPCC. Climate Change, 2001. The Scientific Basis. Contribution of Working Group I to the IPCC Third Assessment Report. 2001
- Islam A. S., Haque A., and Bala S. K. 2010. “Hydrologic characteristics of floods in Ganges Brahmaputra–Meghna (GBM) delta.” *Nat. Hazard.* 54 (3): 797–811.
- Islam, Z. 2011a. A Review on Climate Change Modeling for Hydrological Impact Studies, Tech. Report, doi, 10.13140/2.1.1398.8648.
- Islam, Z. and Gan, T., 2015. Hydrologic Modeling of the Blue River Basin Using NEXRAD Precipitation Data with a Semi-distributed and a Fully Distributed Model. *J. Hydrol. Eng.*, 10.1061/(ASCE)HE.1943-5584.0001179,04015015.
- Jha, M., Arnold, J.G., Gassman, P.W., Giorgi, F. and Gu, R.R., 2006. Climate change sensitivity assessment on Upper Mississippi River Basin stream flows using SWAT. *Journal of the American Water Resources Association*, 42(4), 997-1016.
- Jha, M., Pan, Z., Tackle, E.S. and Gu, R., 2004b. Impacts of climate change on streamflow in the Upper Mississippi River Basin: A regional climate model perspective. *Journal of Geophysical Research D: Atmospheres*, 109(9), D09105 1-12.

- Jian, J., Webster, P.J. and Hoyos, C.D., 2009. Large-scale controls on Ganges and Brahmaputra river discharge on intra-seasonal and seasonal time-scales. *Quarterly Journal of the Royal Meteorological Society*, 135(639), 353-370.
- Jones, P. G. and Thornton P K., 1993, A rainfall generator for agricultural allocations in the tropics, *Agricultural and Forest Meteorology*, 63, 1-19.
- Jones, P. G. and Thornton P K., 1997. Spatial and temporal variability of rainfall related to a third-order Markov model, *Agricultural and Forest Meteorology*, 86, 127-138.
- Jones, P.G. and Thornton P.K., 2013, Generating downscaled weather data from a suite of climate models for agricultural modelling allocations, *Agricultural System*, 114, 1-5.
- Karyn, T. and Williams, J.W., 2010. Globally downscaled climate projections for assessing the conservation impacts of climate change. *Ecological Applications*, 20(2), 554- 565.
- Kerkhoven, E. and Gan T.Y., 2011. Unconditional Uncertainties of Historical and Simulated River Flows Subjected to Climate Change. *Journal of Hydrology*, 396 (1-2), 113-127.
- Khalil, G., 1990. Floods in Bangladesh: A question of disciplining the rivers. *Nat. Hazard.*, 3(4), 379-401.
- Khandu, E., Schumacher M., Awange J. L, and Schmied H. M. 2016. “Exploring the influence of precipitation extremes and human water use on total water storage (TWS) changes in the Ganges-Brahmaputra-Meghna river basin.” *Water Resour. Res.* 52 (3): 2240–2258
- Kite, G.W., 1995. The SLURP Model. In, Singh, V.P., (Ed.), *Computer Models of Watershed Hydrology*, 17. Water Resources Publications, Highlands Ranch, CO, 15, 521-562.

- Kitoh, A., Endo, H., Krishna Kumar, K., Cavalcanti, I.F., Goswami, P. and Zhou, T., 2013. Monsoons in a changing world: a regional perspective in a global context. *Journal of Geophysical Research: Atmospheres*, 118(8), 3053-3065.
- Knox, J.C., 1993. Large increases in flood magnitude in response to modest changes in climate. *Nature*, 361, 430 - 432.
- Krasovskaia, I. and Gottschalk, L., 1992. Stability of River Flow Regimes. *Nordic Hydrology*, 23, 137-154.
- Kripalani, R., Oh, J., Kulkarni, A., Sabade, S. and Chaudhari, H., 2007. South Asian summer monsoon precipitation variability: Coupled climate model simulations and projections under IPCC AR4. *Theoretical and Applied Climatology*, 90(3-4), 133- 159.
- Kumar, K.K., Rajagopalan, B. and Cane, M.A., 1999. On the weakening relationship between the Indian monsoon and ENSO. *Science*, 284(5423), 2156-2159.
- Kumarl N. and Kumar S., 2018 “Investigation of impacts of land use/land cover change on water availability of Tons River Basin, Madhya Pradesh, India” Springer International Publishing AG, part of Springer Nature.
- Labat, D. and Godd ris, Y., Probst, J.L., Guyot, J.L., 2004. Evidence for global runoff increase related to climate warming. *Advances in Water Resources*, 27(6), 631-642.
- Lu, X., and Hulme, M., 2002. A short note on scaling GCM climate response pattern, Tech. Report, Prepared for AIACC regional study team.
- Luo, Y., He, C., Sophocleous, M., Yin, Z., Hongrui, R. and Ouyang, Z., 2008. Assessment of crop growth and soil water modules in SWAT2000 using extensive field experiment data in an irrigation district of the Yellow River Basin. *Journal of Hydrology*, 352(1), 139-156.
- Miller N.L., Bashford K.E. and Strem E. 2003. Potential impacts of climate change on California hydrology. *Journal of the American Water Resources Association*, 39(4), 771-784.

- Miller, J.D., Immerzeel, W.W. and Rees, G., 2012. Climate change impacts on glacier hydrology and river discharge in the Hindu Kush-Himalayas. *Mt. Res. Dev.*, 32(4), 461-467.
- Mirza, M.M.Q., Warrick, R.A. and Ericksen, N.J., (2003) The implications of climate change on floods of the Ganges, Brahmaputra and Meghna rivers in Bangladesh. *Clim Change* 57(3):287–318.
- Mirza, M. Q. and Dixit A., 1997. Climate Change and Water Management in The GBM Basins; *Journal of water resources development*. ISSN, 1027-0345.
- Mirza, M. Q., 2002. Global warming and changes in the probability of occurrence of floods in Bangladesh and implications *Global Environmental Change*, 12, 127–138.
- Mirza, M. Q., Warrick, R. A., Ericksen, N. J. and Kenny, G. J. (1998). Trends and persistence in precipitation in the Ganges, Brahmaputra and Meghna river basins. *Hydrological Sciences Journal*, 43(6), 845-858.
- Mirza, M.Q., 2011. Climate change, flooding in South Asia and implications. *Regional Environmental Change*, 11(1), 95-107.
- Mirza, M.Q., Warrick, R.A., Ericksen, N.J. and Kenny, G.J., 2001. Are floods getting worse in the Ganges, Brahmaputra and Meghna basins? *Global Environmental Change Part B: Environmental Hazards*, 3(2), 37-48.
- Mohammed, K., Islam, A.S., Islam, G.M.T., Alferi, L., Bala, S.K. and Khan, M.J.U. 2018 “Future floods in Bangladesh under 1.5°C, 2°C and 4°C global warming scenarios”, *Journal of Hydrological Engineering*, 23(12): 04018050-13.
- Moriasi, D. N., Arnold, J. G., Van Liew, M. W., Bingner, R. L., Harmel, R. D. and Veith, T. L, 2007. *Model Evaluation Guidelines for Systematic Quantification of Accuracy in Watershed Simulations*.
- Narsimlu, B., Gosain, A. K. and Chahar, B. R. (2013), “Assessment of Future Climate Change Impacts on Water Resources of Upper Sind River Basin, India Using SWAT Model.” *Water resources management*, Vol.27 (10), pp. 3647-3662.

- Neitsch, S.L., J.G. Arnold; J.R. Kiniry, J.R. and K.W. King, "Soil and Water Assessment Tool Theoretical Documentation", Version 2000. Grassland, Soil and Water Research Laboratory, Temple, TX and Blackland Research Center, Temple, TX, (2002).
- Nemec, J. and Schaake, J., 1982. Sensitivity of water resources system to climate variation. *Hydrol. Sci. J.* 27, 327-343.
- Nishat, A. and Faisal, I.M., 2000. An assessment of the Institutional Mechanism for Water Negotiations in the Ganges–Brahmaputra–Meghna system. *International Negotiations*, 289–310.
- NOAA, Ashville, N.C. Pandey, V.P., Babel, M.S., Shrestha, S. and Kazama, F., 2010. Vulnerability of freshwater resources in large and medium Nepalese river basins to environmental change. *Water Sci. Technol.*, 61(6), 1525-1534.
- Nolihan, J, and Mahfouf, J., 1996. ISBA land surface parameterization scheme. *Global and Planetary Change*, 13, 145-159.
- Nolihan, J, and Planton, S., 1989. A simple parameterization of land surface processes for meteorological models. *Monthly Weather Review*, 17.
- Oglesby, R. J., and Saltzman, B., 1992, Equilibrium climate statistics of a GCM as a function of atmospheric carbon dioxide. Part I, geographic distributions of primary variables. *Journal of Climate*5, 66-92.
- Oki, T. and Kanae, S., 2006. Global Hydrological Cycles and World Water Resources. *Science*, 313(5790), 1068-1072.
- Palutikof, J., Goodess, C., Watkins, S. and Holt, T., 2002. Generating Rainfall and Temperature Scenarios at Multiple Sites: Examples from the Mediterranean. *Journal of Climate*, 15(24).
- Parry, M.L., T.R. Carter, and M. Hulme, 1996. What is a dangerous climate change? *Global Environ. Change*, 6, 1 -6.

- Paul, S., Liu, C.M., Chen, J.M. and Lin, S.H., 2008. Development of a statistical downscaling model for projecting monthly rainfall over East Asia from a general circulation model output. *J. Geophys. Res.*, 113(15), art. no. D15117.
- Perazzoli, M., Pinheiro, A. and Kaufmann, V., “Assessing the impact of climate change scenarios on water resources in southern Brazil”. *Hydrological Sciences Journal*, Vol. 58(1), pp. 77-87, (2013).
- Qian, Y., Ghan, S.J. and Leung, L.B., 2010. Downscaling hydroclimatic changes over the Western US based on CAM sub-grid scheme and WRF regional climate simulations. *Int. J. Climatol.*, 30, 675-693.
- Rajeevan, M., Bhate, J. and Jaswal, A.K., 2008. Analysis of variability and trends of extreme rainfall events over India using 104 years of gridded daily rainfall data. *Geophysical Research Letters*, 35(18), L18707.
- Rajkumar, G. and Narasimha, R., 1996. Statistical analysis of the position of the monsoon trough *Proceedings of the Indian Academy of Science*, 105(3), 343-355.
- Ramesh, K.V. and Goswami, P., 2007. Reduction in temporal and spatial extent of the Indian summer monsoon. *Geophys. Res. Lett.*, 34(23), L23704.
- Refsgaard, J.C., and Abbott, M.B., 1996. The role of distributed hydrological modelling in water resources management, 1-16.
- Rossi, C. G., Dybala, T. J., Moriasi, D. N., Arnold, J. G., Amonett, C., and Marek, T., 2008. Hydrologic calibration and validation of the soil and water assessment tool for the Leon River watershed, *Soil Water Conserv.*, 6, 533-541.
- Roy, B., Khan, S. M., Islam, A. K. M., Mohammed, K. & Khan, J. U, 2021. Climate-induced flood inundation for the Arial Khan River of Bangladesh using open-source SWAT and HEC-RAS model for RCP8.5-SSP5 scenario. *SN Applied Sciences* volume 3, Article number: 648 (2021).
- Saji, N.H., Goswami, B.N., Vinayachandran, P.N. and Yamagata, T., 1999. A dipole mode in the tropical Indian Ocean. *Nature*, 401(6751), 360-363.

- Salehin M., Chowdhury, J.U., and Islam, A.K.M.S. (2011), " Development of a water resources model as a decision support tool for national water management", Tech. report, Institute of water and flood management, BUET.
- Seidel, K., Jaroslav, M. and Michael, F., 2000. Baumgartner; modelling runoff and impact of climate change in large Himalayan basins, ICIWRM-2000. Roorkee, India.
- Sharma, M., Coulibaly, P. and Dibike, Y., 2011. Assessing the need for downscaling RCM data for hydrologic impact study. *Journal of Hydrologic Engineering*, 16(6), 534- 539.
- Shashikanth, K., Salvi, K., Ghosh, S. and Rajendran, K., 2013. Do CMIP5 simulations of Indian summer monsoon rainfall differ from those of CMIP3? *Atmospheric Science Letters*, 15(2), 79-85.
- Siddique, A.K., Baqui, A.H., Eusof, A. and Zaman, K., 1991. 1988 floods in Bangladesh: pattern of illness and causes of death. *Journal of Diarrhoeal Diseases Research*, 9(4), 310-314.
- Singh, P., Arora, M. and Goel, N.K., 2006. Effect of climate change on runoff of a glacierized Himalayan basin. *Hydrological Processes*, 20(9), 1979-1992.
- Singh, V.P., Sharma, N., Shekhar, C. and Ojha, P. (Eds.), 2004. *The Brahmaputra basin water resources*. Kluwer Academic Publishers, Dordrecht, The Netherlands
- Solaymani, H. R. 2015. "Assessment of climate change impacts in a semi-arid watershed in Iran using regional climate models". *Journal of Water and Climate Change* 6(1):161–180.
- Sood, A., Muthuwatta, L. and McCartney, M., 2013. A SWAT evaluation of the effect of climate change on the hydrology of the Volta River basin. *Water International*, 38(3), 297-311.
- Srinivasan, R. and J. G. Arnold., "Integration of a basin-scale water quality model with GIS". *Water Resour. Bull.* Vol. 30 (3). pp. 453- 462, (1994).

- Sushama, L., Laprise, R., Caya, D., Frigon, A. and Slivitzky, M., 2006. Canadian RCM projected climate -change signal and its sensitivity to model errors. *Int. J. Climatol.*, 26, 2141-2159.
- SWAT-CUP, 2012. SWAT Calibration and Uncertainty Programs, User Manual.
- Teutschbein, C., Wetterhall, F. and Seibert, J., 2011. Evaluation of different downscaling techniques for hydrological climate-change impact studies at the catchment scale. *Clim. Dyn.*, 37(9-10), 2087-2105.
- The representative concentration pathways, an overview, van Vuuren et. al, 2011. *Climatic Change* 109, 5-31.
- USDA Soil Conservatism service. 1972. National Engineering Handbook Section 4 Hydrology, 4-10.
- USDA-SCS, Hydrology, 1972. National Engineering Hand Book Sect. 4, Washington, DC, USDA-SCS.
- Varis, O., Kummu, M. and Salmivaara, A., 2012. Ten major rivers in monsoon Asia-Pacific: An assessment of vulnerability. *Appl. Geogr.*, 32(2), 441-454.
- Webster, P.J., Moore, A.M., Loschnigg, J.P. and Leben, R.R., 1999. Coupled ocean atmosphere dynamics in the Indian Ocean during 1997-98. *Nature*, 401(6751), 356-360.
- Wetterhall, F., Bárdossy, A., Chen, D., Halldin, S. and Xu, C.Y., 2009. Statistical downscaling of daily precipitation over Sweden using GCM output. *Theoretical and Applied Climatology*, 96(1-2), 95-103.
- Whetton, P.H., Fowler, A.M., Haylock, M.R. and Pittock, A.B., 1993, Implications of climate change due to the enhanced greenhouse effect on floods and droughts in Australia. *Climatic Change*, 25(3-4), 289-317.
- Wilby, R. L., Troni, J., Biot, Y., Tedd, L., Hewitson, B. C., Smithe, D. M. and Suttonf, R. T., 2009. A review of climate risk information for adaptation and development planning. *Int. J. Climatol.*, 29, 1193-1215.

- Williams, J.R. and R.W. Hann. 1973. HYMO, a problem-oriented computer language for building hydrologic models. *Water Resour. Res.*, 8(1),79-85.
- Williams, J.R., 1969. Flood routing with variable travel time or variable storage coefficients. *Trans. ASAE* 12(1),100-103.
- Wu, R. and Wang, B., 2002. A contrast of the East Asian summer monsoon-ENSO relationship between 1962-77 and 1978-93. *J. Clim.*, 15(22), 3266-3279.
- Xu, C., 2000. Modelling the Effects of Climate Change on Water Resources in Central Sweden. *Water Resources Management*, 14, 177-189.
- Xu, C-Y. and Halldin, S., 1997. The Effect of Climate Change on River Flow and Snow Cover in the NOPEX Area Simulated by a Simple Water Balance Model. *Nordic Hydrology*, 28 (4/5), 273-282.
- Yao, H., Scott, L., Guay, C. and Dillon, P., 2009. Hydrological impacts of climate change predicted for an inland lake catchment in Ontario by using monthly water balance analyses. *Hydrol. Process.* 23, 2368-2382.
- Yu, P.-S., Yang, T.-C. and Wu, C.-K., 2002. Impact of climate change on water resources in southern Taiwan. *Journal of Hydrology*, 260(1), 161-175.
- Zhang, H., Huang, G.H., Wang, D. and Zhang, X., 2011. Uncertainty assessment of climate change impacts on the hydrology of small prairie wetlands. *Journal of Hydrology*, 396, 94-103.
- Zhang, X. and Cai, X., 2011. Climate change impacts on global agricultural land availability. *Environmental Research Letters*, 6(1), 014014.
- Zhu, T. and Ringler, C., 2012. Climate change impacts on water availability and use in the Limpopo River Basin. *Water*, 4(1), 63-84.
- Zorita, E. and von Storch, H., 1999. The Analog Method as a Simple Statistical Downscaling Technique, Comparison with more Complicated Methods. *J. Climate* 12, 2474-2489.

APPENDIX A

Table A1: Sample CFSR dataset for weather input.

| | Jan | Feb | Mar | Apr | May | Jun | Jul | Aug | Sept | Oct | Nov | Dec |
|------------------|------------|------------|------------|------------|------------|------------|------------|------------|-------------|------------|------------|------------|
| TMPMX1 | 38.61 | 40.87 | 42.60 | 42.25 | 39.62 | 36.73 | 32.60 | 30.70 | 32.44 | 36.58 | 39.17 | 38.36 |
| TMPMN1 | 16.61 | 18.10 | 22.53 | 26.60 | 26.26 | 24.67 | 22.91 | 22.28 | 22.61 | 22.94 | 19.95 | 17.34 |
| TMPSTDMX1 | 2.26 | 2.48 | 2.94 | 3.18 | 3.63 | 3.55 | 3.92 | 3.85 | 3.75 | 3.72 | 2.15 | 1.83 |
| TMPSTDMN1 | 2.31 | 3.42 | 4.11 | 2.00 | 1.21 | 1.19 | 1.25 | 1.04 | 1.02 | 1.45 | 3.09 | 2.39 |
| PCPMM1 | 0.18 | 0.75 | 6.45 | 20.59 | 73.90 | 88.20 | 159.15 | 257.51 | 192.37 | 54.08 | 6.34 | 0.14 |
| PCPSTD1 | 0.13 | 0.27 | 1.20 | 6.01 | 9.44 | 10.70 | 12.16 | 16.08 | 13.07 | 7.26 | 3.14 | 0.07 |
| PCPSKW1 | 23.62 | 13.01 | 13.58 | 18.21 | 7.84 | 7.25 | 5.71 | 4.50 | 4.62 | 12.10 | 25.47 | 15.84 |
| PR_W1_1 | 0.00 | 0.01 | 0.06 | 0.11 | 0.21 | 0.29 | 0.43 | 0.53 | 0.42 | 0.16 | 0.03 | 0.01 |
| PR_W2_1 | 0.00 | 0.23 | 0.23 | 0.26 | 0.33 | 0.35 | 0.41 | 0.44 | 0.42 | 0.35 | 0.20 | 0.00 |
| PCPD1 | 0.09 | 0.41 | 2.50 | 4.19 | 9.31 | 11.47 | 18.34 | 21.97 | 18.41 | 7.94 | 1.09 | 0.16 |
| RAINHHMX1 | 1.18 | 1.73 | 9.17 | 46.47 | 48.37 | 41.75 | 49.49 | 55.57 | 44.47 | 50.97 | 31.58 | 0.46 |
| SOLARAV1 | 21.35 | 22.79 | 22.62 | 22.10 | 21.15 | 20.64 | 17.75 | 16.52 | 18.89 | 20.91 | 21.06 | 20.58 |
| DEWPT1 | 0.17 | 0.19 | 0.29 | 0.39 | 0.48 | 0.57 | 0.69 | 0.78 | 0.77 | 0.61 | 0.33 | 0.19 |
| WNDV1 | 2.54 | 2.39 | 2.35 | 2.92 | 3.07 | 2.92 | 2.67 | 2.32 | 2.09 | 2.17 | 1.90 | 2.34 |

Where:

| UNITS | | |
|-----------------|--------------------------|--|
| TMPMX | [deg c] | Average maximum air temperature for month. |
| TMPMN | [deg c] | Average minimum air temperature for month. |
| TMPSTDMX | [deg c] | Standard deviation for maximum air temperature in month. |
| TMPSTDMN | [deg c] | Standard deviation for minimum air temperature in month. |
| PCPMM | [mm/dd] | Average amount of precipitation falling in month. |
| PCPSTD | [mm/dd] | Standard deviation for daily precipitation in month. |
| PCPSKW | na | Skew coefficient for daily precipitation in month. |
| PR_W1 | [fraction] | Probability of a wet day following a dry day in the month. |
| PR_W2 | [fraction] | Probability of a wet day following a wet day in the month. |
| PCPD | [days] | Average number of days of precipitation in month. |
| RAINHHMX | [mm] | Maximum 0.5hour rainfall in entire period of record for month. |
| SOLARAV | [MJ/m ² -day] | Average daily solar radiation in month. |
| DEWPT | [deg c] | Average dew point temperature in month. |
| WNDV | [m/s] | Average wind speed in month. |

Table A2: Sample output tables, provided by SWAT after simulation for the year of 2000.

| SUB | YEAR | MON | AREAk² | FLOW_IN cms | FLOW_OUT cms | EVAP cms |
|------------|-------------|------------|--------------------------|------------------------|-------------------------|---------------------|
| 351 | 2000 | Jan | 1171000 | 1942 | 1918 | 24.18 |
| 351 | 2000 | Feb | 1171000 | 720.8 | 696.7 | 24.03 |
| 351 | 2000 | Mar | 1171000 | 814 | 776 | 37.92 |
| 351 | 2000 | Apr | 1171000 | 1613 | 1552 | 60.69 |
| 351 | 2000 | May | 1171000 | 13040 | 13010 | 33.5 |
| 351 | 2000 | Jun | 1171000 | 25480 | 25460 | 26.51 |
| 351 | 2000 | Jul | 1171000 | 46900 | 46870 | 26.74 |
| 351 | 2000 | Aug | 1171000 | 65050 | 65030 | 24.67 |
| 351 | 2000 | Sep | 1171000 | 63860 | 63840 | 19.52 |
| 351 | 2000 | Oct | 1171000 | 30440 | 30420 | 21.59 |
| 351 | 2000 | Nov | 1171000 | 14880 | 14860 | 21.05 |
| 351 | 2000 | Dec | 1171000 | 4753 | 4733 | 20.17 |

- Hardinge bridge outlet point is on the Sub basin no 351 in Model.
- cms = Cubic meter per second.

APPENDIX B

Table B1: Future monthly flow (m³/s) at SW 90 for 2020s for different Climate Change scenarios.

| Month | Observed (2000-2016) | Wettest (BCC-CSM 1.1 RCP 8.5) | Driest (HadGEM-2 ES RCP 2.6) | Coolest (IPSL-CM5A- LR RCP 2.6) | Warmest (HadGEM-2 ES RCP 8.5) |
|--------------|---------------------------------|--|---|--|--|
| Jan | 1863.5 | 2856.9 | 1677.1 | 2283.3 | 2228.0 |
| Feb | 1519.2 | 2068.0 | 1766.4 | 1831.5 | 1671.7 |
| Mar | 1189.1 | 1455.1 | 1070.2 | 1344.4 | 1217.9 |
| Apr | 1073.8 | 1474.4 | 1300.2 | 1127.1 | 1188.6 |
| May | 1308.4 | 992.3 | 1177.6 | 1430.2 | 1002.9 |
| Jun | 2945.3 | 4208.6 | 2650.7 | 2570.9 | 3351.4 |
| Jul | 18601.0 | 30246.1 | 23023.3 | 18872.5 | 32026.3 |
| Aug | 33800.7 | 51717.3 | 30420.6 | 40368.2 | 40354.6 |
| Sep | 31755.7 | 52802.1 | 28580.1 | 38541.9 | 40247.1 |
| Oct | 16618.9 | 22009.7 | 16325.4 | 22365.4 | 18652.0 |
| Nov | 6307.4 | 9420.7 | 5676.7 | 6900.9 | 7403.0 |
| Dec | 3298.7 | 4938.2 | 2968.9 | 3992.1 | 3878.0 |

Table B2: Future monthly flow (m³/s) at SW 90 for 2050s for different Climate Change scenarios.

| Month | Observed (2000-2016) | Wettest (BCC-CSM 1.1 RCP 8.5) | Driest (HadGEM-2 ES RCP 2.6) | Coollest (IPSL-CM5A- LR RCP 2.6) | Warmest (HadGEM-2 ES RCP 8.5) |
|--------------|---------------------------------|--|---|---|--|
| Jan | 1863.48 | 3041.50 | 1770.31 | 2245.50 | 2184.38 |
| Feb | 1519.20 | 2615.30 | 1443.24 | 1815.29 | 2236.32 |
| Mar | 1189.14 | 1909.80 | 1129.68 | 1383.44 | 1187.36 |
| Apr | 1073.76 | 1527.70 | 1020.07 | 1569.32 | 1632.32 |
| May | 1308.40 | 984.90 | 1242.98 | 1963.32 | 1326.23 |
| Jun | 2945.27 | 4405.62 | 3625.32 | 3829.74 | 3329.04 |
| Jul | 18600.96 | 29989.80 | 17670.91 | 23546.95 | 24568.14 |
| Aug | 33800.69 | 55033.33 | 32110.65 | 40053.81 | 45032.65 |
| Sep | 31755.67 | 57218.85 | 29656.32 | 44410.30 | 43265.32 |
| Oct | 16618.92 | 26167.44 | 19236.33 | 25632.32 | 22365.32 |
| Nov | 6307.42 | 9968.59 | 5992.05 | 7889.32 | 7665.41 |
| Dec | 3298.73 | 5228.21 | 4236.32 | 4056.78 | 2763.32 |

Table B3: Future monthly flow (m³/s) at SW 90 for 2080s for different Climate Change scenarios.

| Month | Observed (2000-2016) | Wettest (BCC-CSM 1.1 RCP 8.5) | Driest (HadGEM-2 ES RCP 2.6) | Coollest (IPSL-CM5A- LR RCP 2.6) | Warmest (HadGEM-2 ES RCP 8.5) |
|--------------|---------------------------------|--|---|---|--|
| Jan | 1863.48 | 6917.58 | 1770.31 | 2006.27 | 2349.07 |
| Feb | 1519.20 | 2637.72 | 3456.32 | 4856.00 | 2236.32 |
| Mar | 1189.14 | 4309.73 | 1129.68 | 1385.05 | 1336.86 |
| Apr | 1073.76 | 1625.71 | 1020.07 | 1569.32 | 4658.32 |
| May | 1308.40 | 941.78 | 1242.98 | 1963.32 | 7365.32 |
| Jun | 2945.27 | 4743.39 | 3625.32 | 3179.42 | 3605.23 |
| Jul | 18600.96 | 30246.13 | 27670.32 | 23551.14 | 32653.32 |
| Aug | 33800.69 | 57304.71 | 32110.65 | 38623.32 | 43265.32 |
| Sep | 31755.67 | 74604.69 | 29656.32 | 44696.10 | 37654.32 |
| Oct | 16618.92 | 26391.07 | 19236.33 | 12632.32 | 15632.32 |
| Nov | 6307.42 | 4994.13 | 5992.05 | 7747.88 | 7549.06 |
| Dec | 3298.73 | 5700.88 | 4236.32 | 4055.79 | 2763.32 |

Table B4: Future monthly flow (m³/s) at SW 90 for different Land Use scenarios.

| Month | Observed (2000-2016) | 20% Urbanization increase | 30% Urbanization increase | 40% Urbanization increase |
|--------------|---------------------------------|--------------------------------------|--------------------------------------|--------------------------------------|
| Jan | 1863.48 | 2347.99 | 2958.47 | 3727.67 |
| Feb | 1519.20 | 1428.05 | 1342.36 | 1261.82 |
| Mar | 1189.14 | 1117.79 | 1050.72 | 987.68 |
| Apr | 1073.76 | 1009.33 | 948.77 | 891.85 |
| May | 1308.40 | 1059.80 | 858.44 | 695.34 |
| Jun | 2945.27 | 2385.67 | 1932.39 | 1565.24 |
| Jul | 18600.96 | 15066.77 | 12204.09 | 9885.31 |
| Aug | 33800.69 | 36235.00 | 45482.20 | 52759.36 |
| Sep | 31755.67 | 32653.00 | 42730.43 | 49567.29 |
| Oct | 16618.92 | 19277.94 | 22362.42 | 25940.40 |
| Nov | 6307.42 | 7947.35 | 10013.66 | 12617.21 |
| Dec | 3298.73 | 4156.40 | 5237.06 | 6598.70 |

APPENDIX C

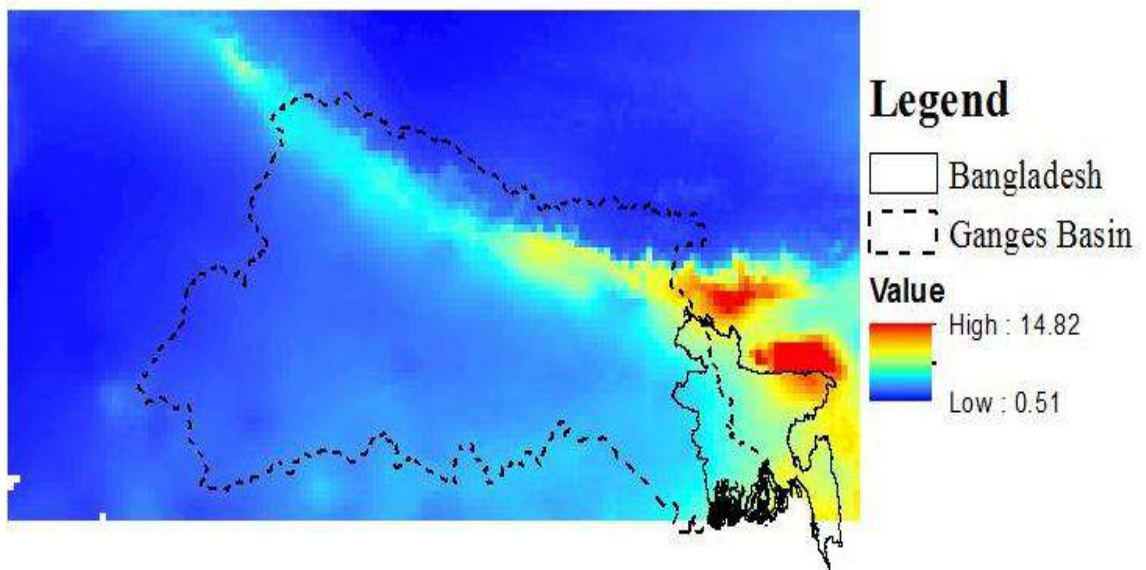


Figure C1: Spatial variation of precipitation (mm) for IPSL-CM5A-LR 8.5 in 2020s (Wettest Scenario)

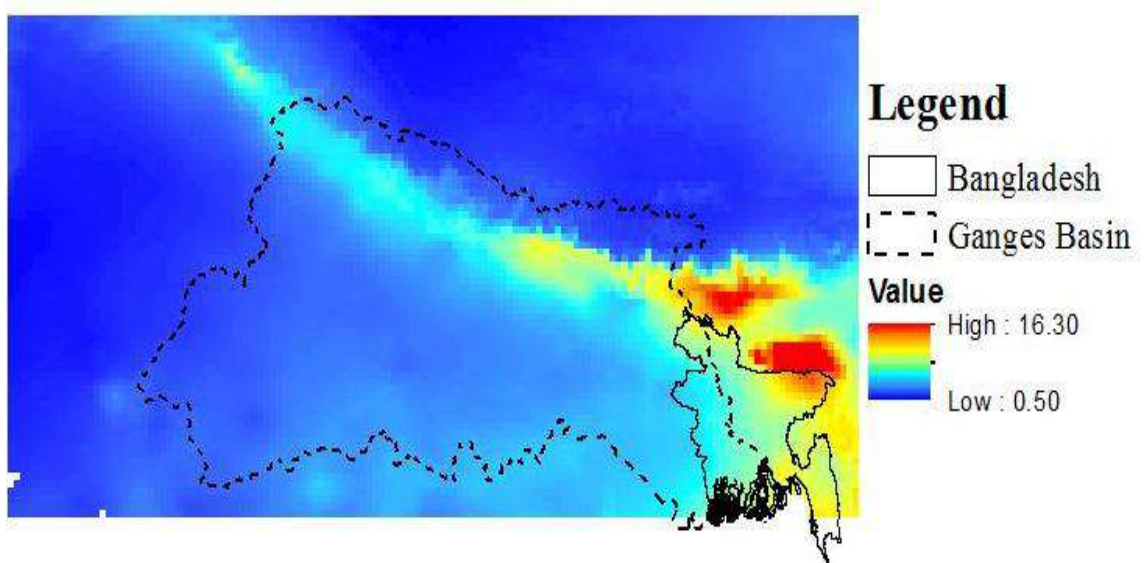


Figure C2: Spatial variation of precipitation (mm) for IPSL-CM5A-LR 8.5 in 2050s (Wettest Scenario)

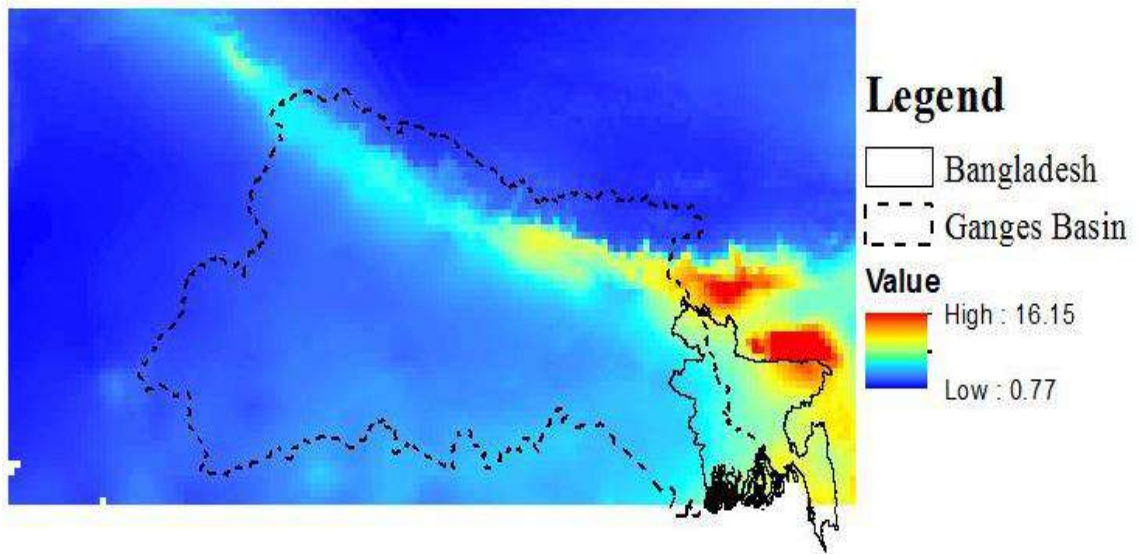


Figure C3: Spatial variation of precipitation (mm) for IPSL-CM5A-LR 8.5 in 2080s (Wettest Scenario)

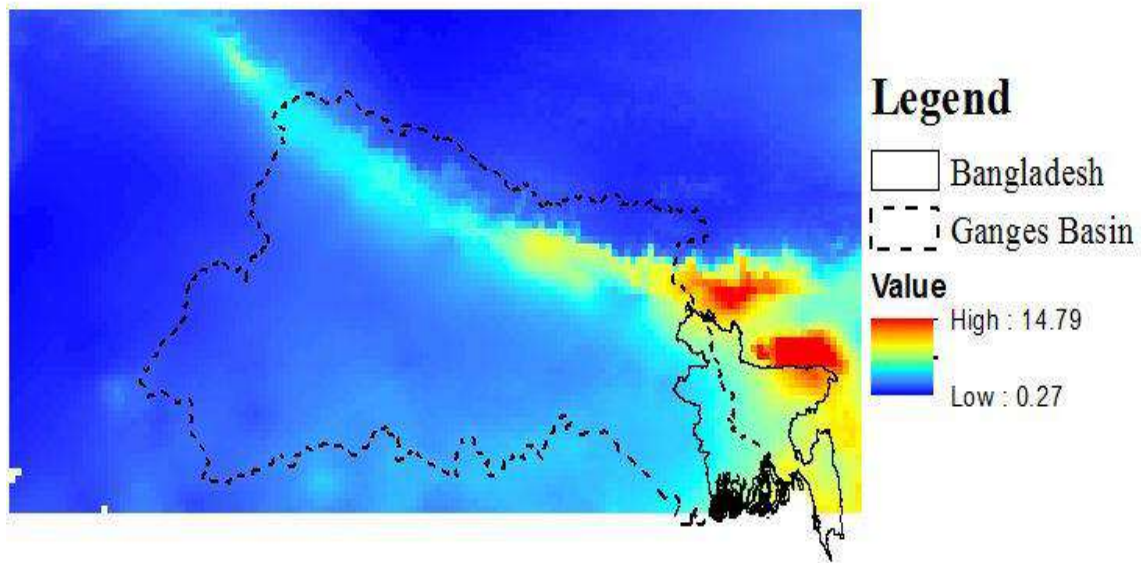


Figure C4: Spatial variation of precipitation (mm) for HadGEM-2 ES-2.6 in 2020s (Driest Scenario)

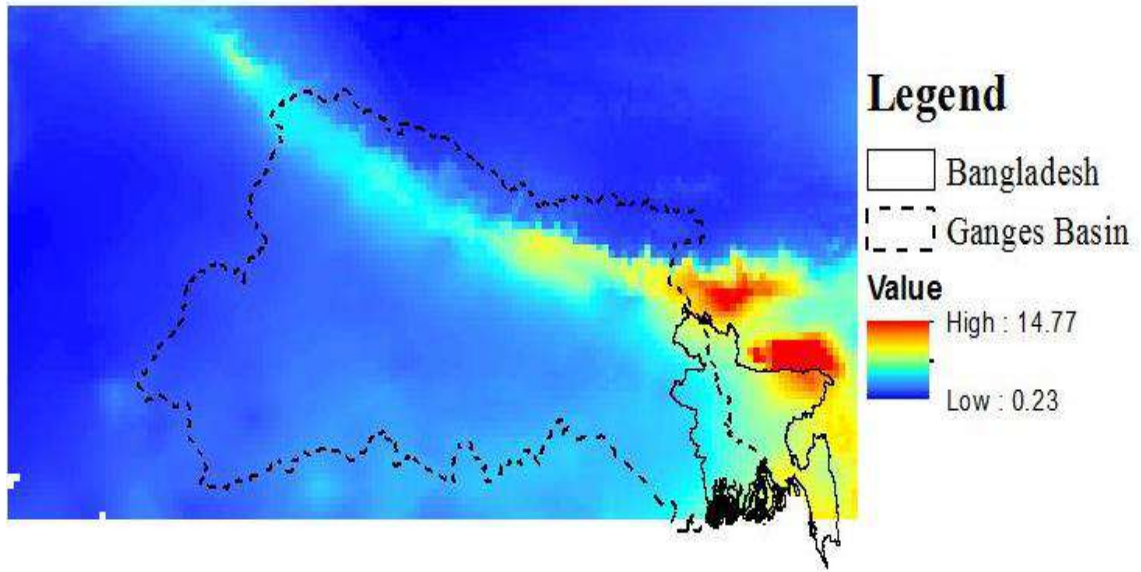


Figure C5: Spatial variation of precipitation (mm) for HadGEM-2 ES-2.6 in 2050s (Driest Scenario)

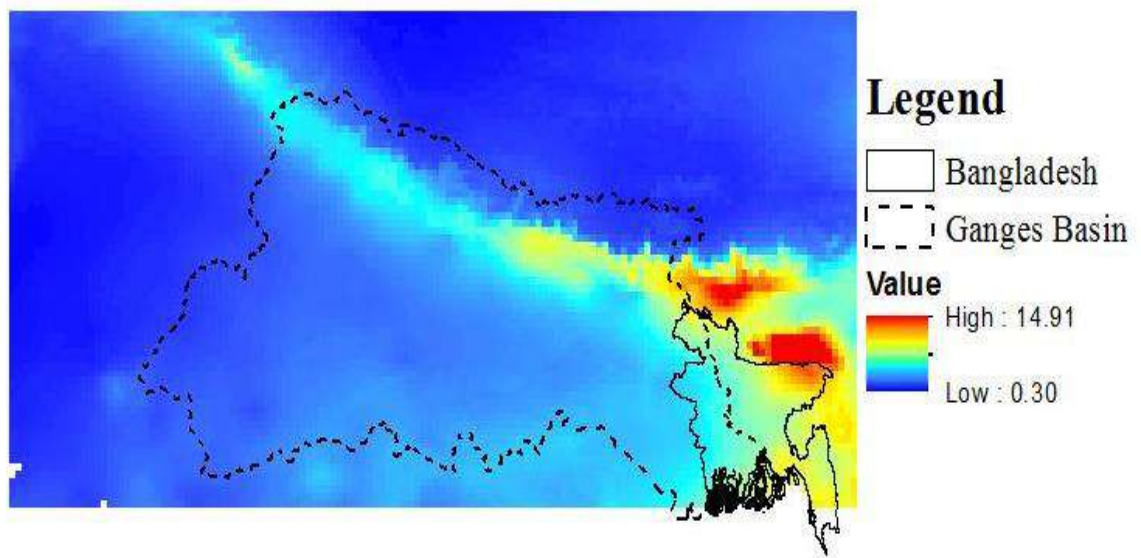


Figure C6: Spatial variation of precipitation (mm) for HadGEM-2 ES-2.6 in 2080s (Driest Scenario)

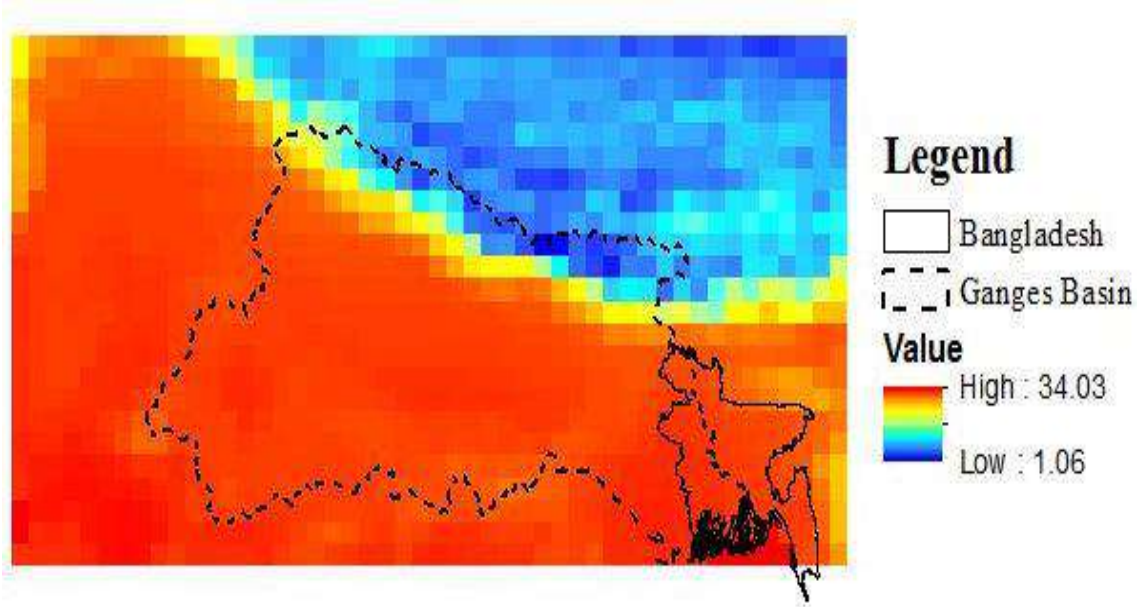


Figure C7: Spatial distribution of Maximum temperature (°C) for HadGEM-2 ES-8.5 in 2020s (Warmest Scenario)

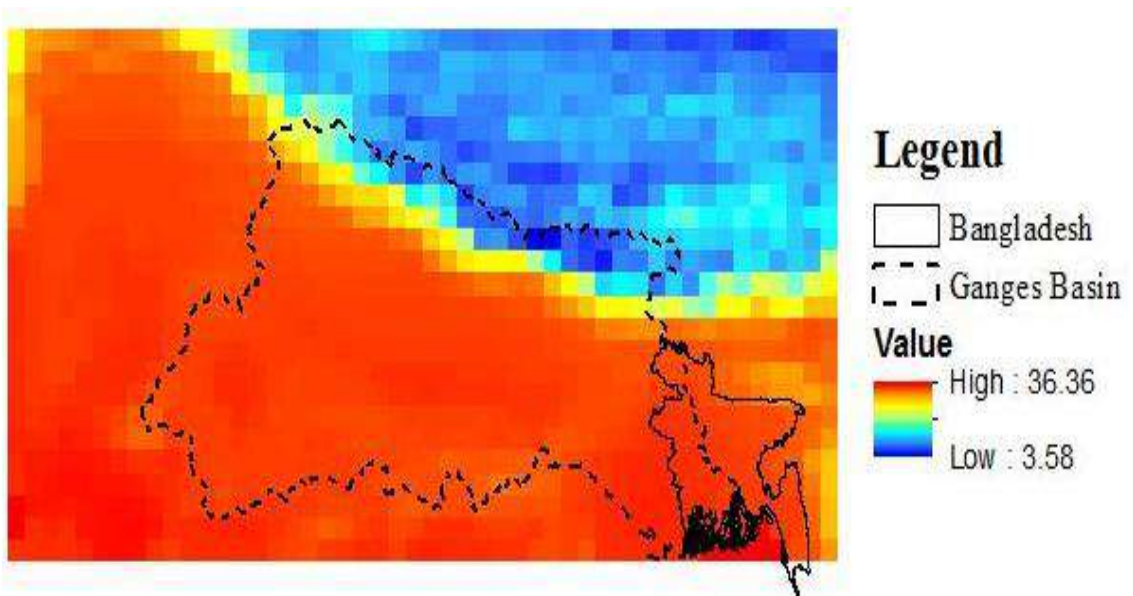


Figure C8: Spatial distribution of Maximum temperature (°C) for HadGEM-2 ES-8.5 in 2050s (Warmest Scenario)

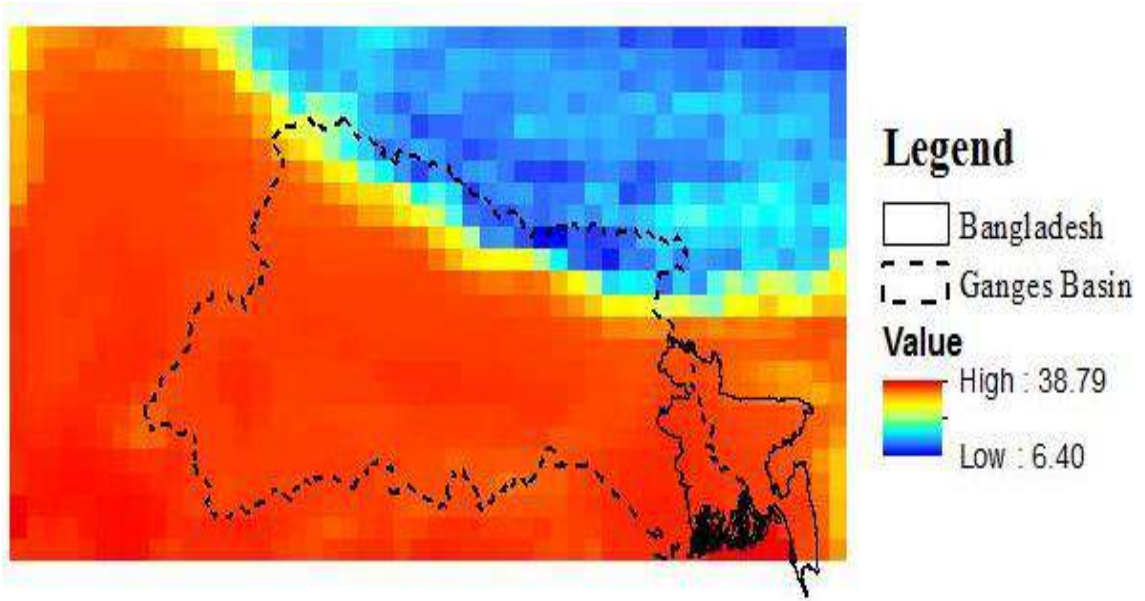


Figure C9: Spatial distribution of Maximum temperature (°C) for HadGEM-2 ES-8.5 in 2080s (Warmest Scenario)

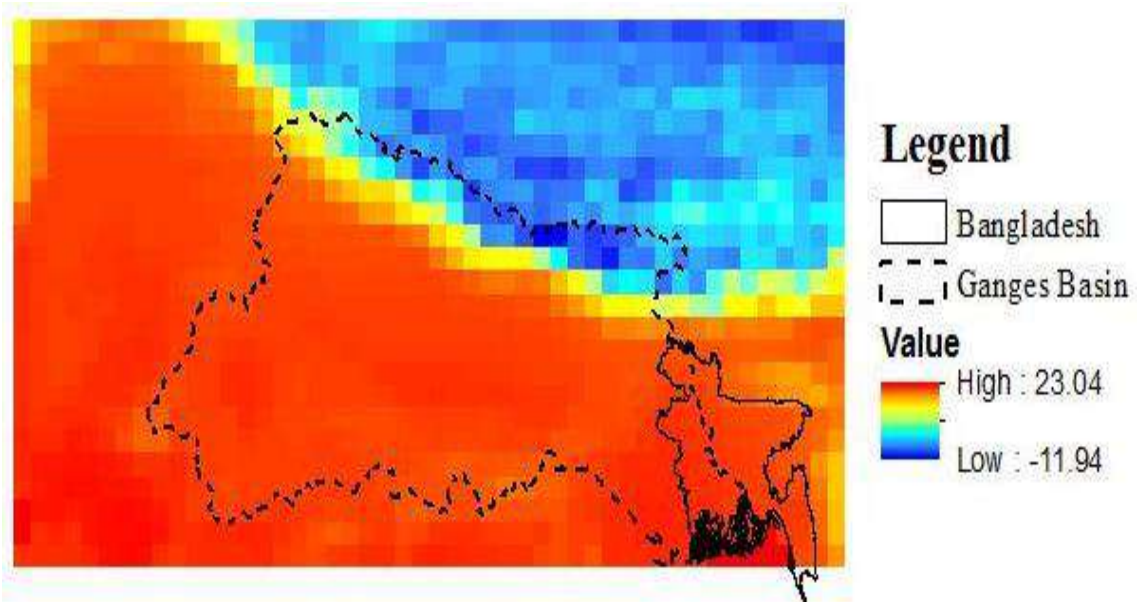


Figure C10: Spatial distribution of Minimum temperature (°C) for HadGEM-2 ES-8.5 in 2020s (Warmest Scenario)

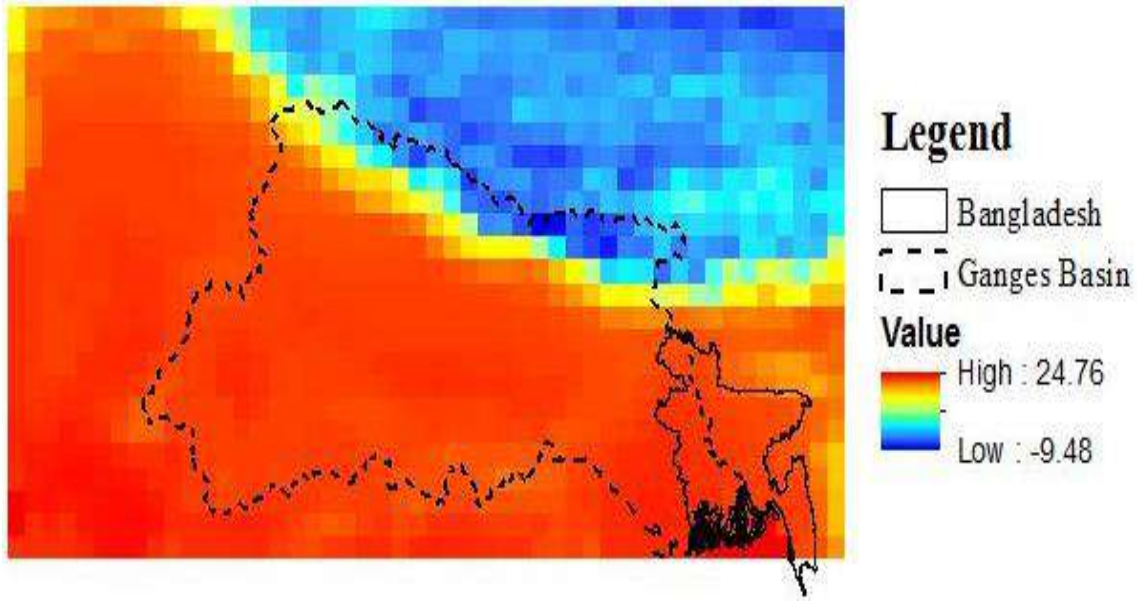


Figure C11: Spatial distribution of Minimum temperature (°C) for HadGEM-2 ES-8.5 in 2050s (Warmest Scenario)

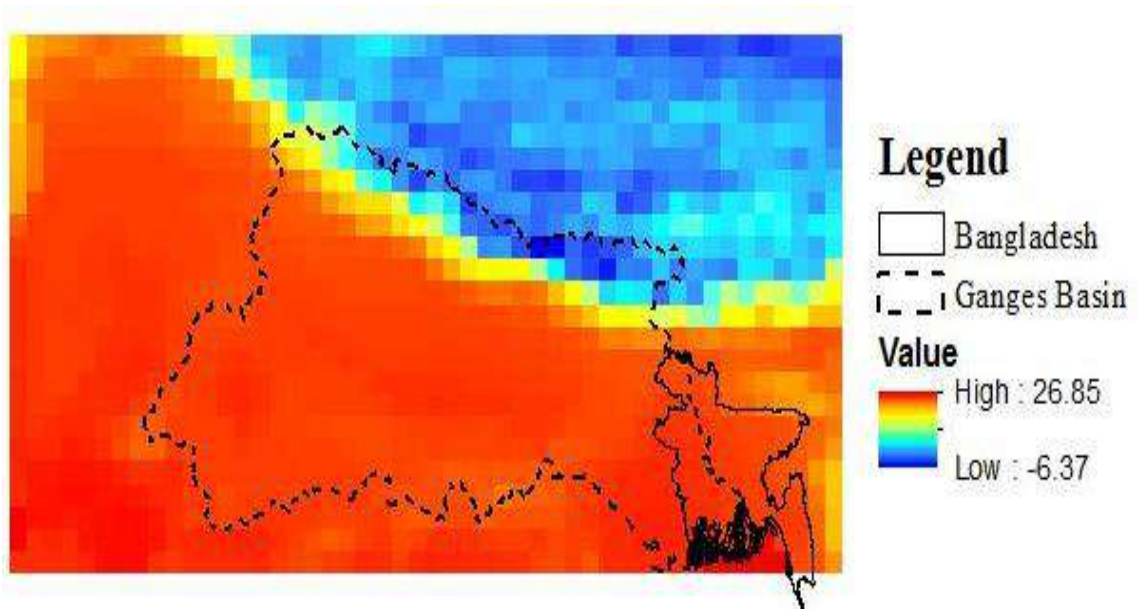


Figure C12: Spatial distribution of Minimum temperature (°C) for HadGEM-2 ES-8.5 in 2080s (Warmest Scenario)

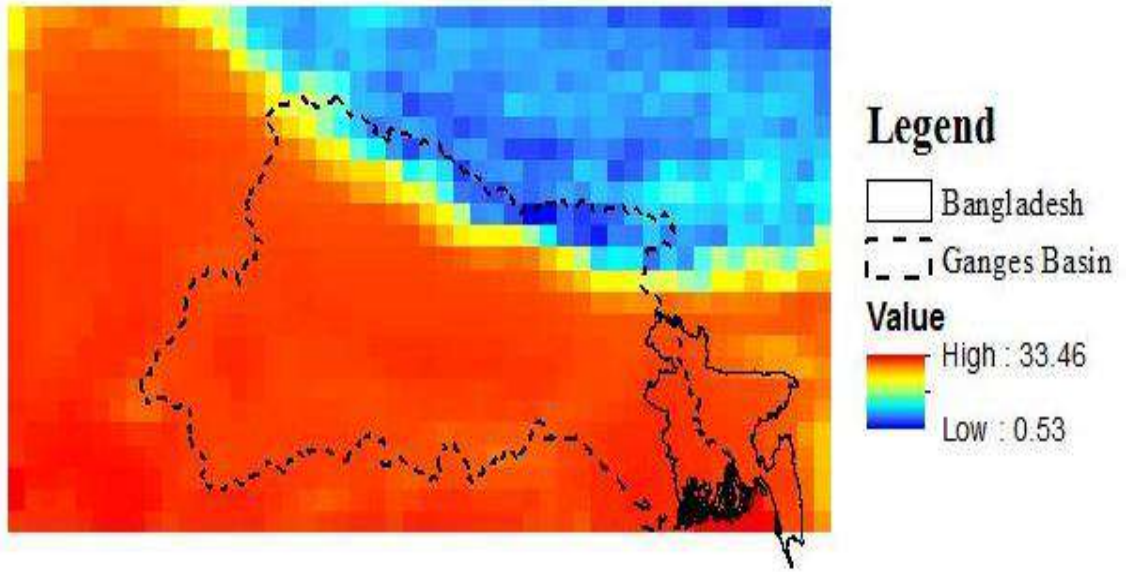


Figure C13: Spatial distribution of Maximum temperature (°C) for IPSL-CM5A-LR 4.5 in 2020s (Coolest Scenario)

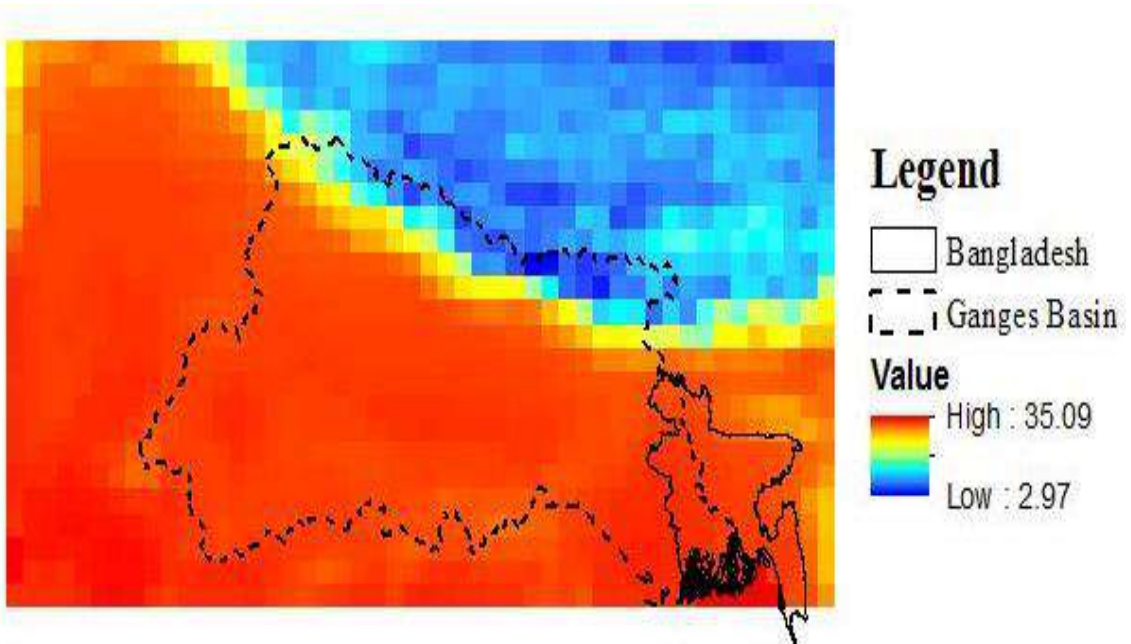


Figure C14: Spatial distribution of Maximum temperature (°C) for IPSL-CM5A-LR 4.5 in 2050s (Coolest Scenario)

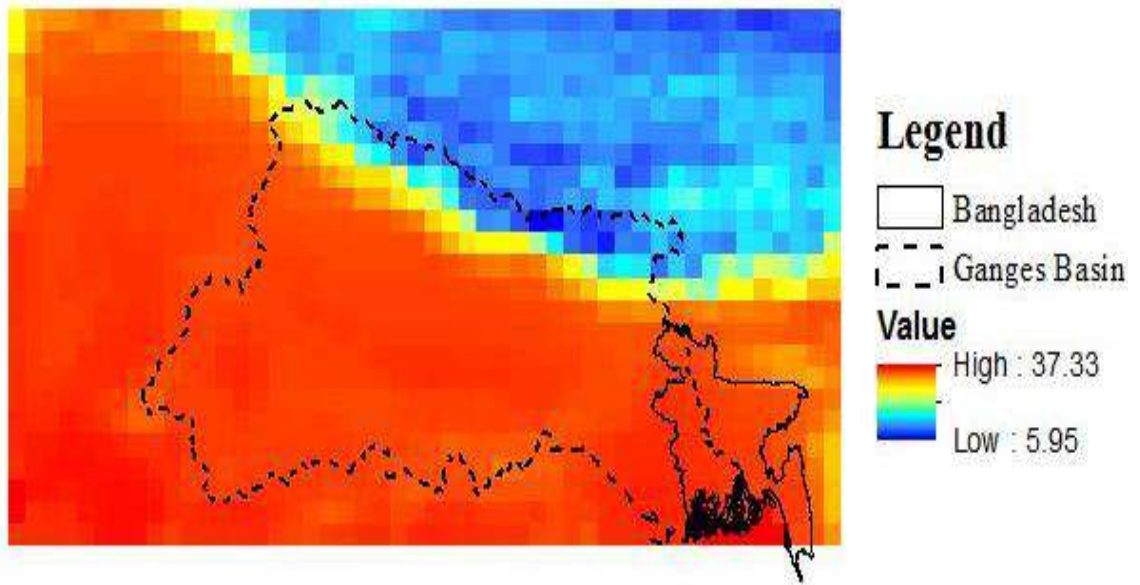


Figure C15: Spatial distribution of Maximum temperature (°C) for IPSL-CM5A-LR 4.5 in 2080s (Coolest Scenario)

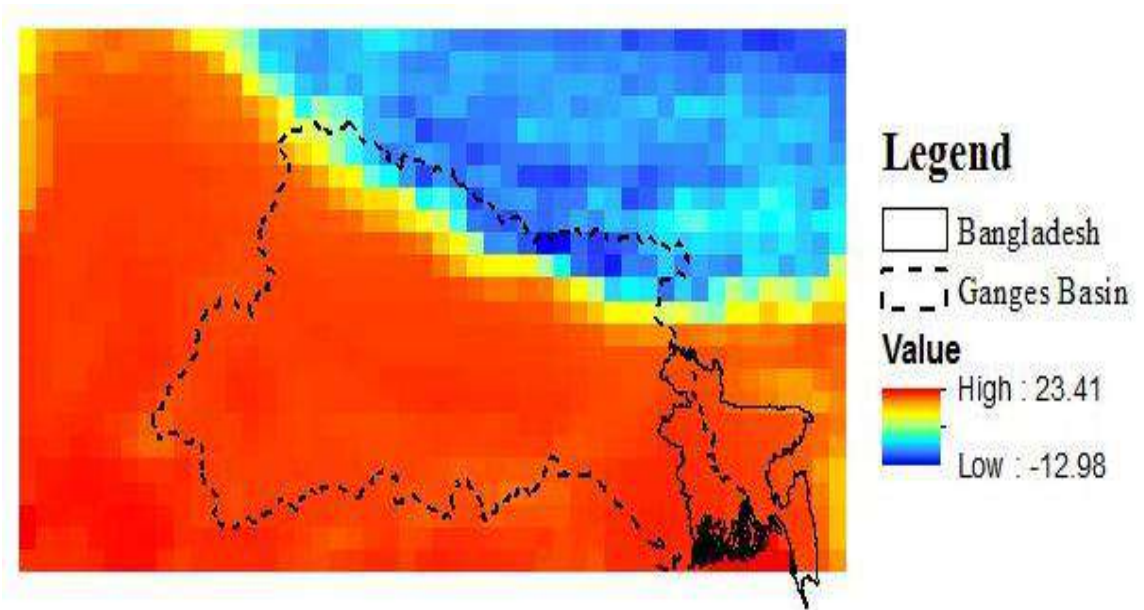


Figure C16: Spatial distribution of Minimum temperature (°C) for IPSL-CM5A-LR 4.5 in 2020s (Coolest Scenario)

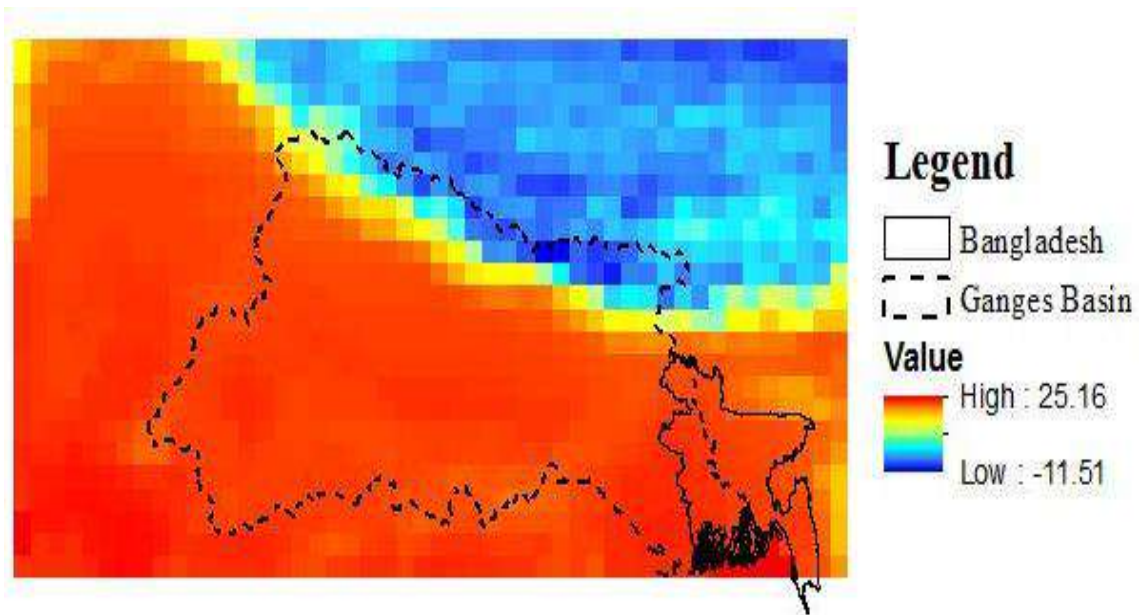


Figure C17: Spatial distribution of Minimum temperature (°C) for IPSL-CM5A-LR 4.5 in 2050s (Coolest Scenario)

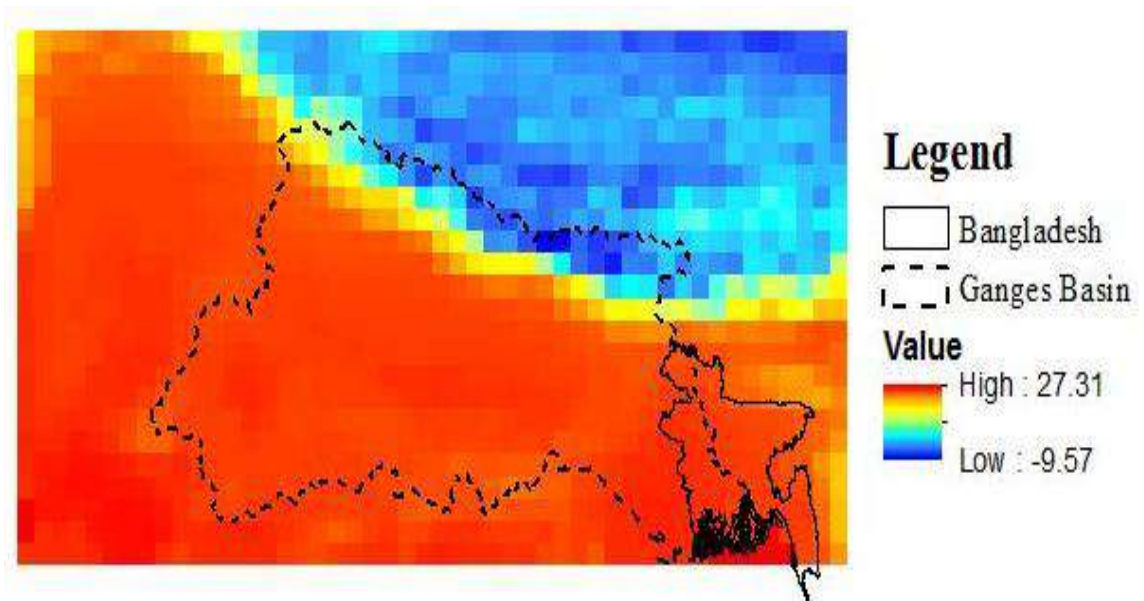


Figure C18: Spatial distribution of Minimum temperature (°C) for IPSL-CM5A-LR 4.5 in 2080s (Coolest Scenario)